

Development of Automatic Measurement System for Surface Profiles

ムハマド, ハズラト, アリ

<https://doi.org/10.15017/1441225>

出版情報：九州大学, 2013, 博士（工学）, 課程博士
バージョン：
権利関係：全文ファイル公表済

DEVELOPMENT OF AUTOMATIC MEASUREMENT
SYSTEM FOR SURFACE PROFILES

MD. HAZRAT ALI

March, 2014

Doctoral Thesis

Department of Mechanical Engineering

Graduate School of Engineering

Kyushu University

ABSTRACT

This thesis presents the research findings of measuring surface profile automatically in manufacturing components where the traditional measurement system is not applicable. In Part I of this study, the laser guided deep-hole measurement system is applied to holes with normal millimeter-level diameters and lengths of several hundred millimeters. A measurement system which can measure a small size hole with a diameter between 17 to 21 mm and having a length between 0 to 800 mm is developed, and the performance has been evaluated experimentally. Accurate measurement of diameter, roundness, cylindricity, and straightness of a deep-hole is essential for improving the performance of manufacturing products and components. However; existing systems have drawbacks to precisely measuring holes with large- length-to- diameter ratios, which require multiple measurement devices. In order to accurately evaluate the parameters of such deep-holes with millimeter-level diameters and meter-level lengths using a single device, a laser-guided deep-hole measurement probe is developed. In Part II of this thesis, the developed gear circumference measurement system has been described with the increment of scanning speed up to 20 times faster than the conventional system. During gear profile measurement, the synchronized movement control of both axes is the key issue to achieve the constant line speed scanning in whole measurement. To justify the proposed measuring strategy, the new Gear Measuring Machine (GMM) is developed with direct axis-driving and 3D probe implementation. A standard cylindrical gear is measured using the developed GMM and the whole shape of the gear outline was successfully obtained with the maximum scanning speed of 7 mm/s without detaching the stylus from the workpiece. The tip edge is one of the challenging shapes to be measured, but it is also obtained with good accuracy by adjusting the nominal data. The proposed method has great advantage over conventional gear measurement system as it gives detail information of tooth profiles of both tooth flanks for all teeth, tip diameter, the edge shapes of tooth tips, root and bottom profiles for all teeth, as well as pitch deviation in one complete measurement. Since those useful deviation parameters can be obtained automatically in only one scanning procedure for a target gear; it is very useful and cost effective in manufacturing industries. In addition; a camera and software system is integrated with the gear measurement system in order to enhance overall safety and reliability of the developed system.

PART I

LASER-GUIDED DEEP-HOLE MEASUREMENT SYSTEM FOR HOLES HAVING SMALL DIAMETERS AND LONG LENGTHS

Table of Contents

Contents	Page no.
ABSTRACT	ii
PART I	iii
Table of Contents	iv
List of Figures	ix
List of Tables	xiii
CHAPTER 1	1
INTRODUCTION	1
1.1 Introduction.....	1
1.2 Deep-hole.....	2
1.3 Problem statement	3
1.4 Research objectives	3
1.5 Research methodology.....	4
1.6 Research scope.....	5
1.7 Thesis organization	5
CHAPTER 2	6
BACKGROUND STUDY	6
2.1 Introduction.....	6
2.2 Surface roughness measurement system	9
2.2.1 Measurement probe with various measurement units.....	9
2.2.2 Working principle of previous measurement system for larger holes.....	10
2.3 Roundness error evaluation technique.....	12

2.4 Three point roundness measurement	13
2.5 Non-contact based roundness measurement	13
2.6 Surface measurement applied optical instruments	14
2.7 Laser based macrostructure measurement	14
2.8 Measurement system based on confocal laser scanning microscope	15
CHAPTER 3	16
MEASUREMENT SYSTEM COMPONENTS	16
3.1 Measurement system	16
3.2 Design of measurement unit	16
3.3 Pentaprism	16
3.4 Integrated optical components	18
3.4.1 Pentaprism and its working principle.....	18
3.4.2 Corner-cube prism and its working principle.....	19
3.5 Laser system	20
3.5.1 Laser beam radiation and reflection	20
3.5.2 Laser interferometer's output.....	21
3.5.3 Basic laser beam testing.....	23
3.6 Front axis setting by PSD sensor	24
3.7 Setting main axis.....	26
3.8 Complete system setting	27
3.9 Rear axis setting.....	27
3.10 Rear CCD camera	29
3.11 Rear CCD camera spot detection.....	29
3.12 Summary.....	31

CHAPTER 4	32
WORKING PRINCIPLES OF ROUNDNESS MEASUREMENT	32
4.1 Introduction.....	32
4.2 Working principle of laser interferometer.....	34
4.2.1 Laser interferometer and its function	36
4.2.2 Experimental procedure using laser interferometer	36
4.3 Working principle of PSD sensor	38
4.4 Working principle of rear CCD cameras	40
4.4.1 Rear optical device.....	43
4.4.2 Rear probe's coordinate calculation based on CCD spot.....	43
4.4.3 Measurement effects on the spot changes of CCD camera.....	44
4.5 Working principle of rotation detector sensor	45
4.5.1 Features of the rotation detecting sensor.....	45
4.5.2 Specifications of rotation detecting sensor	46
4.6 Working principle of measurement unit	46
4.6.1 Detection of hole deviation	46
4.6.2 Deviation of probe from hole center	47
4.6.3 Effect of initial inclination on detection accuracy	48
4.7 Measurement unit control	49
4.8 Working principle of integrated computer system.....	51
4.8.1 Measurement probe	51
4.8.1.1 Measurement system without actuator.....	52
4.8.1.2 Integrated measurement system with actuator	52
4.8.2 Editing program	54

4.8.3 Saving program after editing.....	54
4.8.4 Compiling program.....	55
4.8.5 Table feed	55
4.8.6 Roundness measurement.....	56
4.9 Summary.....	56
CHAPTER 5	57
RESULTS AND DISCUSSION	57
5.1 Introduction.....	57
5.2 Experimental results	57
5.2.1 Experiment # 1: Hole depth = 40 mm.....	57
5.2.2 Experiment # 2: Hole depth = 50 mm.....	60
5.2.3 Experiment # 3: Hole depth = 60 mm.....	62
(1) Trial # 1	62
(2) Trial # 2	65
(3) Trial # 3	68
(4) Trial # 4	71
5.2.4 Experiment # 4: Hole depth = 100 mm.....	74
5.2.5 Experiment # 5: Hole depth = 200 mm.....	76
5.2.6 Experiment # 6: Hole depth = 300 mm.....	78
5.2.7 Experiment # 7: Hole depth = 400 mm.....	80
5.2.8 Experiment # 8: Hole depth = 800 mm.....	82
5.2.8.1 Intermediate feed and circumferential scanning	83
5.3 Experimental results at different conditions	85
5.3.1 Case 1: $N=6 \text{ min}^{-1}$, $f=0.5 \text{ mm/rev}$, distance 100 mm	85

5.3.2 Case 2: $N=6 \text{ min}^{-1}$, $f=0.5 \text{ mm/rev}$, distance 200 mm and 400 mm	85
5.4 Experimental results for longitudinal scanning	86
5.5 Key achievements	86
5.6 Performance analysis of the developed deep-hole measurement system	87
5.6.1 Performance evaluation of roundness measurement.....	87
5.6.2 Performance evaluation of 3d shape measurement.....	87
5.6.3 Performance evaluation of CCD data measurement	88
5.7 Summary	88
CHAPTER 6	89
CONCLUSION AND FUTURE WORKS.....	89
6.1 Introduction.....	89
6.2 Conclusion	89
6.3 Future works	90
6.4 Mechanical actuator for the measurement system.....	91
6.5 Assembly design of the mechanical actuator.....	93
REFERENCES	95

List of Figures

Figures	Page no.
Fig. 2. 1 Laser guided deep-hole measurement probe.....	10
Fig. 2. 2 Fundamental structure of deep-hole measurement probe	10
Fig. 2. 3 Overview of the measurement system	11
Fig. 3. 1 Pentaprism for the measurement head	16
Fig. 3. 2 Combined assembly design of the measurement head.....	17
Fig. 3. 3 Measurement head checking	17
Fig. 3. 4 Pentaprim and its working principle	18
Fig. 3. 5 The reflection principle of pentaprism.....	19
Fig. 3. 6 Corner cube prism and its working principle.....	20
Fig. 3. 7 State of the working laser interferometer.....	20
Fig. 3. 8 (a) A correct laser beam radiation; (b) an error occurred during laser beam radiation	21
Fig. 3. 9 (a) An active laser interferometer during manufacturing process; (b) an example of correct laser beam radiation before measurement	21
Fig. 3. 10 (a) An example of active measurement while generates alarm in monitor; (b) Laser interferometer monitor after resetting the button	22
Fig. 3. 11 Laser and optical error checking	23
Fig. 3. 12 PSD sensor for front axis setting.....	24
Fig. 3. 13 Adjustment of position and slope of laser optical axis.....	25
Fig. 3. 14 Overview of the measurement system	27
Fig. 3. 15 Positioning of the rear CCD camera	28
Fig. 3. 16 CCD camera (LU 125)	29

Fig. 3. 17 Laser spots on computer monitor from (a) CCD1 and (b) CCD2 cameras.....	30
Fig. 3. 18 (a) CCD camera shows the spot position in terms of ‘X’ and ‘Y’ axes; (b) rear measurement deviation result recorded by CCD cameras.....	30
Fig. 4. 1 Axis setting for laser interferometer.....	35
Fig. 4. 2 A set of complete laser interferometer	36
Fig. 4. 3 Shape of the workpiece	36
Fig. 4. 4 Measurement unit.....	37
Fig. 4. 5 Calculation of radius of the hole	37
Fig. 4. 6 Measurement principle of the PSD: Determination of (b) x coordinate, Determination of (c) y coordinate	40
Fig. 4. 7 Flow chart for acquiring CCD camera data	41
Fig. 4. 8 Measurement method for probe position and inclination	42
Fig. 4. 9 (a) Rear laser beam setting, (b) mirror 1 and (c) mirror 2 of the rear optical system.....	43
Fig. 4. 10 Rotation detector sensor.....	45
Fig. 4. 11 Hole shapes measurement	47
Fig. 4. 12 Deviation of probe from hole center	47
Fig. 4. 13 Motor and controller used for measurement head	49
Fig. 4. 14 Measurement head controlling program using Microchip programmer	50
Fig. 4. 15 Controlling method of DC motor.....	50
Fig. 4. 16 Measurement probe design	51
Fig. 4. 17 Manufactured measurement probe.....	52
Fig. 4. 18 Laser-guided deep-hole measurement system without actuators.....	52
Fig. 4. 19 Integrated experimental set up	53
Fig. 4. 20 Flow chart for editing the program	54

Fig. 4. 21 Flow chart for saving the program after editing	54
Fig. 4. 22 Flow chart for compiling the program	55
Fig. 4. 23 Flow chart for moving the table	55
Fig. 4. 24 Flow chart for roundness measurement	56
Fig. 5. 1 Measured roundness curve of the hole.....	58
Fig. 5. 2 3d inner shape of the measured deep-hole	59
Fig. 5. 3 Rear view obtained from CCD camera	59
Fig. 5. 4 Measured roundness curve of the hole.....	60
Fig. 5. 5 Measured 3d shape of the inner hole surface	61
Fig. 5. 6 Rear CCD camera data for 50mm.....	61
Fig. 5. 7 Measured roundness curve.....	63
Fig. 5. 8 3d inner shape of the measured deep-hole	64
Fig. 5. 9 Rear view obtained from CCD camera	64
Fig. 5. 10 Measured roundness curve of the hole.....	66
Fig. 5. 11 3d inner shape of the measured deep-hole	67
Fig. 5. 12 Rear view obtained from CCD camera	67
Fig. 5. 13 Measured roundness curve of the hole.....	69
Fig. 5. 14 3d inner shape of the measured deep-hole	70
Fig. 5. 15 Rear view obtained from CCD camera	70
Fig. 5. 16 Measured roundness curve of the hole.....	72
Fig. 5. 17 3d inner shape of the measured deep-hole	73
Fig. 5. 18 Rear view obtained from CCD camera	73
Fig. 5. 19 Measured roundness curve of the hole.....	74

Fig. 5. 20 3d shape of the inner hole surface.....	75
Fig. 5. 21 Rear CCD camera data for 100mm.....	75
Fig. 5. 22 Measured roundness curve of the hole.....	76
Fig. 5. 23 Measured 3d shape of the inner hole surface	77
Fig. 5. 24 Rear CCD camera data for 200mm.....	77
Fig. 5. 25 Measured roundness curve of the hole.....	78
Fig. 5. 26 Measured 3d shape of the inner hole surface	79
Fig. 5. 27 Rear CCD camera data for 300mm.....	79
Fig. 5. 28 Measured roundness curve of the hole.....	80
Fig. 5. 29 Measured 3d shape of the inner hole surface	81
Fig. 5. 30 Rear CCD camera data for 400 mm.....	81
Fig. 5. 31 Spirally scanned hole shape measured by the laser interferometer	82
Fig. 5. 32 Circumferentially scanned hole shape: measured every hole depth of 50 mm by the laser interferometer.....	83
Fig. 5. 33 Corrections of measured roundness profile using fitting method, and locational delay of rotation-detection sensor	84
Fig. 5. 34 Hole deviation obtained from $CCD\delta$ and $CCDi$	86
Fig. 5. 35 Longitudinal scanning of four hole walls	86
Fig. 6. 1 Middle part of the actuator.....	91
Fig. 6. 2 Connecting part of the actuator.....	92
Fig. 6. 3 Assembly design of different parts of the actuator.....	93
Fig. 6. 4 Assembly drawing with integrated worm gear	94

List of Tables

Table	Page no.
Table 3. 1: Pentaprism specification (Sigma Koki.co.jp).....	19
Table 3. 2 : Laser specification.....	23
Table 3. 3 : Specifications of PSD sensor.....	25
Table 3. 4 : CCD camera specification (Lu 125).....	29
Table 4. 1 : CCD1 camera's coordinate effects	44
Table 4. 2 : CCD2 camera's coordinate effects	44

CHAPTER 1

INTRODUCTION

1.1 Introduction

Nowadays, the production quality is a major stake specially for fields like mechanical and nuclear industries which have to produce extremely accurate parts. Large hole can be found in jet engine shaft, wheel shaft of high speed train or in the cylinder liner of a large ship for example. It is very difficult to measure precisely the accuracies of these kind of hole parameters, such as its diameter, roundness, cylindricity and straightness; particularly when the hole has high length to diameter ratio (L/D). Currently, all these hole parameters are measured by different kind of devices such as roundness tester, cylinder gauge and so on. Using several measuring devices instead of one is very time consuming. This operation does not create any added value on the produced parts, therefore it is important to reduce the time duration.

The purpose of this research is to design a measurement probe which would allow us to determine the hole surface parameters accurately in a short time. This probe uses a laser system to scan the hole wall and can be controlled to correct the position and inclination of the probe. The aim of this research is to develop a system that can solve the problem in measuring unreachable holes such as long length and small diameter in mechanical components. The misalignment of main spindle, guide bush, workpiece and table (machining system) also could bring the hole deviation. The precise adjustment of this machining system could decrease the deviation although it is impossible to prevent perfectly this misalignment. At present condition, the possible depth of internal grinding finishing is very low. If the hole diameter is 110 mm, possible grinding depth will be just 350 mm, so to reach 1000 mm of depth is still facing with impossibility.

There is a high importance of online measurement in deep-hole boring. Nowadays, often lasers are used to keep machine on target and a precision of as good as 0.1 μm can be reached, as discussed by Hallum [1]. System applying lasers in combination with Position Sensitive Detector (PSD) are widely in use for measurement and adjustment

tasks. But their application to deep-hole boring is not known except for the actual case in the present research. Optical sensors like laser, CCD and PSD have been developed because of their immunity to harsh environment such as intense electromagnetic fields, high temperatures and corrosive environments [2]. Necessity of adjustment of the tool's course to reduce axial hole deviation has led to development of a deep-hole boring tool guided by laser, which builds the basis for the present research work. The detail system structure, specifications, and working process could be read deeply at the later chapter of this thesis. System works in general, but precision and depth of hole are limited by rigidity of connecting shafts.

1.2 Deep-hole

All boring operations count for approximately 30% of all metal cutting operations, whereas, solid boring alone stands for 22%. Conventional twist drills are applied without any problems up to length to diameter (L/D) ratio of about 3 to 5. Deep-hole boring operations find many wide fields of applications, as there are manufacturing of precision cylinders for extrusion machinery and injection molding machinery, weight reduction of rotating shafts, or even mass production in case of engine cylinders. A hole with a depth more than five times of diameter usually defined as a deep-hole. Deep-hole boring is one of the most difficult processes in cutting and grinding, specially when the ratio of L/D is bigger than the normal ratio. In comparison to small holes, deep-holes have special features that require specially designed tool for application.

At present, the deep-hole boring is done by the use of BTA (Boring and Trepanning Association)/ STS (Single Tube System), DTS (Double Tube System) or gun drill. Although these tools have self-guiding action for keeping the straightness of forward movement as the excellent point of these tools, but when the ratio of hole length to diameter is increasing, the stiffness of boring bar is getting insufficient to support the tool and causes a hole deviation during process. The non-homogeneity of material and vibration during boring also cause this hole deviation which results in the degradation of product quality. Usually, boring is conducted by rotating the workpiece (stationary tool

and rotating workpiece together) to avoid hole deviation. Unfortunately, this process is limited to symmetric workpiece only. When the shape of workpiece is asymmetric, this process only could be done by rotating the tool (stationary workpiece and rotating tool system), but it could also causes deviation because the tool will move forward to thin or weak point of workpiece material. It also causes the degradation of hole precision.

1.3 Problem statement

The main problem of surface parameter measurement in unreachable hole or in another word we name it as deep-hole is that there is no conventional hole parameter measurement tools. One of the existing tools can measure open surface by using laser beam reflection technique on the surface area. Some other existing machines can measure inner hole shapes of larger diameter without the application of laser such as Talyrond. Traditional measurement systems do not support in measuring inner deep-hole's surface parameters. Another system is used for deep-hole roundness measurement purpose but that is applicable only for a minimum hole diameter of 70 mm. Thus a system is necessary to measure deep-hole having a range of target diameter between 17-21 mm so that it can be applied for certain types of deep-holes and having a length between 0-800 mm. As the existing system is applicable for a minimum hole diameter of 70 mm; the downsizing of the deep-hole is very useful and will add a new technique in measuring surface roundness.

1.4 Research objectives

This dissertation presents experimental results of measuring hole parameters having small diameter and long length by a measurement unit fixed at the end of a cylindrical long measurement bar. The system consists of a measurement unit in order to scan hole wall; laser interferometer for detecting topography of the hole wall; and optical device at the back for detecting attitude of the measurement unit. As a result of experimental analysis, it is observed that deep-hole having less than 20 mm-diameter and long-length about 0-800 mm can be measured by the new developed measurement system. Measurement in machining process is vital in order to acquire target outputs from the

manufactured machine parts. In addition, the measurement of hole surface parameters and its monitoring system during measurement is also very important. The monitoring system works as feed-back control system for the complete process. The system for this measurement consists of a laser interferometer, measurement head, laser diode, CCD cameras; and optical devices such as pentaprism, corner cube prism as well as display monitors for the CPU, CCD camera and data measured by the laser interferometer. The measurement performance is monitored by the display monitors and graphs plotted by the acquired experimental data as elaborated later in this research.

Currently, deep-hole in various mechanical parts has been made in the manufacturing industries. Among them, large rotational shaft; aircraft jet engine; the cylinder liners for large marine engines and Shinkansen; power generation turbine rotor; the generator, and centrifugal casting mold where there exist deep-holes. For the measurement of the hole, the instrument such as cylinder gauge and roundness measuring machine is generally used, but application is very difficult as commercially available tools has restrictions on size, in case of deep-hole; problem such as thermal deformation, and the size of the instrument while maintaining high measurement accuracy is also difficult. Therefore, in case of drilling; deep hole actually measuring the thickness from the outer surface by using an ultrasonic instrument, and estimates that the shape of the hole. This method is simple; the measurement accuracy is not good because of the environmental disturbance compare to the new developed system by which it can be measured reasonably and accurately the shape of the deep-holes.

1.5 Research methodology

To solve this problem in deep-hole measurement, a combination of laser interferometer, optical components such as pentaprism, corner cube prism, PSD sensor; laser diode, CCD camera based integrated system is designed and developed. Optical components are used in order to keep the axis on its correct axis during measurement specially for rear probe attitude. PSD sensor is used in order to set the workpiece axis. Laser interferometer gives the data for roundness and 3D spiral shape of the inner holes. To scan the deep-hole's wall the probe's head must rotate during measurement to scan the

hole wall continuously. DC motor is used to control the measurement head's rotational speed. A hall element or rotation detection sensor is used to get the accurate sampling data by detecting and recording the data for each rotation in complete measurement. A servo motor is used to feed the workpiece which is set on the table.

1.6 Research scope

The dissertation also presents computational results of deep-holes evaluated by a measurement unit fixed at the end of a cylindrical long measurement bar. The measurement unit which is fixed at the end of the measurement bar and positioned along a hole center is supported by a pair of skids. As a result of computational analysis, it is found that deep-hole between 0 to 800 mm-length and 18 mm-diameter can be measured by the measurement unit with the cylindrical long measurement bar. The measuring depth can be increased by extending the long measurement bar.

1.7 Thesis organization

Chapter 2 discussed background studies of the similar system. New developed measurement system is described in Chapter 3. Chapter 4 elaborates experimental methods of roundness measurement. Finally, the result of this research is discussed in chapter 5. Chapter 6 summarizes the results of this research and suggests for future works.

CHAPTER 2

BACKGROUND STUDY

2.1 Introduction

Deep-holes are bored with the meter, millimeter, and micrometer level diameters in engineering. Their lengths can be as large as several tens of meters to as short as a few micrometers. Examples of holes with large 100 millimeter level diameters and meter level lengths are the rotation shafts of jet engines, generators, and high-speed trains; the large cylinder used in plastic injection molding; the cylindrical liners of ship engines and cannons. Holes with normal 10 millimeter level diameters and lengths of several hundred millimeters are used for the main spindles of machines, the small cylinder in plastic injection molding, the tube sheet for heat exchanger and guns. Accurate measurement of the diameter, roundness, cylindricity, and straightness of a deep-hole is essential for improving the performance of products. However, existing systems have drawbacks to precisely measure holes with large length to diameter ratios that require multiple measurement devices. In order to accurately evaluate the parameters of such deep-holes with 100-millimeter-level diameters and meter-level lengths, using a single device, a laser-guided deep-hole evaluation probe was developed [1-6].

It is very important to monitor the mechanical behavior of precision measurement system in manufacturing devices. The monitoring system has the advantages such as compare simple structure, high precision, low price and great expandability, which has huge application potentiality for the manufactured components. With the goal of developing more effective nuclear weapon, new instruments that brought greater accuracy to measurements of dimensions, shapes, densities, and surface finishes than the existing instruments is developed. A manufacturing process for machining and finishing which is more precise than anything commercially available is proposed [7]. The science of measurement (known as metrology) and precision engineering is necessary to produce new parts, because without the ability to measure a dimension or other quantity, one can never know whether a given level of precision has been achieved. As measuring

capabilities improved, components for industrial applications are designed to tighter tolerances, leading to an increased emphasis on precision manufacturing.

Metrology tools have varieties of applications. The most obvious is to measure shape errors in the part being produced. But they also can measure the errors arising in the equipment used to manufacture the part, a practice known as machine tool metrology. And they are often used to measure a process such as characterization of a grinding wheel. Precision engineering requires, among other things, a systematic approach to determine dimensional errors. When measurements are made, precision engineering requires a quantitative assessment of the total uncertainty of the measurement. A few breakthrough technologies, such as the laser interferometer, optical devices, cameras and the personal computer have revolutionized the machine design procedure while most advances in precision engineering today are incremental [8].

Xpress probes are designed for high accuracy dimensional measurements on a wide range of components [9]. Whereas the Gannen XP probe is designed for ultimate precision, the Gannen XM and Heimen probes are designed for high precision measurements on miniaturized parts. These include micro holes with a diameter in the region of several tens of micrometers, micro trenches, e.g. for micro-fluidics, freeform surfaces, etc. [9]. Leading technology in ultra-precision metrology components, systems and machines are also designed [10]. Accuracy and precision can be defined as follows; the accuracy of the measurement refers to how close the measured value is to the true or accepted value; on the other hand precision refers to how close together a group of measurement actually are to each other. Precision has nothing to do with the true or accepted value of a measurement, so it is quite possible to be very precise and totally inaccurate [11].

The application of laser in measurement is increasing day by day. Isara (IBS Precision Engineering) is an ultra-precision Coordinate Measuring Machine (CMM) that is now available in the market; it comprises a moving product table and a metrology frame with thermal shielding on which three laser sources are mounted [12]. Multi-probe measurement system also plays vital role in micro machining in recent years. The results from the pre-experiment verify that the multi-probe measurement method performs the

yaw and straightness motion error measurement extremely well. Comparisons with the simulation results demonstrate that the multi-probe measurement method can also measure the reference bar mirror profile with a small standard deviation of 10 nm [13]. The measurement and monitoring framework mainly has three purposes:

- To provide evidence of how well the approved measurement system is meeting the requirements.
- To improve measurement system by applying the most efficient method.
- To determine how well the complete measurement system is being followed.

Automatic measurement system in order to measure a mechanical tool or workpiece is not widely used. It is essential to accurately measure the surface parameters of a hole for applications such as the rotation shafts of a jet engine, generator and high-speed train; the cylinder used in plastic injection molding; and the cylinder liner of a ship engine. Available system has disadvantages in precise measurement of the hole with large length to diameter ratio, in which different measurement devices are required separately. To evaluate the accuracies of such deep-holes using a single device, a laser-guided deep-hole evaluation probe is necessary. In some other studies, expensive piezoelectric actuators are used to control attitude of the measurement probe [14]. It is still difficult to measure the accuracy of holes with depths in the order of a few meters and with diameters varying in the order of a few millimeters.

Deep-hole with 3m-length and 63mm-diameter was measured by the measurement unit with the cylindrical long measurement bar [17]. In our past study [16], measurement unit which can measure holes with a diameter of 70 to 168 mm was developed and discussed. In the piezoelectric actuator stroke is 0.35mm, allowable load is 16kg and fast speed response. Piezoelectric actuator is also introduced in self-sensing measurement for micro manipulator and micro assembly context [15]. The improvement of control strategy in measuring high performance laser guided deep-hole tool has been elaborated in details. Control strategy for the attitude control is also discussed [18]. The objective of the current study is to design laser-guided probe to satisfy the following two conditions:

- To downsize deep-hole measurement probe with the range of diameters between 17-21 mm and lengths between 0-800 mm.
- Deep-hole's roundness, inner shape and rear probe's attitude measurement during experiment.

2.2 Surface roughness measurement system

Surface roughness measurement system has various techniques. Some are contact base and some are non-contact base. Some have larger hole-diameter and long-length and some are vice-versa.

2.2.1 Measurement probe with various measurement units

To evaluate the accuracies of such deep-holes using a single device, a laser-guided deep-hole evaluation probe is developed as in **Fig. 2.1**. The attitude (position and inclination) of the probe is controlled as if it is on the right measurement axes as shown in **Fig. 2.2**. A measurement unit rotates and its stylus scans the hole wall. The movement of the stylus is detected by a laser interferometer located in front of the probe. It is still difficult to measure the accuracy of deep-holes in the order of a few meters and with diameters varying in the order of a few millimeters, such as the rotating shaft holes of jet engines and high-speed-trains. In this case, different measurement devices are required separately for measuring hole accuracy. An investigation on the correlation between surface topography and its mechanical properties measured by a novel multi-function Tribological Probe Microscope (TPM) at the micro/ nanometre level is discussed in this research [19]. A scanning multi-probe system for measuring straightness profiles of cylinder workpieces is discussed [20]. The system consists of two probe-units, each having three displacement probes. The two probe-units that are placed on the two sides of the test cylinder, are moved by a scanning stage to scan the two opposed straightness profiles of the cylinder simultaneously by this system.

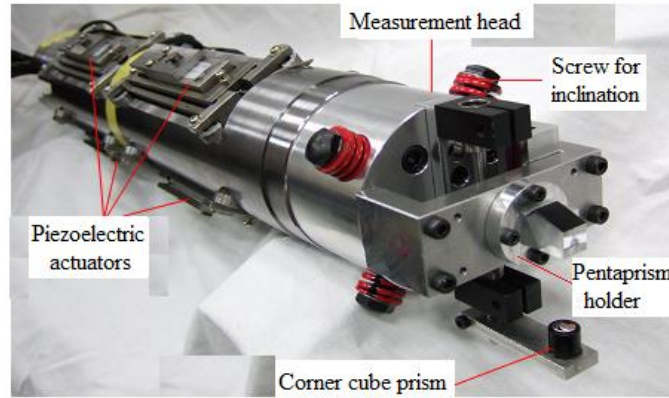


Fig. 2. 1 Laser guided deep-hole measurement probe

2.2.2 Working principle of previous measurement system for larger holes

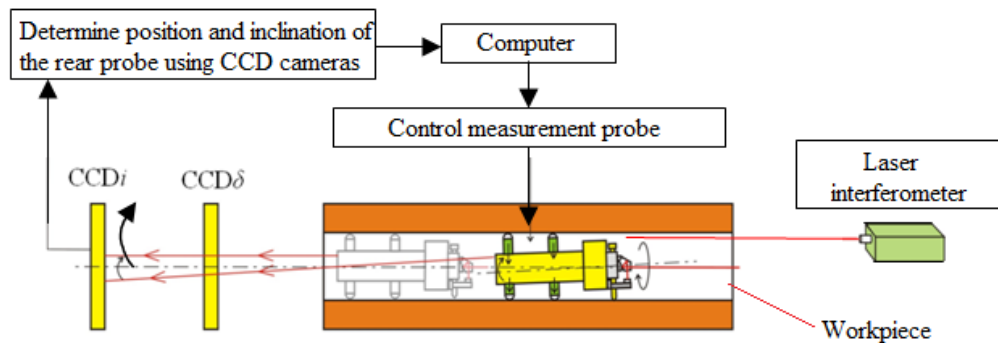


Fig. 2. 2 Fundamental structure of deep-hole measurement probe

Conventional lathe is used for the above experiment. One end of measurement bar is fixed by a collet chuck and the other end supported by a pair of skids behind the measurement unit [6]. In that measurement system, the laser diode is placed on measurement axis which is a center line of the spindle of headstock. Attitude of measurement unit can be accurately detected. On the other hand, in the measurement system described in [6, 19], a laser diode is fixed on the measurement probe apart from the measurement axis. Therefore rotational deviation of the laser diode due to the rolling of the measurement probe affected detection accuracy of the probe the probe attitude [22].

- ① Deep hole boring machine
- ② Guide bush
- ③ Measurement probe
- ④ Laser interferometer

- ⑤ Optical system for measuring probe attitude
- ⑥ Optical system for setting a guiding axis
- ⑦ Personal computer
- ⑧ Monitor

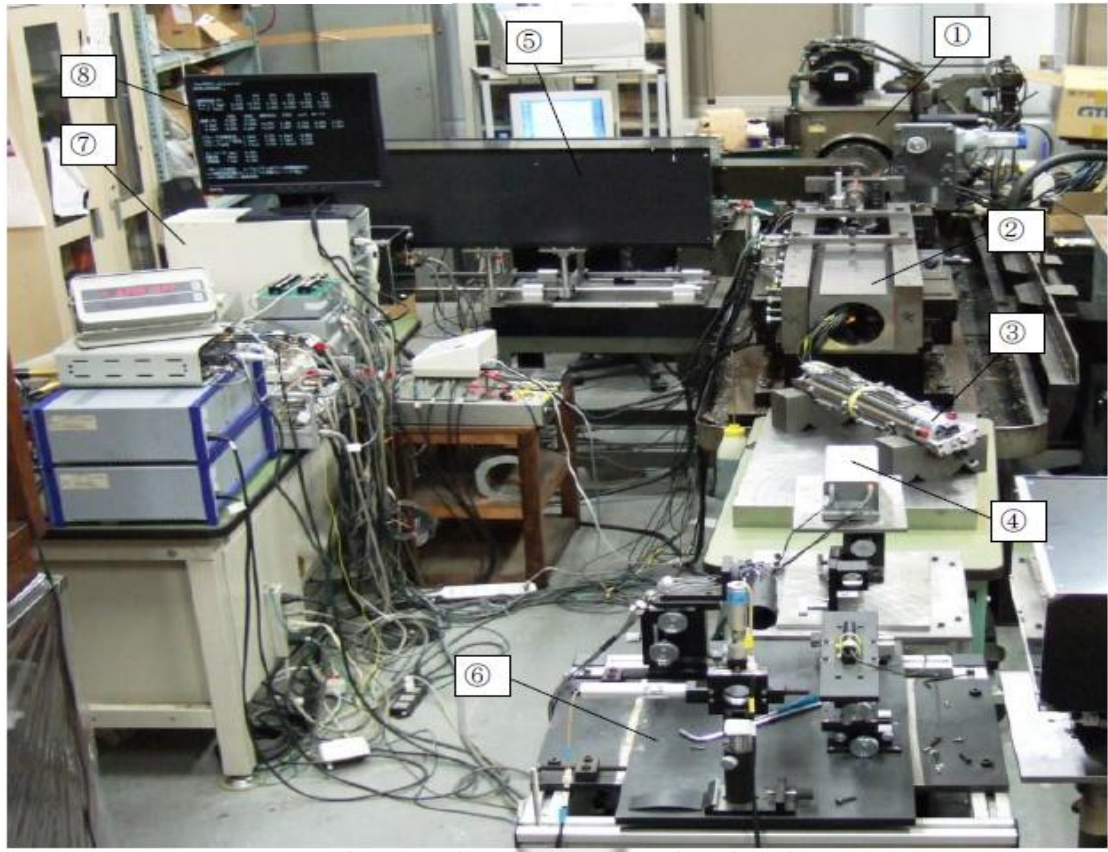


Fig. 2. 3 Overview of the measurement system

The integrated system`s working principles and the necessary commands for the programs are shown below in details. The flow charts are drawn to clarify the processes. **Figure 2.3** shows a complete experimental apparatus for measuring a larger hole profiles. The apparatus descriptions are given above **Fig 2.3**.

This dissertation also presents a distance measurement method based on pixel number variation of CCD images by referencing to two arbitrarily designated points in the image frames. By establishing a relationship between the displacement of the camera movement along the photographing direction and the difference in pixel count between reference points in the images, the distance from an object can be calculated via the

proposed method. To integrate the measuring functions into digital cameras, a circuit design implementing the proposed measuring system in selecting reference points, measuring distance, and displaying measurement results on CCD panel of the digital camera is proposed in this paper. In comparison to pattern recognition or image analysis methods, the proposed measuring approach is simple and straightforward for practical implementation into digital cameras. To validate the performance of the proposed method, measurement results using the proposed method and ultrasonic rangefinders are also presented in this paper [23].

2.3 Roundness error evaluation technique

Theoretical error was conducted for on-machine measurements of roundness profiles based on the assessment of radial variations in [21]. Another new method for roundness error evaluation using polar coordinate system, named as Polar Coordinate Transform Algorithm (PCTA), is presented in this paper. The algorithm first allocates a circular region around the least square circle center following certain rules, then calculates the polar radius for all measured points by translating polar coordinate system to each point in the region in turn, and finally obtains minimum circumscribed center point, maximum inscribed center point and minimum zone center point from comparing each polar radius relative to each polar coordinate system. With accurate center point, the algorithm could give more accurate roundness evaluation. In that paper, the process of PCTA is described in detail including geometrical dimensions. Theoretical calculation and testing results show that PCTA can evaluate roundness error effectively and accurately [24].

Another research work presents a new architecture of a roundness measuring system in which the roundness measuring accuracy is not dependent on motion accuracy of the rotary element. In this architecture, the influence of motion errors on roundness measurement is minimized by applying a new error separation technique, the Improved Reversal Method (IRM). A prototype that uses: a rotary table supported by ball bearings, non-contact gap sensors and a computer system that collects and process sensor readings has been developed. Experimental results have shown that even using a rotary table supported by ball bearings that has non-repetitive motion errors larger than 2mm, the

final measurement repeatability is better than 0.3mm of peak-to-peak value. In order to ensure the same levels of accuracy of the proposed system, a traditional roundness measuring system design must use a more precise and therefore more expensive type of bearing with a motion error no larger than 0.1mm [25].

2.4 Three point roundness measurement

This research [26] presents two enhancements to three-point method for roundness measurement. They enable measuring a larger bandwidth and also present a logical progression from two-point profile to three-point roundness measurement using the combined method. Simulated profiles with and without step variations are used to demonstrate these improvements [26]. A novel time-domain method, which can reconstruct straightness profile of workpiece exactly for on-machine measurement, has successfully been developed. The proposed method is based on difference measurement and can use two or three displacement probes [27].

2.5 Non-contact based roundness measurement

A new in-process and non-contact probe is proposed to measure the diameter and the roundness of turned workpieces as shown in [28]. The initial probe discussed in previous publications exhibited diameter measurements with good accuracy (uncertainty 5 μm over 100 mm). This paper discusses the implementation of roundness measurement into the initial probe and its performance. The principle of the roundness measurement is based on the relationship between the displacement and the light intensity. The probe delivers a maximum error of 0.5 μm with an uncertainty of 1 μm for roundness measurement over a range of 100 mm diameter [28].

A gear surface measurement system is highlighted by camera [33]. A simplified drawing of the optical stylus and its detection system is shown in [34]. It operates with an optical head incorporating a 780 nm wavelength semiconductor laser, yielding a measurement spot size of 1 μm diameter and a height sensitivity of 0.03 μm . A critical comparison between an optical laser stylus measurement system and a Talystep mechanical stylus profilometer is discussed. Sixteen surfaces having root mean square

roughness from 0.002 μm to 3 μm for cut-off lengths less than 0.8 mm have been used in that study. The quality of surfaces is obtained by the utilization of scattered laser light examined by a neural network and extracted features from the scattered angular spectrum that are then used as inputs to a hierarchical neural network as presented in [34].

2.6 Surface measurement applied optical instruments

In [35], the laser light is attenuated by a polarizer to ensure that the detector is not saturated. The concave mirror focuses the light to a spot approximately 0.5 mm in diameter. The scattered light is collected over an angle of approximately 25.6 degrees by the Plano -convex lens. The line array camera has 256 pixels [35].

2.7 Laser based macrostructure measurement

A laser based device for pavement macrotexture measurement is presented in [36]. In this study, a practical laser device was developed, which is lightweight and portable with low cost. Pavement surface macrotexture greatly contributes to tire-pavement skid resistance which has a direct effect on traffic operation and safety particularly at high speeds. Therefore, a strong motivation is necessary to develop effective and practical devices to measure macrotexture profile.

As described in [36], a system designed where a laser is projected onto a rough surface it will be scattered by its microscopic surface irregularities. The layer of the surface, caused by the direction of machining, determines the general light scattering pattern. A surface is perceived as changing from smooth or mirror-like to rough or diffuse when the surface roughness increases. A smooth surface scatters light mainly in a specular direction [37]. A novel method of profile measurement for reflective surface based on optical feedback is proposed in this paper [38]. With so-called self-mixing structure, a fraction of the light emitted from a laser diode (LD) is reflected back by the target under test and returns the laser cavity and changes the operation mode of this LD.

A laser-based measurement system for evaluation of the scraping workpiece quality that can eliminate contact-induced measurement errors and increase measurement accuracy is proposed [39]. The laser-based measurement system consists of a light-scattering-type triangulation laser, a Computer Numerical Control (CNC) machine tool, and an analog-to-digital (A/D) converter. The triangulation laser measures the depth of the scraping spots and the CNC machine tool locates their position [40].

2.8 Measurement system based on confocal laser scanning microscope

An experimental study of the roughness analyses for the flat and spherical surfaces of machined metal in order to compare the roughness data taken from the cloud data produced by the stylus type profilometer and two optical based measurement instruments, namely the infinite focus microscope and the confocal laser scanning microscope is presented [41]. The scattered light pattern reflected from a machined surface generally contains much information concerning the surface roughness. This study examines and proposes a surface roughness measurement technique for the on-machine measurement of the roughness of machined surfaces. The technique is based on the measurement of scattered light patterns and the statistical analysis of the light intensity distribution [43]. Another study showed that the 3D point cloud data contains a wealth of information typically not available. The surface roughness measurements can be made across the entire image to generate a surface roughness map. Joint characteristics such as surface roughness anisotropy can be evaluated efficiently [44].

2.9 Summary

As a summary, it can be said that this chapter extensively discussed some important surface measurement techniques or methods that have been used in precision measurement. Mainly it highlights the implemented previous methods applying laser and optical instruments.

CHAPTER 3

MEASUREMENT SYSTEM COMPONENTS

3.1 Measurement system

The integrated measurement system consists of several individual parts. Some parts are complex in design in order it to be fixed with others. Some others are very small and thin; precise manufacturing is depends upon proper design of the parts.

3.2 Design of measurement unit

Design of measurement unit or measurement head is very crucial in conjunction with integrated measurement system. The important steps of the probe design and the system components are briefly discussed below.

3.3 Pentaprism

Figure 3.1 shows a pentaprism which has been designed in order to fix with the measurement head to work with laser beam and corner cube prism. Its working method is described later in this chapter.

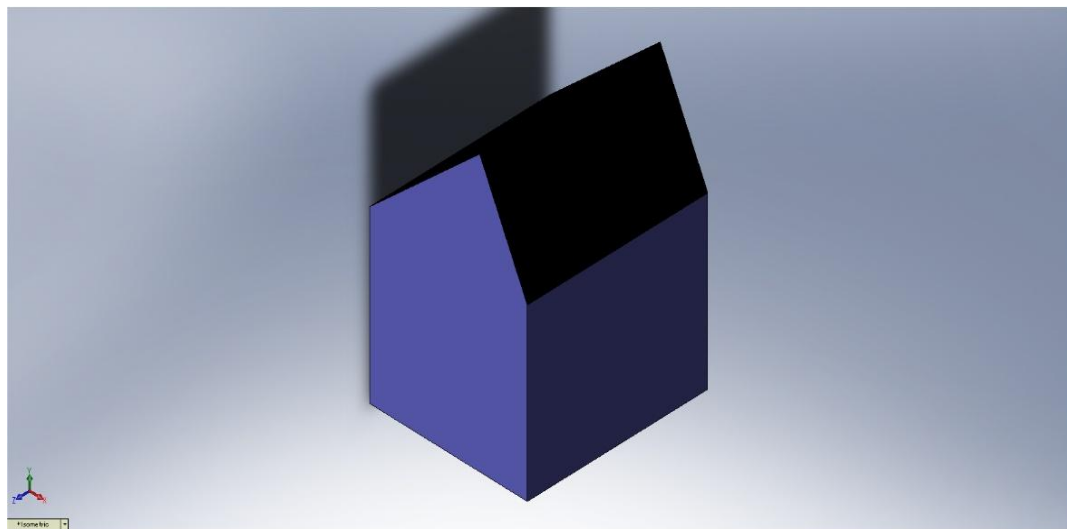


Fig. 3. 1 Pentaprism for the measurement head

Figure 3.2 shows the complete assembly drawing of the measurement unit. Important components of this unit are shown in this figure. All components are very important for the system. In front of the measurement unit laser beam is radiated which reflects to the pentaprism and deflects to the corner cube-prism, finally the deflected beam returns to the interferometer through pentaprism and gives the reading of the beam in terms of distance in mm.

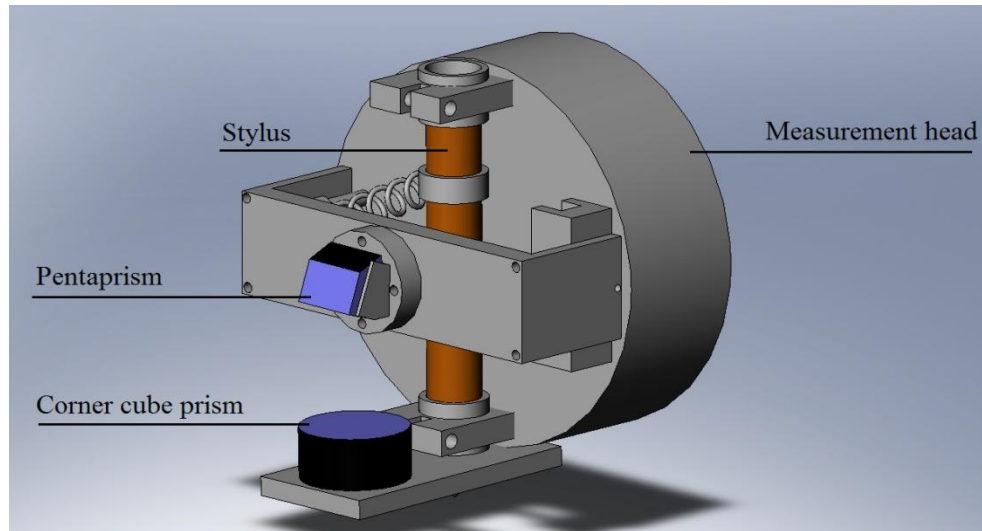


Fig. 3. 2 Combined assembly design of the measurement head

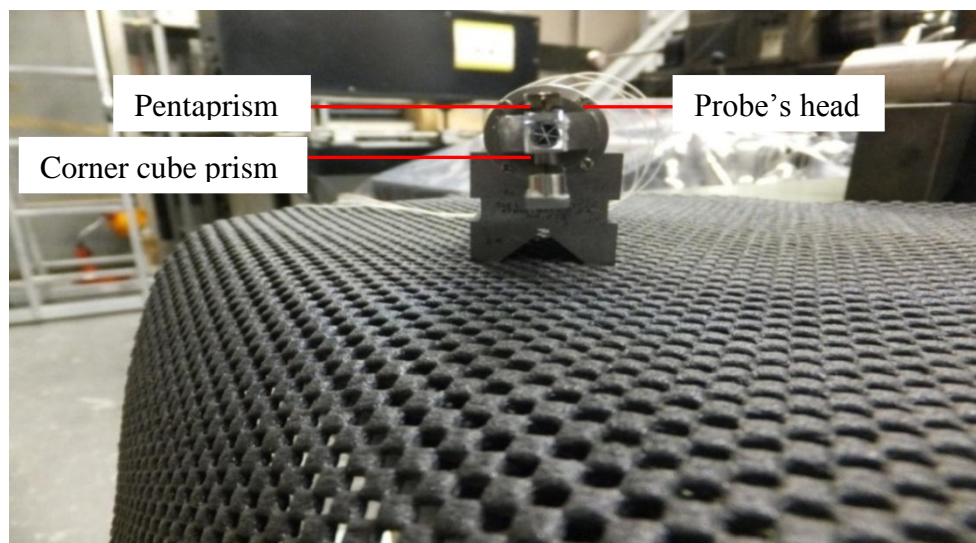


Fig. 3. 3 Measurement head checking

Figure 3.3 shows the probe with measurement unit attached to it where pentaprism, corner cube prism and stylus are connected together.

3.4 Integrated optical components

The working principles of the optical components are described below.

3.4.1 Pentaprism and its working principle



Fig. 3. 4 Pentaprim and its working principle

Figure 3.4 shows the pentaprism which is a five-sided reflecting prism. This is integrated with the measurement head so that it can divert the laser beam by a constant angle of 90° even if the entry beam is not at 90° to the prism. The beam reflects inside the prism twice, allowing the transmission of an image through a right angle without inverting it as a normal right-angle prism or mirror. The reflections inside the prism are not caused by total internal reflection, since the beams are incident at an angle less than the critical angle (the minimum angle for total internal reflection). Instead, the two faces are coated to provide mirror surfaces. The two opposite transmitting faces are often coated with an antireflection coating to reduce spurious reflections. The fifth face of the prism is not used optically but truncates that; otherwise it would be an awkward angle joining the two mirrored faces.

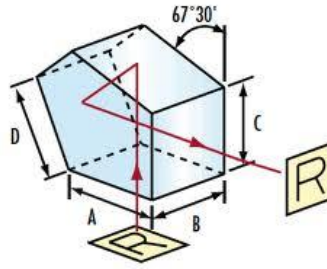


Fig. 3. 5 The reflection principle of pentaprism

Figure 3.5 explains geometrically that even if the light incidents at any angle; it has the property of emitting by bending the return beam exactly 90° . **Table 3.1** shows the specifications of the integrated pentaprism.

Table 3. 1: Pentaprism specification (Sigma Koki.co.jp)

Material	BK7
Surface flatness of substrate	$\lambda/4$
Angle tolerance	$\pm 3'$
Surface Quality (Scratch-Dig)	40-20
Coating	Aluminum coating + Black Paint MgF ₂ Single-layer anti-reflection coating
Clear aperture	Circle inscribed in a square of 90% of the dimensions
Dimensions[mm]	A x B x C x (10x10x10.8)

3.4.2 Corner-cube prism and its working principle

Figure 3.6 shows a corner cube prism which is used as a retroreflector consisting of three mutually perpendicular, intersecting flat surfaces, which reflects waves back directly towards the source, but shifted (translated). The three intersecting surfaces often have square shapes. For this reason, metal made radar corner reflectors are used to reflect radio waves from radar sets.

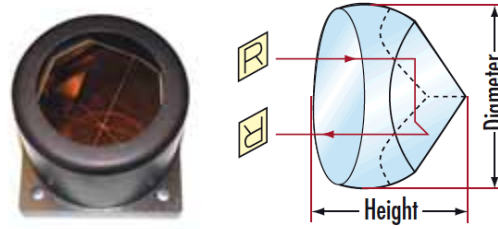


Fig. 3. 6 Corner cube prism and its working principle

Corner cubes, made of three-sided glass prisms are used in surveying and laser range finding purposes. The term is also used for a corner reflector antenna, consisting of two flat metal surfaces at a right angle, with a dipole antenna in front of them. In this research, we used this component for laser range finding purpose.

3.5 Laser system

Laser system mainly consists of two parts; laser interferometer and laser diode. Below the working method of laser system is described with figures.

3.5.1 Laser beam radiation and reflection

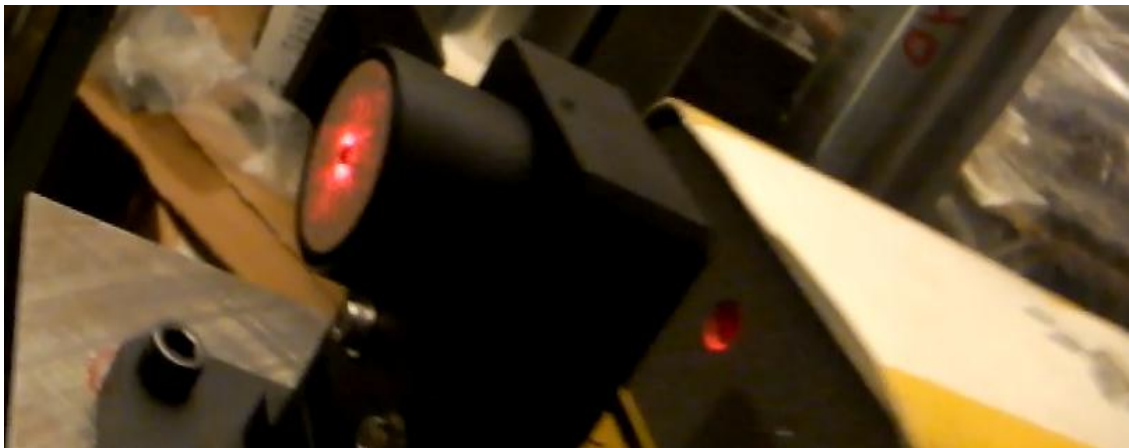


Fig. 3. 7 State of the working laser interferometer

Figure 3.7 shows the correct state of the laser interferometer during experiments. The laser beam must return to the interferometer through the same path after reflecting at

pentaprism via corner cube prism in order to acquire correct measurement data from the laser interferometer.

Figure 3.8 (a) shows the correct state of the laser interferometer during measurement while possible error state is shown in **Fig. 3.8 (b)**. Green spot is indicated as an error state in this experiment. Before proceeding with the experiment; the laser beam must be corrected to acquire correct measurement data.

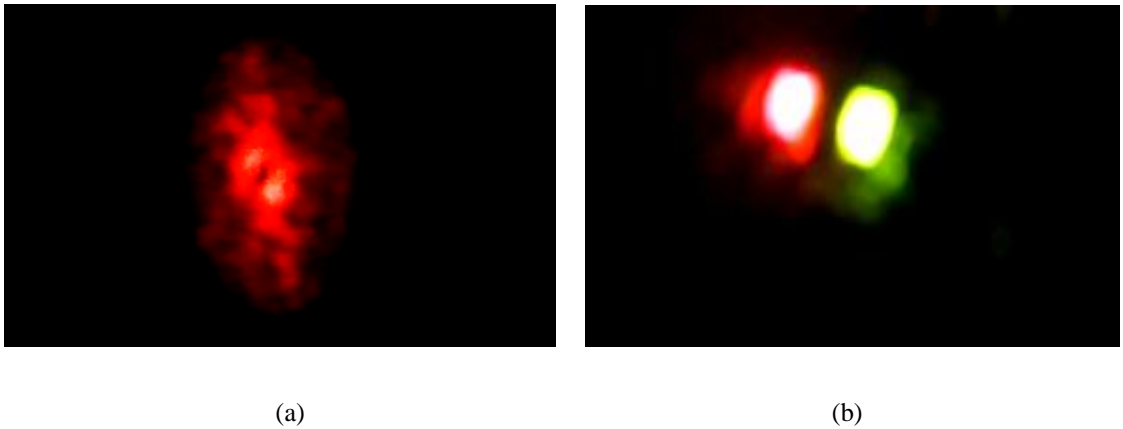


Fig. 3. 8 (a) A correct laser beam radiation; (b) an error occurred during laser beam radiation

3.5.2 Laser interferometer's output

Figure 3.9 (a) is an example of application of laser beam in manufacturing industries.



Fig. 3. 9 (a) An active laser interferometer during manufacturing process; (b) an example of correct laser beam radiation before measurement

The laser interferometer radiates laser beam to the target distance as shown in this figure. **Figure 3.9 (b)** shows an idle state of the laser interferometer where the laser beam is found to be stable. On the other hand, **Fig 3.10 (a)** shows the measurement value during experiment where ‘A’ denotes generated alarm during measurement and the dotted red bar denotes the stability of the data. During alarm generation in measurement; correct data is possible to acquire until the minimum 5 red dotted bars are visible and stable. The data will generate errors if the dotted bars go below 5 during experiment. **Figure 3.10 (b)** shows a resetting condition of the laser interferometer before the experiment started. Initial value denoting ‘-’ and ‘+’ do not affect the acquired results at all. **Table 3.2** shows the specifications for laser interferometer below. This interferometer needs to warm-up about 30 minutes in order to acquire correct experimental data.



Fig. 3. 10 (a) An example of active measurement while generates alarm in monitor; (b) Laser interferometer monitor after resetting the button

Table 3. 2 : Laser specification

Type	Lv-9110A
Measurement range	0-10m
Response speed	0- ±2.0 m/s
Laser materials	He-Ne
Wavelength	632.8nm
Light power	1mW
Warm-up time	30minutes
Display talent	0.01μm

3.5.3 Basic laser beam testing

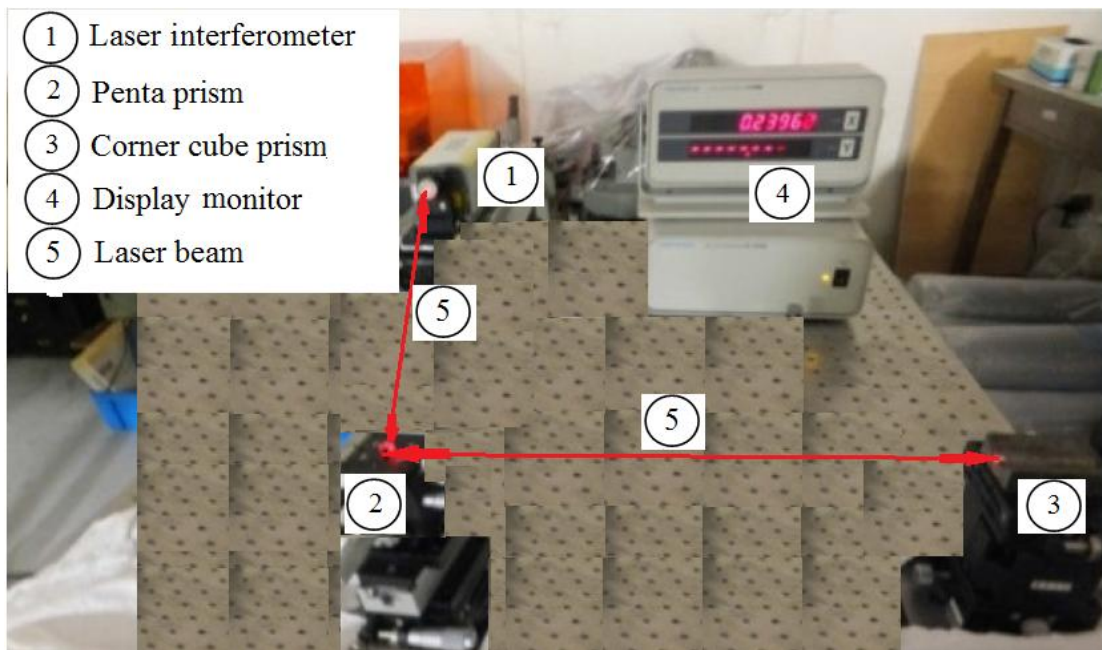


Fig. 3. 11 Laser and optical error checking

Figure 3.11 shows the optical components for laser beam experiment which was set up in order to justify the workability of the 2 mm laser diode, small pentaprism, small corner cube prism and laser interferometer display monitor. The names of the components are shown top-left corner of this figure. Laser beam radiates from the laser

interferometer and it reflects to the pentaprism. Finally; the reflected beam from pentaprism and deflected beam from corner cube prism returns to laser interferometer through pentaprism.

3.6 Front axis setting by PSD sensor

In **Fig. 3.12** a double-sided split-type two-dimensional PSD sensor is shown (manufactured by Hamamatsu Photonics, S1300). **Table 3.3** shows the specifications for this PSD sensor.



Fig. 3. 12 PSD sensor for front axis setting

Laser optical axis adjustment is shown in **Fig. 3.13**. First the PSD sensor is set inside the fixture (1) on the workpiece table. Then the fixture is placed to the workpiece in order to keep the axis on correct alignment. The PSD sensor cable is connected to the A/D converter; and A/D converter is connected to the computer. When the optical axis program starts, PSD sensor's coordinate data from the laser beam is displayed in the computer monitor. Position (2) is the rear fixture position of the PSD sensor. Both the x

and y coordinate values of front side and rear side have to be very close to each other in order to make sure that the laser spot is always on the center of the workpiece.

Table 3. 3 : Specifications of PSD sensor

Features	Applications
High position resolution	Optical position and angle sensing
Wide spectral response range	Remote optical control systems
High-speed response	Automatic range finder systems
Simultaneous measurements of position and intensity	Displacement and vibration monitors
Position is measured independent of light-spot size	Laser beam alignment
High reliability	Medical equipment

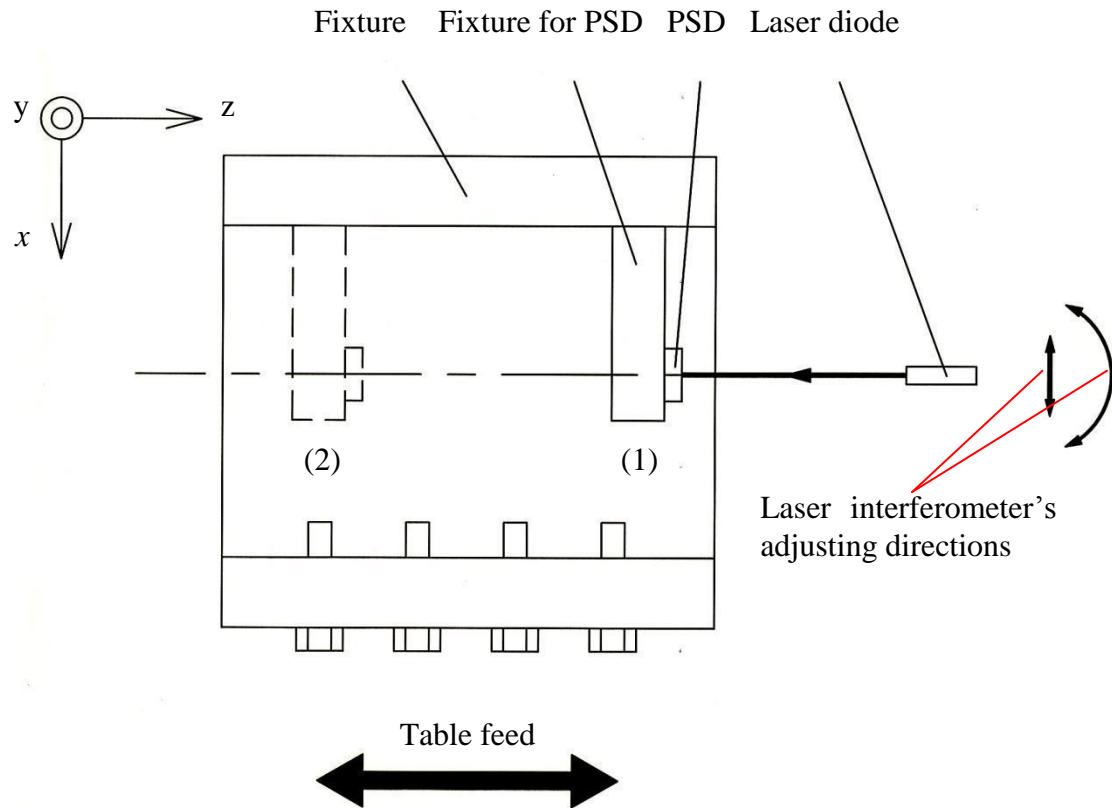


Fig. 3. 13 Adjustment of the position and slope of laser optical axis

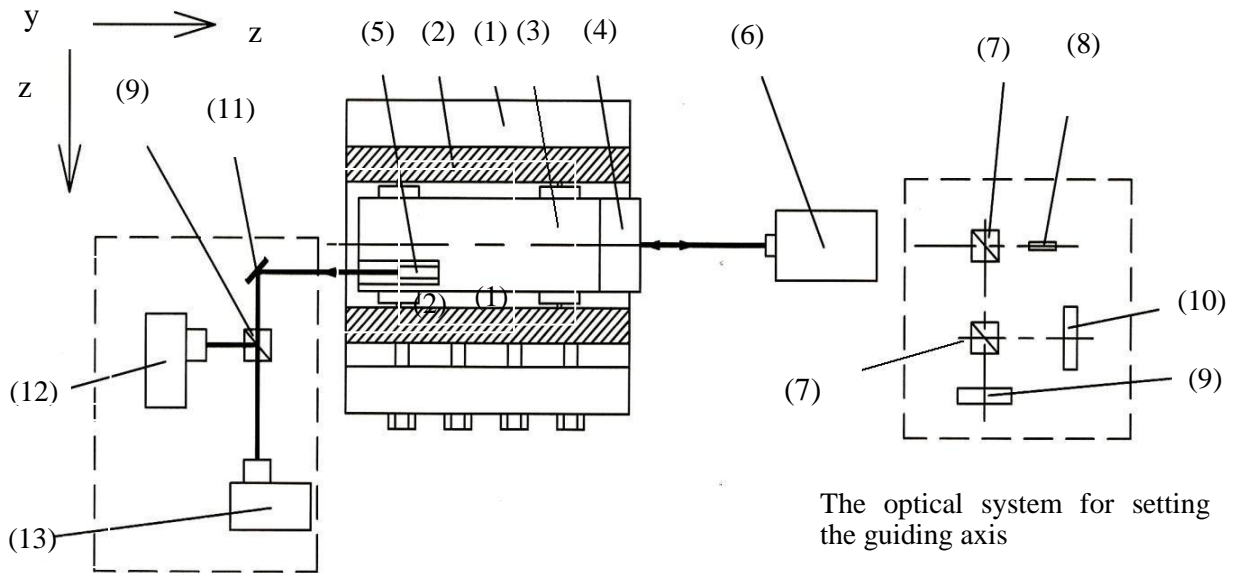
The setting is time consuming but once if it is set then there is no problem to continue the experiment until the laser axis or workpiece axis is changed from its initial setting.

3.7 Setting main axis

A semi conductor laser diode is positioned in front of the workpiece in order to set the main axis of the measurement table as well as workpiece. The laser beam is radiated from the laser diode and it reflects from the mirror and travel back to the beam splitter where PSD1 and PSD2 are initially set. PSD1 and PSD2 are connected to the A/D converter and the data of the mirror position is displayed on the computer monitor in terms of (x, y) coordinate values. The PSD data acquiring program must be run at the same time when the laser interferometer switched is on and mirror is placed in front of the workpiece on the measurement table. If the primary data is not acceptable then the laser diode must be moved and inclined to the correct position and angle. By this method; the front and the rear side of the workpiece is set to the correct axis initially. Repeating this process, we will get the desire values of the coordinate data; thus based on the (x, y) values it can be decided whether the measurement should start or not.

3.8 Complete system setting

- | | | |
|---------------------|--------------------------|-------------|
| (1) Fixture | (6) Laser interferometer | (11) Mirror |
| (2) Guide bush | (7) Beam splitter | (12) CCD 1 |
| (3) Measuring probe | (8) Laser diode | (13) CCD 2 |
| (4) Measuring head | (9) PSD 1 | |
| (5) Laser diode | (10) PSD 2 | |



The optical system for measuring probe attitude

The optical system for setting the guiding axis

Fig. 3. 14 Overview of the measurement system

General overview of the optical instrument setting with other main components is shown in **Fig. 3.14**. Experimental apparatus setting is shown in details in this figure indicating internal components.

3.9 Rear axis setting

Rear CCD camera positioning is shown in **Fig. 3.15**. In order to set the position of the CCD posture for the optical system; laser beam from the rear side of the workpiece is

radiated. Two mirrors are installed in the optical system to adjust the position of the CCD cameras in order to know the positions of the cameras from the radiated laser beam spot to determine the center.

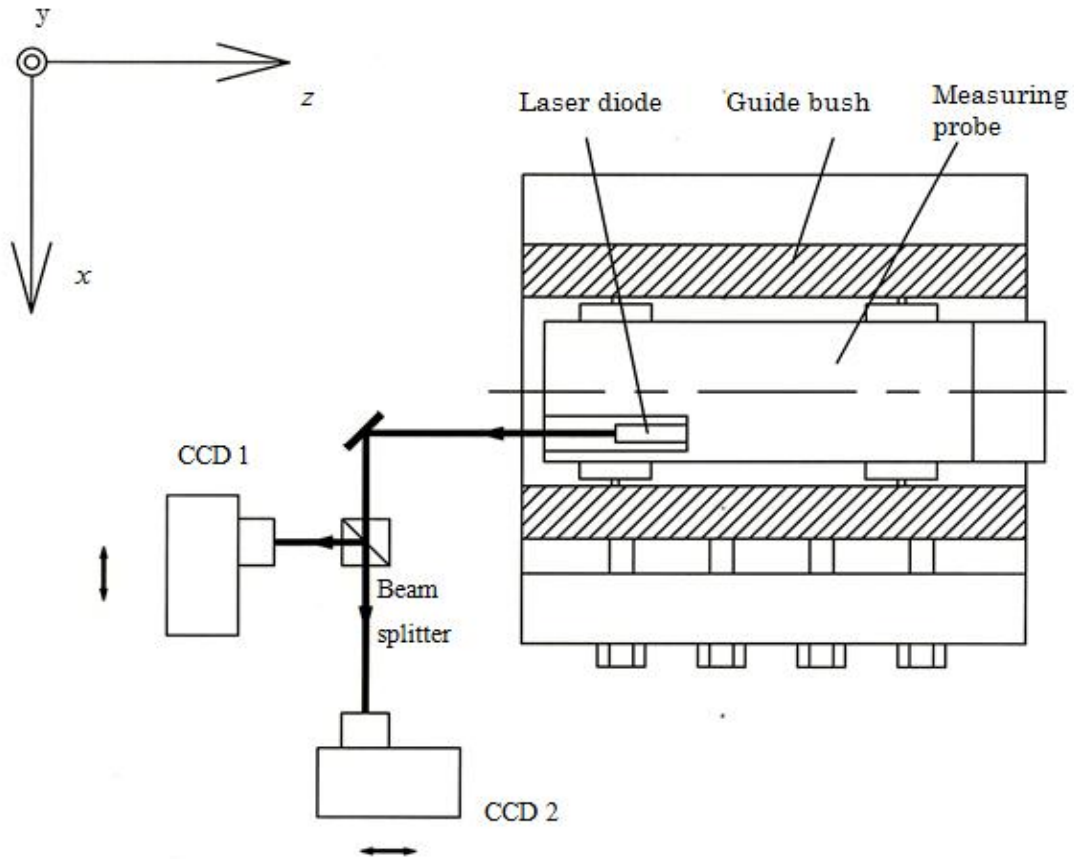


Fig. 3. 15 Positioning of the rear CCD camera

The positioning of the rear CCD cameras is shown in the figure above. First; it is necessary to run the attitude control program; then the displayed value is considered as the initial value of the CCD camera. If the center of the CCD camera deviates from its original axes then the camera is set by looking at the display spot of the laser beam in the computer monitor and compare with the values to confirm that the CCD cameras are on the right axes. The procedure should be repeated until the display spot and the shown numerical values are acceptable. The numerical acceptable values are in μm level. Performing attitude control of the measurement probe on the basis of the initial value is

required in order to keep the rear attitude on its center axis at all times during measurement.

3.10 Rear CCD camera



Fig. 3. 16 CCD camera (Lu 125)

Table 3. 4 : CCD camera specification (Lu 125)

Type	Lu125
Image sensor size	8.6 mm x 6.9 mm
Effective pixels	1280 x 1024
Pixel size	6.7 μm x 6.7 μm
Sensor size	1.3 megapixel
Frame rate	15 fps at 1280 x 1024, 60 fps at 640 x 480

Figure 3.16 shows the integrated CCD camera and its model name is Lu125. Camera specifications are shown in **Table 3.4**. The camera has resolution in μm level.

3.11 Rear CCD camera spot detection

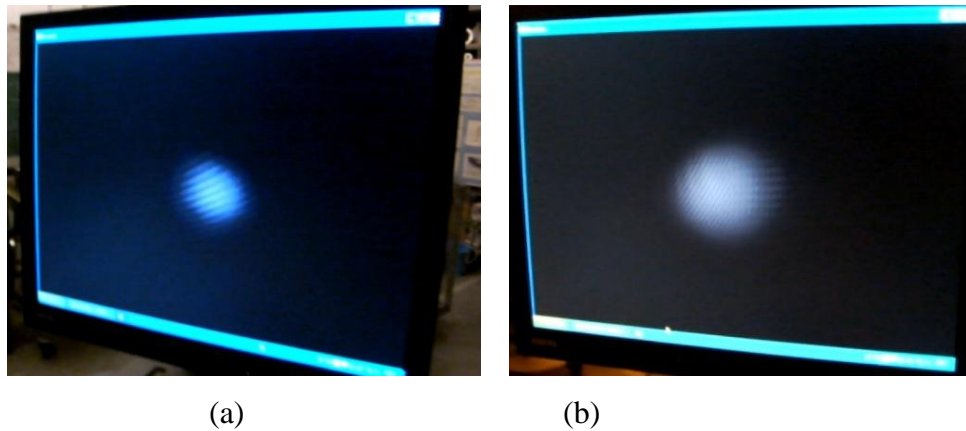


Fig. 3.17 Laser spots on computer monitor from (a) CCD1 and (b) CCD2 cameras

Figure 3.17 (a) and (b) show the spots of the laser beam from the rear laser diode to the CCD cameras.

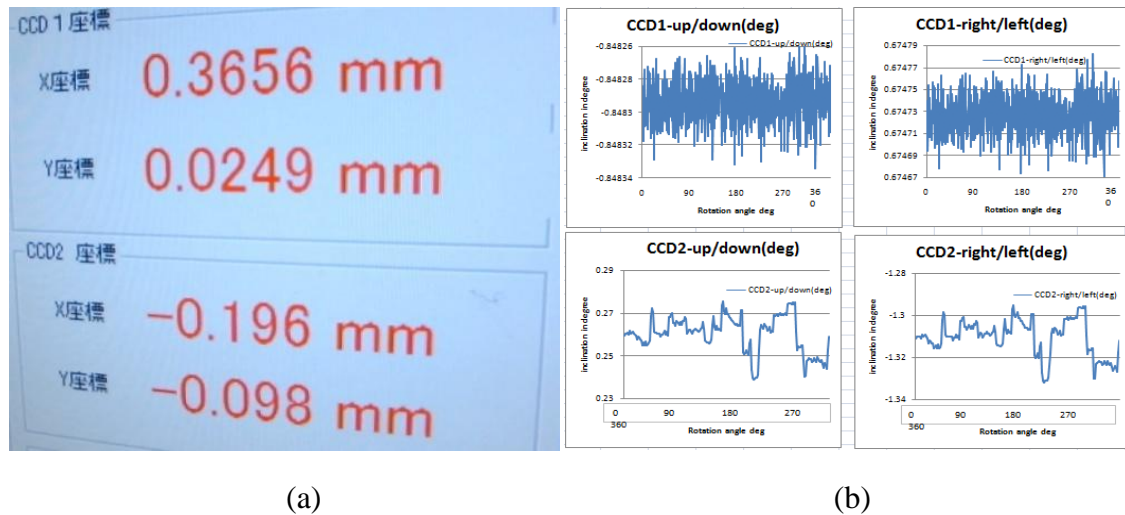


Fig. 3.18 (a) CCD camera shows the spot position in terms of 'X' and 'Y' axes; (b) rear measurement deviation result recorded by CCD cameras

These spots can be viewed on the computer monitor and it is necessary to adjust the spots on the camera and the checking must be carried out before the measurement starts. If the initial position deviates from the center; the center should be corrected first. **Figure 3.18 (a)** shows CCD camera initial position in the direction of 'X' and 'Y' axes. Final measurement data can be compared with the initial value which is shown on the monitor. **Figure 3.18 (b)** shows rear position of the long measurement bar during

experiment. The figures are drawn in terms of deviation and rotation angle of rear side of the measurement bar.

3.12 Summary

This chapter elaborates the experimental components and their applications in measuring small diameter based deep-holes. It gives an extensive explanation of the system components from very close view which clarifies and makes the system easy to understand and thus; easy to implement in industries.

CHAPTER 4

WORKING PRINCIPLES OF ROUNDNESS MEASUREMENT

4.1 Introduction

The principle of roundness measurement is based on the fact that the light intensity varies with respect to the displacement from the reflective object. The deviation between the actual radius at each point around its circumference and the measured radius is called out-of-roundness (OOR). The displacement between the probe and the rotating workpiece may change according to the OOR of the workpiece, the error of the rotational system, and the radial displacement of the workpiece. The variation of the displacement causes variation of the light intensities reflected from the rotating workpiece. The OOR of the rotating workpiece can be defined by analyzing the variation of the light intensities. The developed probe configured for diameter measurement can be easily reconfigured to measure the OOR of the rotating workpiece by blocking only one laser beam. All components in the probe configured for roundness measurement remain the same as those configured for radius measurement. In diameter measurement, two laser beams are produced. In roundness measurement, one laser beam is blocked before reaching the focusing lens. A blockage can be placed between the beam splitter and the focusing lens. The laser beam is directed to the workpiece surface. The receiving lens collects the scattered lights and focuses them to the photodiode. The intensities of the scattered lights are converted to an electrical signal by the photodiode. The electrical signal from the photodiode is sent to an amplifier circuit to eliminate unwanted noise and prepare the signal to match the input requirement of the Data Acquisition (DAQ) system. The signal from the amplifier circuit is sent to the computer with LabView environment and processed to extract the OOR of the rotating workpiece as in [28].

In another study [29], the combined method, which combines the generalized 2-point method with the inclination method, has been developed to measure profiles that include high-frequency components whose spatial wavelengths are shorter than the probe interval. It is suitable for measuring discontinuous profiles that include step-wise

variations and abrupt changes. In the above mentioned research, the influence of the setting error of the probe interval is discussed specially when it is used the combined method to measure a step-wise profile. Results of theoretical analyses show that these errors cause the same kind of evaluation errors in the profile measured with the combined method; and large profile evaluation errors are caused by the edge part of a step-wise profile. The value of the profile evaluation error is concerned with the aperture size of the displacement probe and the height of the step-wise profile. The influence of the gain errors of the probe is also investigated. An automatic selection method that can select the standard area properly and quickly is developed to improve the accuracy of the combined method. A machined surface with a stepwise profile is measured by using two capacitance-type displacement probes. Experimental results that confirm the effectiveness of the combined method are also presented [29].

In another article [30], the authors described a new differential method for on-machine roundness measurement of cylindrical workpieces, which is called the combined three-point method. This method combines the advantages of the generalized three-point method and the sequential three-point method and can accurately measure roundness profiles including step-wise variations. In the combined three point method, some data points in the roundness profile evaluated by the generalized three-point method are chosen as the reference points of the standard area and used to determine the relationships among the data groups of the sequential three-point method. An interpolation technique is employed in the data processing of the generalized three-point method to improve the accuracy of the standard area. Theoretical analyses and computer simulations confirming the feasibility of the combined three-point method are shown in this paper. A roundness measurement system using three capacitance-type displacement probe is constructed. The measurement system and the experimental results are also presented in [30].

Other researchers presented a novel algorithm for evaluating roundness from discrete coordinate data measured by a Coordinate Measuring Machine (CMM) [31]. The main feature of this algorithm is the concept and quantification of profile confidence

level, which is used to reduce the uncertainty associated with fitting the sampled data points in the determination of the roundness zone. This algorithm starts by characterizing the deterministic profile of a circular feature. After the deterministic profile is obtained, the normally distributed fitted residuals are available and regarded as random errors. With the established random errors, the roundness zone corresponding to a satisfactory profile confidence level can be determined. Extensive experimental data analysis has been carried out to validate the unique advantage of the present algorithm: if the circular deterministic profile is characterized correctly, the evaluated roundness values are consistent under different sample sizes and/or sampling locations. Also, these consistent roundness values are very close to the minimum-zone solution of a large sample size, which often provides a good approximation to the true roundness value. The applied algorithm for the above mentioned research is thus very useful and able to reliably evaluate roundness with a relatively small number of data points [31].

A real time monitoring and diagnosis system to measure spindle center displacement (roundness error) during turning operation is introduced in this research [32]. The system was developed based on the three-point method. The error generated during cutting process was monitored and diagnosed by using a system equipped with a designed DSP Digital Signal Processor (DSP) board and Fast Fourier Transform (FFT) algorithm. The system could estimate cutting force and predict other cutting characteristics such as chattering and tool wear. Using the spindle center fluctuation, i.e. a roundness error movement from the center, the relationship between the cutting force and the roundness error could also be investigated. The roundness error that eliminated geometric shape error and eccentric error from the measured signals in the frequency domain proved to be a dominating factor in determining cutting characteristics [32].

4.2 Working principle of laser interferometer

Figure 4.1 shows the flow chart of the front axis setting program. The front axis of the measurement probe setting is very important before the measurement is conducted. For

this axis setting; laser beam is radiated from the laser interferometer and reflects to the PSD sensor. The main notations that are used for the main program are q = quit; m = measurement; c = control attitude.

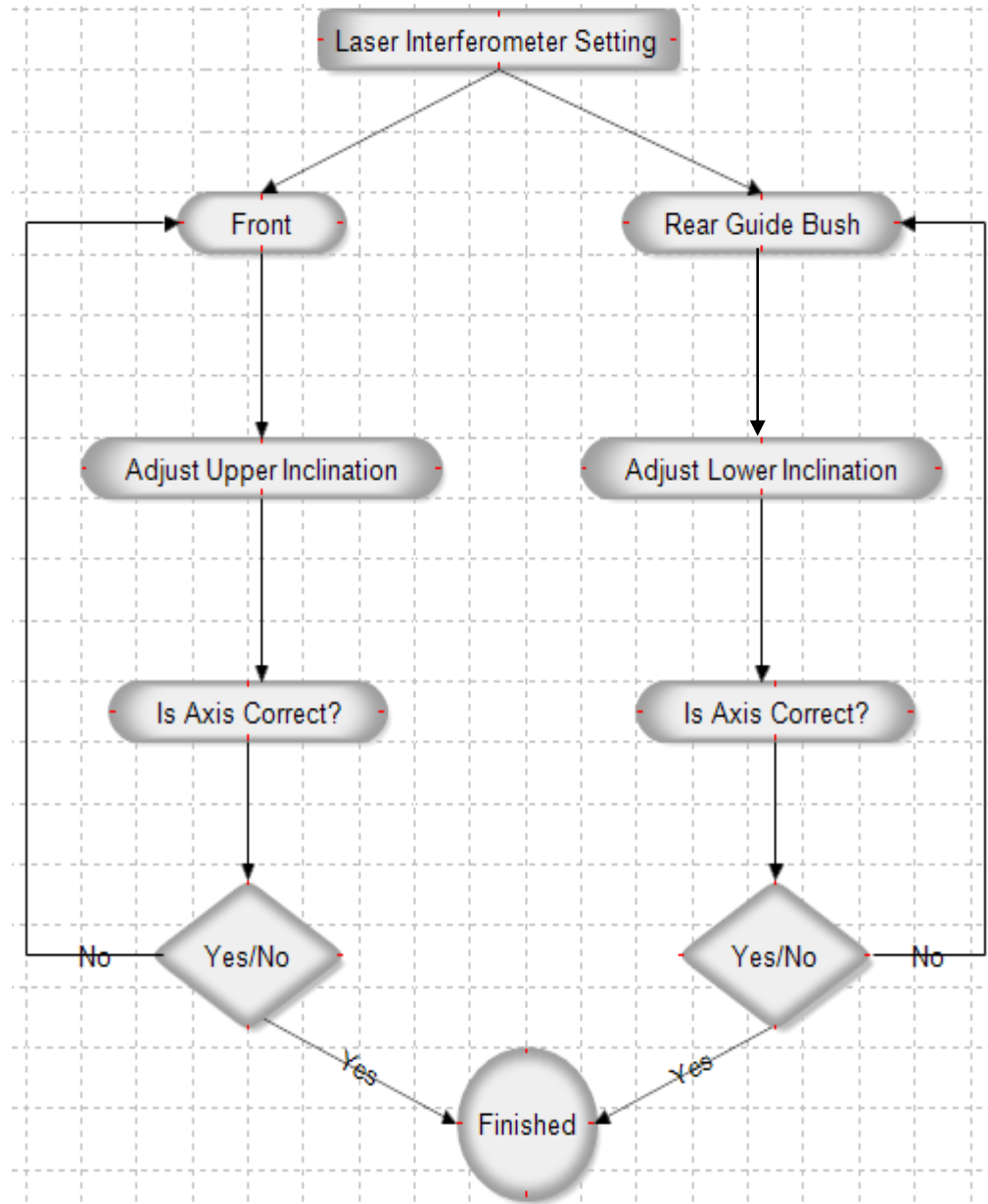


Fig. 4. 1 Axis setting for laser interferometer

4.2.1 Laser interferometer and its function

Figure 4.2 shows the complete set of laser interferometer for measurement. This consists of a laser beam radiator, a display monitor and data converter from analog to digital (A/D). The measurement data usually need to reset before starting to record the data. Before recording data; reset is necessary for the laser interferometer in order to start with the initial value.



Fig. 4. 2 A set of complete laser interferometer

4.2.2 Experimental procedure using laser interferometer

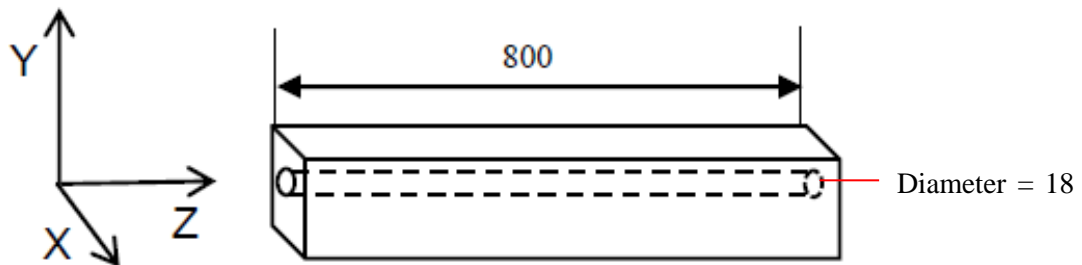


Fig. 4. 3 Shape of the workpiece

Figure 4.3 shows the workpiece model. Measurement starts at a longitudinal position where two skids are inserted to the entrance of the hole of workpiece. After that, measurement starts at the hole entrance. The range of hole diameter is between 17 to 21 mm. Probe center is set to the hole center by four skids which move radial direction by their screws. Experiments are carried out under the above conditions. The optical system consists of a laser interferometer placed in front of the measurement probe as well as measurement unit which comprises with the pentaprism and corner cube prism as in **Fig. 4.4**.

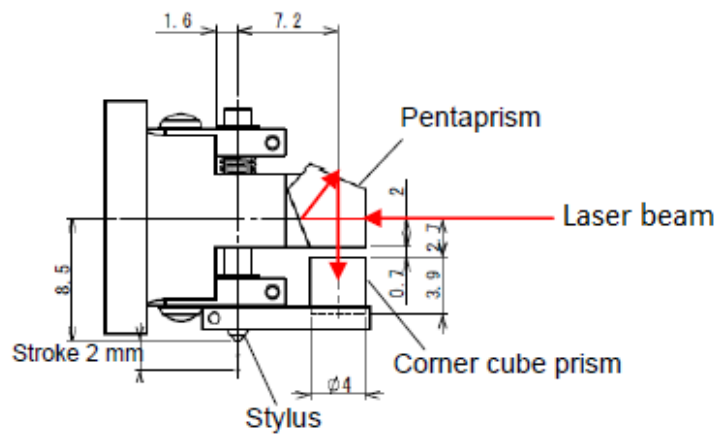


Fig. 4. 4 Measurement unit

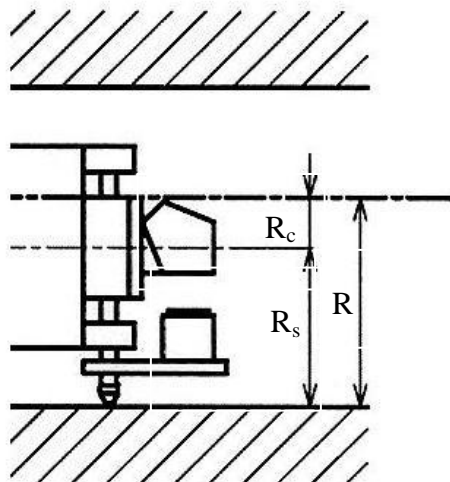


Fig. 4. 5 Calculation of radius of the hole

Main structure of the measurement unit is similar to a dial gauge. Its fabrication error is 0.01 mm. The corner cube prism is fixed to its holder and connected to the stylus. The stylus scans the hole wall of a workpiece which is set on a carriage toward the tangential direction. The laser beam from the interferometer is deflected by the pentaprism to the corner cube prism. The pentaprism deflects the input beam precisely by 90°. The corner cube prism returns the output beam to pentaprism. Then the returning beam reaches the interferometer along the same path In **Fig. 4.5**, it is shown how to determine the radius of the hole inside the workpiece. The radius of the hole, i.e. the distance to the inner wall of the hole measurement reference axis can be determined by adding the distance to the feeler tip from the measurement probe and the center displacement of the measurement probe center is as shown in **Eqn. (4.1)**.

$$R = R_c + R_s \quad (4.1)$$

Total distance to the stylus tip from the measurement probe center is equal to the sum of the displacement occurred to the feeler tip from the measurement probe center which is detected by the laser interferometer as well as the initial value of the distance to the stylus tip from the measurement probe center. The value is obtained by the following **Eqn. (4.2)**.

$$R_s = R_{s0} + \Delta R_s \quad (4.2)$$

4.3 Working principle of PSD sensor

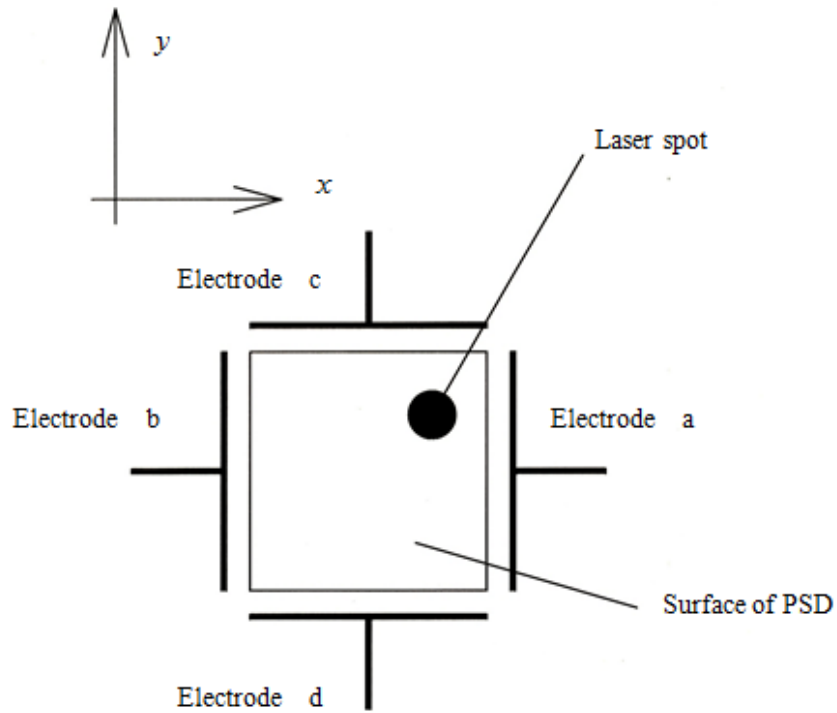
Working principle of the PSD sensor is shown in **Figs. 4.6 (a), (b) and (c)**. Light spot incidents on the PSD sensor surface of **Fig. 4.6 (a)** where corresponding voltage to the amount of light is generated in its place. Photo current flows through four electrodes named a, b, c, and d accordingly. The magnitude of the current flowing through each electrode becomes inversely proportional to the distance from the respective electrodes of the light spot. Therefore; by detecting the ratio of the current flowing through the

four electrodes, it is possible to determine the position of the optical spot on PSD sensor.

Theoretical formulas are given below based on the flowing currents I_a , I_b , I_c , I_d , through the electrodes a , b , c , and d respectively.

$$x \text{ coordinate : } \frac{I_a}{I_b} = \frac{L+x}{L-x} \qquad \therefore x = \frac{I_a - I_b}{I_a + I_b} \cdot L \quad (4.3)$$

$$y \text{ coordinate : } \frac{I_c}{I_d} = \frac{L+y}{L-y} \qquad \therefore y = \frac{I_c - I_d}{I_c + I_d} \cdot L \quad (4.4)$$



(a) Working principle of PSD sensor

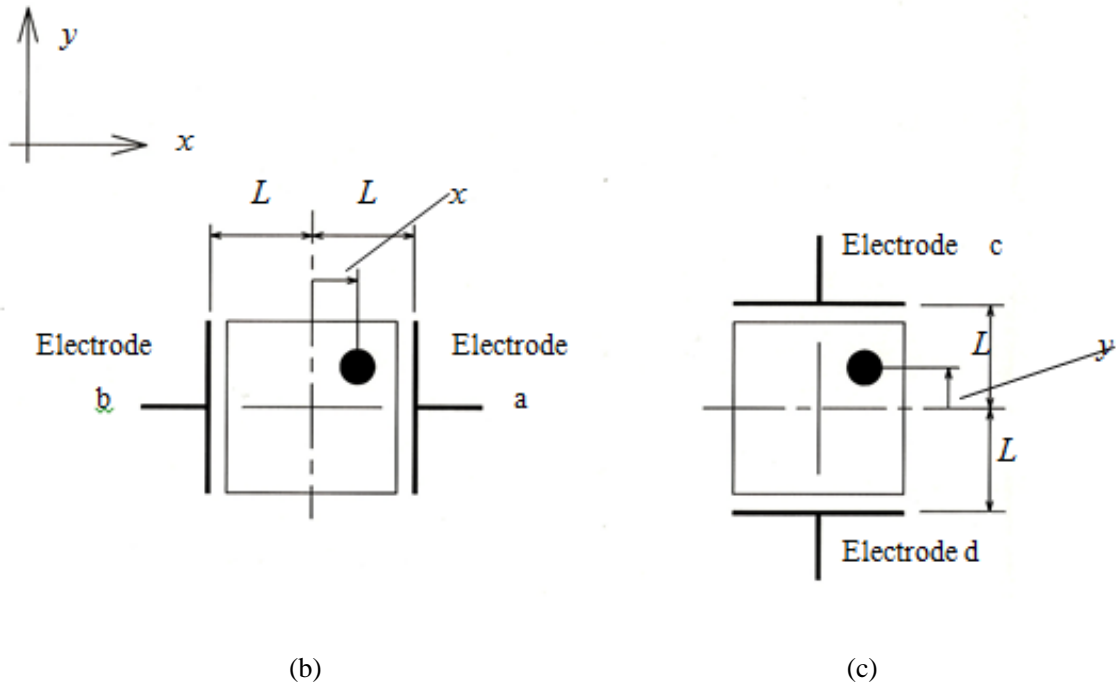


Fig. 4. 6 Measurement principle of the PSD: Determination of (b) x coordinate, Determination of (c) y coordinate

The procedure of setting the main axis position of the optical system is shown above. Setting the laser and optical axes are necessary before beginning the experiment. In order to align the position of the optical axis by the laser beam from the lead axis; the tilt is adjusted accordingly.

4.4 Working principle of rear CCD cameras

Figure 4.7 explains the method of acquiring rear CCD camera data. Rear optical system consists of a laser diode, mirrors, beam splitter and two CCD cameras. Laser diode radiates laser beam; the mirror reflects the beam and send to the beam splitter. Beam splitter splits the beam and sends them to CCD1 and CCD2 cameras. Finally; the beam spot position is examined on computer monitor. The rear side deviation is recorded in μm levels during experiment.

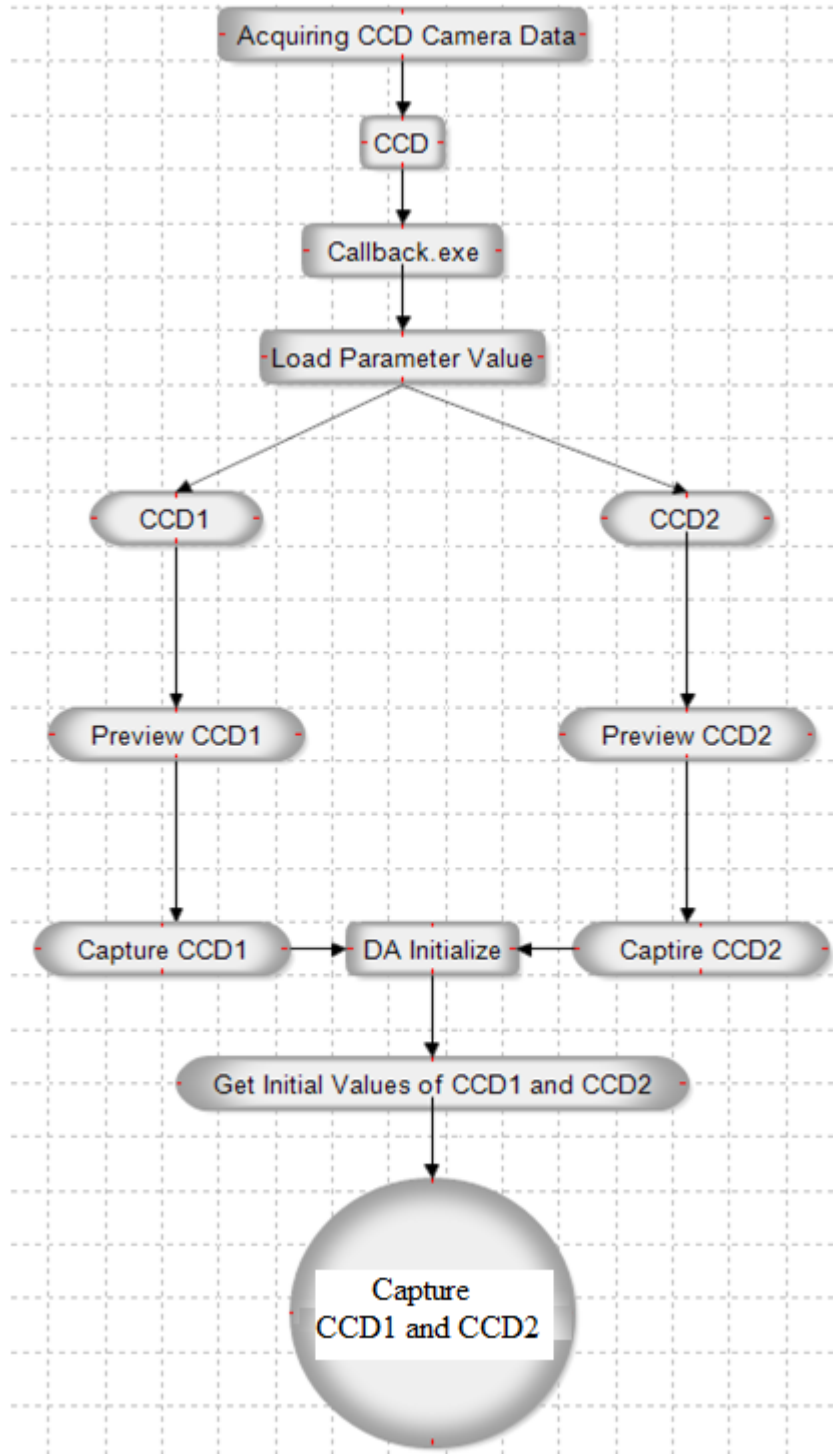


Fig. 4. 7 Flow chart for acquiring CCD camera data

The stylus movement which is placed perpendicular to the hole wall, is detected by the laser interferometer. The measurement length, response speed, and resolution of the laser interferometer are 0-10 m, 0 to ± 2.0 m/s, and $0.01 \mu\text{m}$, respectively. In **Fig 4.8**, $L = 2,814$ mm, $l = 1,192$ mm, and $c = 22.5$ mm.

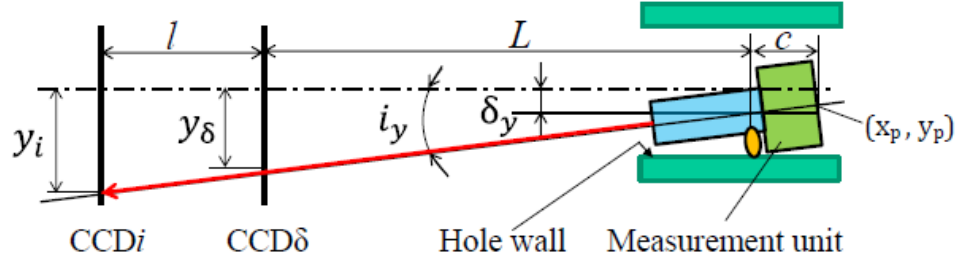


Fig. 4. 8 Measurement method for probe position and inclination

Fig. 4.8 shows the position of the probe which is set to detect the laser beam toward the optical system (CCDi) and backward from the rear end of the semiconductor laser probe (CCDδ). Calculation of displacement and tilt of the probe is accomplished by placing two CCD cameras. Geometric relationship of the camera angle (θ), position (R_c) and tilt displacement of the probe are shown in the following **Eqns. (4.5), (4.6) and (4.7)**.

$$\tan \theta = \frac{R_{c2} - R_{c1}}{l} \quad (4.5)$$

$$R_c = R_{c1} - L \cdot \tan \theta \quad (4.6)$$

$$\theta = \tan^{-1} \left(\frac{R_{c2} - R_{c1}}{l} \right) \quad (4.7)$$

Where, R_{c1} = Coordinates of CCD1, R_{c2} = Coordinates of CCD2, θ = Slope of the center axis of the measurement probe, R_c = Center displacement of the probe. This relationship has been established also with respect to the axial direction 'X'. In **Fig. 4.5**,

the movement of the corner cube prism is reconsidered as a movement of the stylus. In this case, measurement unit detects short distance R_c because in the penta-prism optical path difference is constant. From the equations above; all the CCD camera parameters are calculated. L , l , and R_c are measured in the laboratory using long measurement scale. Finally; all the measurement data from the CCD cameras are recorded and saved in the computer hard disk. If major deviation is detected by the system, feed-back control will eliminate this problem.

4.4.1 Rear optical device

Figure 4.9 (a) shows the setting condition of the rear laser diode in order to check the probe's rear position through the data of CCD cameras. **Figures 4.9 (b)** and **(c)** show the laser beam on mirror 1 and mirror 2. These laser beams go to CCD cameras through the reflection of the mirrors.

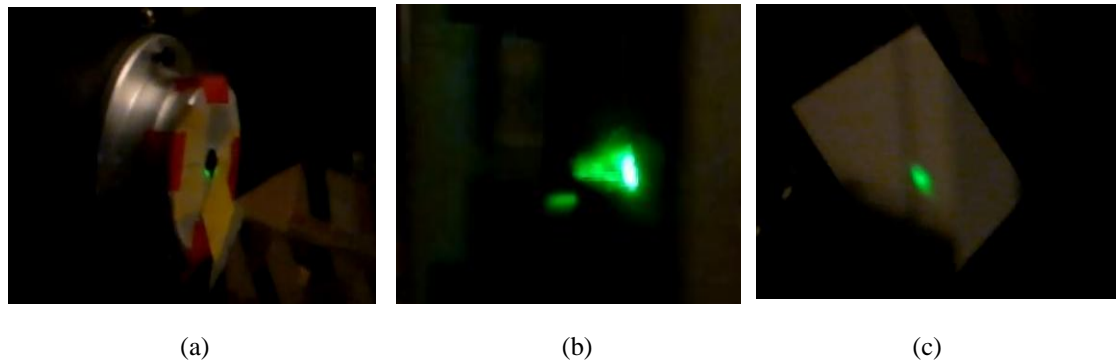


Fig. 4. 9 (a) Rear laser beam setting, (b) mirror 1 and (c) mirror 2 of the rear optical system

4.4.2 Rear probe's coordinate calculation based on CCD spot

When CCD camera is tilted, due to error; the position of the spot from the actual position is deviated. In order to correct this, coordinate correction is performed for the measured CCD camera data. The detail is shown in the next section.

4.4.3 Measurement effects on the spot changes of CCD camera

Table 4. 1 : CCD1 camera's coordinate effects

Deviation of the laser spot from the center	Deviation from the center (mm)			
	X1	Y1	X2	Y2
1mm below	0.0702	0.9469	-0.012	0.011
1mm up	0.1320	-0.992	-0.015	0.014
1mm right	1.1184	0.1018	-0.016	0.011
1mm left	-0.972	0.0188	-0.015	0.007

From **Tables 4.1 and 4.2**, it can be seen that the data for CCD1 and CCD2 are given in terms of x1, y1 and x2, y2. The **Tables** show the initial value of the laser beam on the CCD camera and the deviation can be calculated easily by comparing this value with the recorded value during experiments. The **Tables** also show the coordinate effects of CCD cameras when the camera spots deviate from their origin.

Table 4. 2 : CCD2 camera's coordinate effects

Deviation of the laser spot from the center	Deviation from the center (mm)			
	X1	Y1	X2	Y2
1mm below	0.1598	0.0918	0.040	1.559
1mm up	0.0669	-0.0921	-0.022	-0.783
1mm right	0.0867	0.1018	0.987	0.073
1mm left	0.0751	0.093	-0.860	0.055

4.5 Working principle of rotation detector sensor



Fig. 4. 10 Rotation detector sensor

Figure 4.10 shows a rotation detector sensor which is integrated with the measurement probe. This new version of the JR TLS2-ROT DMSS Rotation Sensor [44] employs an optical infrared detection system that is designed to use with JR XG6, XG7, XG8 and XG11 DMSS radios. Rotation detector sensor is used to count the rotation and save the data accordingly. It generates a maximum and minimum value of 7.35 and 0 volts respectively.

4.5.1 Features of the rotation detecting sensor

Rotation detector sensor has the following properties:

- An infrared sensor is utilized which realizes minimal misdetection. Since rotation can be detected even at a distance from the sensor unit, setting is simple.
- The sensor unit is independent from signal processing unit, making it small in size to allow easy incorporation.
- The rotation detection display unit incorporates an LED so that operation confirmation is simple.

4.5.2 Specifications of rotation detecting sensor

Rotation detector sensor has the following specifications:

- Detection system: Light detecting system
- Detection range: 1,000-50,000 min⁻¹
- Rated voltage: 4.8 V
- Operating voltage: 4.0-8.5 V

4.6 Working principle of measurement unit

The detail of the deep-hole surface measurement steps are described below.

4.6.1 Detection of hole deviation

Hole deviation cannot be detected by the measurement unit due to the movement of the measurement unit along the hole deviation. Hence, the deviation is detected using CCD δ and CCD i as shown in **Fig. 4.8**. In this experiment, the coordinate of the laser spot of each CCD is stable at the micrometer level. **Figure 4.8** shows the locations of the probe, CCD δ and CCD i for detecting the probe position and its inclination. The probe position and its inclination are geometrically calculated at the longitudinal skid position from the relationship between the coordinates of laser spots on the two CCD cameras and the laser source.

4.6.2 Deviation of probe from hole center

Figure 4.11 shows the measurement of hole shapes. The shape is measured by scanning hole wall circumferentially at intervals of various depth. The locus of the probe center is detected by the rear CCD cameras as mentioned in **Fig. 4.8**. However the displacement of the probe from the hole center that influences on the detection accuracy is not detected. The displacement can be obtained as shown geometrically in **Fig. 4.12**. From the triangle $O_P O_H A$ shown in **Fig. 4.12**, the following formula can be obtained.

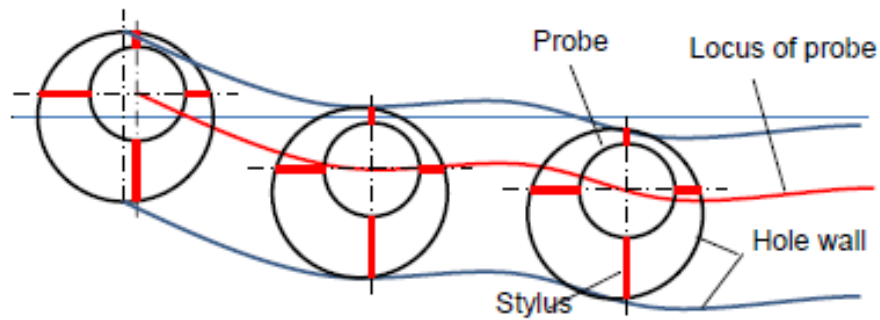


Fig. 4. 11 Hole shapes measurement

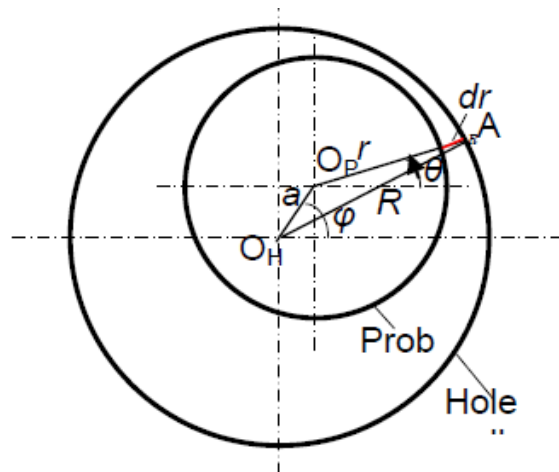


Fig. 4. 12 Deviation of probe from hole center

$$R^2 = a^2 + (r+dr)^2 - 2a(r+dr) \cos\left(\frac{\pi}{2} - \varphi + \frac{\pi}{2} + \theta\right) \quad (4.8)$$

$$r+dr = -a \cos\theta - \varphi + \sqrt{a^2 \cos^2(\theta - \varphi) - (a^2 - R^2)} \quad (4.9)$$

$$r+dr = -a \cos\theta - \varphi + R \sqrt{\left(1 - \frac{a^2}{R^2} \sin^2(\theta - \varphi)\right)} \quad (4.10)$$

$$\frac{a^2}{R^2} \sin^2(\theta - \varphi) \ll 1 \quad (4.11)$$

$$r+dr = R - a \cos(\theta - \varphi) \quad (4.12)$$

Where a and φ are the value and direction of the probe displacement. R and r are radius of hole and distance between probe center and hole wall. θ is rotation angle of stylus. Parameters a and φ can be obtained by compensating the values measured by the interferometer.

4.6.3 Effect of initial inclination on detection accuracy

In case of a cantilever with a supported end, an inclination of supported end is shown as:

$$i_0 = \frac{we^2}{48EI} \quad (4.13)$$

Where Young's modulus, $E=205$ GPa and the length between a fixed end of the beam and skids $e = 1,025$ mm. I is the geometrical moment of inertia. Weight per unit length w is 0.001244 kg/mm. Inside and outside diameters are $d_i = 11$ mm and $d_o = 16$ mm respectively. Calculated inclination angle i_0 is 5.448×10^{-4} . In **Fig.4.8**, a point (X_p, Y_p) where a center line of measurement head and that of a stylus cross can be arranged on measurement axis $(0, 0)$. When the inclination i_0 exists, hole wall is scanned ellipsoidally. In case of a hole with a diameter of 18 mm, scanning point deviates by maximum $18 \times i_0$

$= 18 \times 5.448 \times 10^{-4} = 9.8 \times 10^{-3}$ mm in Z-direction (Depth direction). Major axis of the oval is $18 / \cos(\tan^{-1}(i_0)) = 18.00000267$ mm, which is bigger by $0.00267 \mu\text{m}$ than the original hole diameter (18 mm). This value is very small. Therefore; the effect of scanning deviation due to inclination angle i_0 is negligible.

4.7 Measurement unit control

Integrated DC motor's specifications:

- Power supply = 6V (DC)
- Free-run = 45 min^{-1}
- Free-run current = 40 mA
- Stall current = 360 mA
- Stall torque = 1.8 kg-cm
- Weight = 98 mN
- Sample application = mini-size mobile robot, feather weight mechanism, etc.

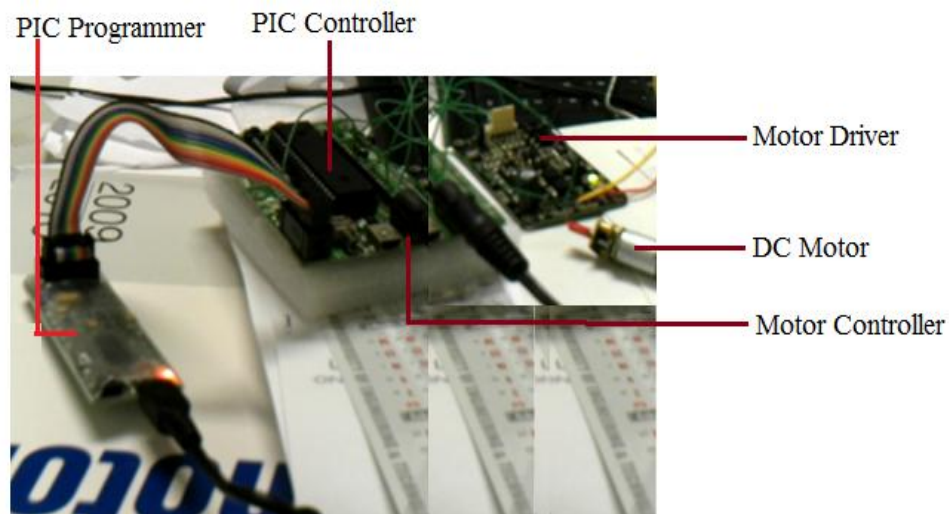


Fig. 4. 13 Motor and controller used for measurement head

Figure 4.13 shows the electrical connections with motor, controller and drivers through programmer. Figure 4.14 highlights program window of the applied microchip programmer.

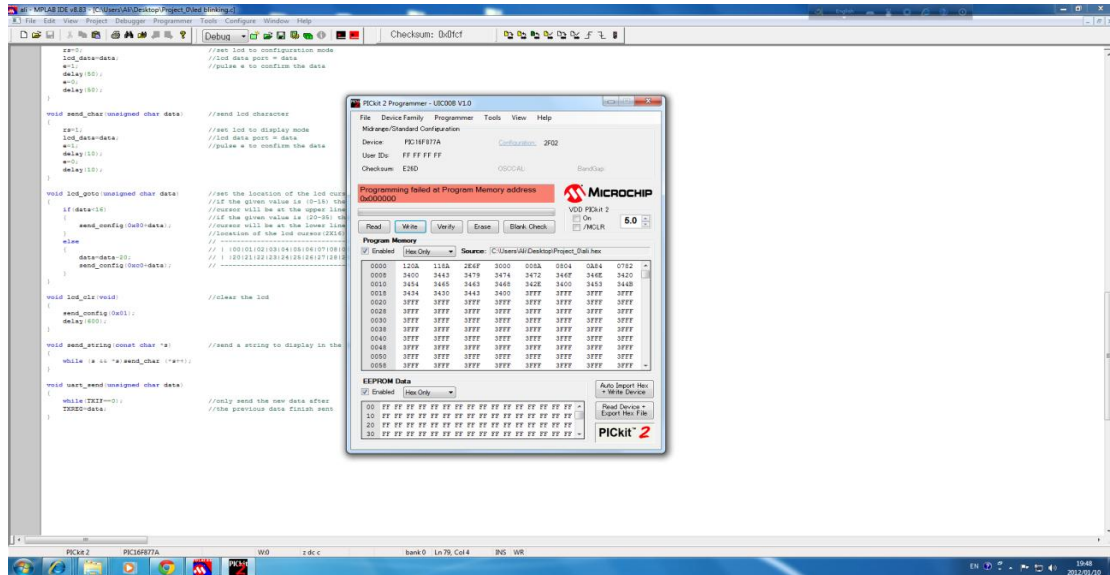


Fig. 4. 14 Measurement head controlling program using Microchip programmer

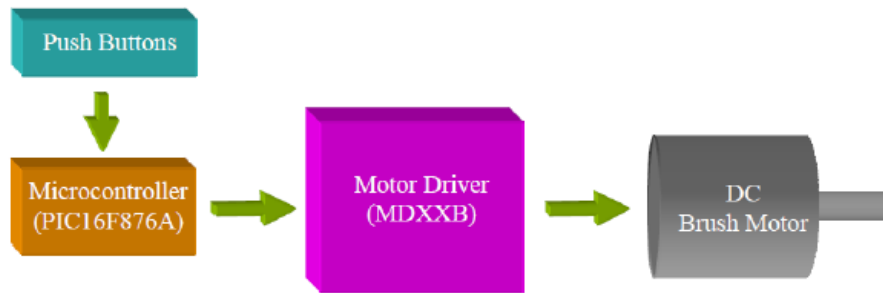


Fig. 4. 15 Controlling method of DC motor

The integrated motor driver name is MD10C. MD10C is an enhanced version of the MD10B which is designed to drive high current brushed DC motor up to 10A continuously. It offers several enhancements over the MD10B such as support for locked-anti phase and sign-magnitude PWM signal as well as using full solid state

components that result in faster response time and eliminate the wear and tear of the mechanical relay. **Figure 4.15** shows the method of controlling measurement head through the connected DC motor.

4.8 Working principle of integrated computer system

Past and present integrated measurement systems are discussed below.

4.8.1 Measurement probe

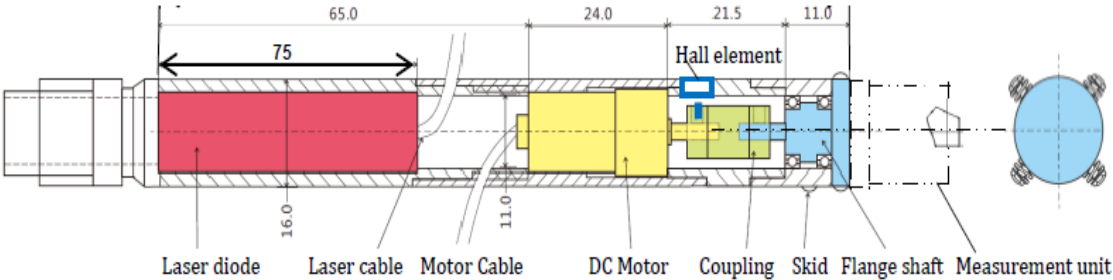


Fig. 4. 16 Measurement probe design

Figure 4.16 shows a sectional view of the probe. **Figure 4.17** shows a measurement probe that can measure a hole with a diameter range between 17 to 21 mm and a length range between 0 to 800 mm. The measurement unit rotates by a DC motor through a reduction gear, coupling, and flange shaft. Integrated DC motor model is DCSPG10. At the coupling, a magnet is molded to detect the rotation of the measurement unit. A collimated laser (Type MLXA, KIKOH GIKEN) is used as a laser diode to detect the probe’s rear attitude. In this experiment; the focus length of the laser diode is 4 m.

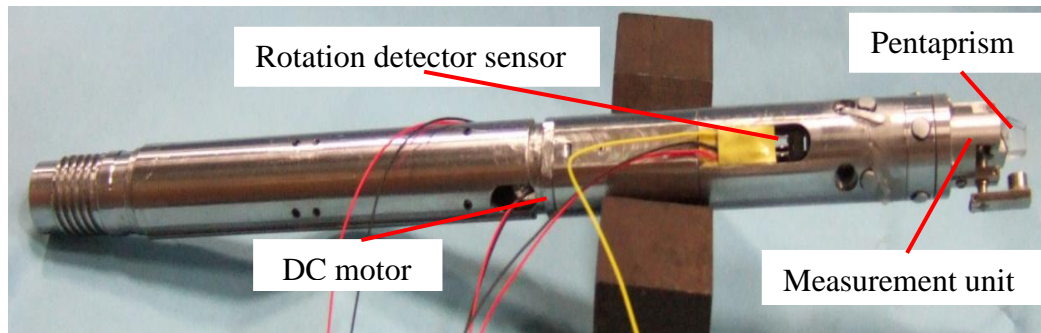


Fig. 4. 17 Manufactured measurement probe

4.8.1.1 Measurement system without actuator

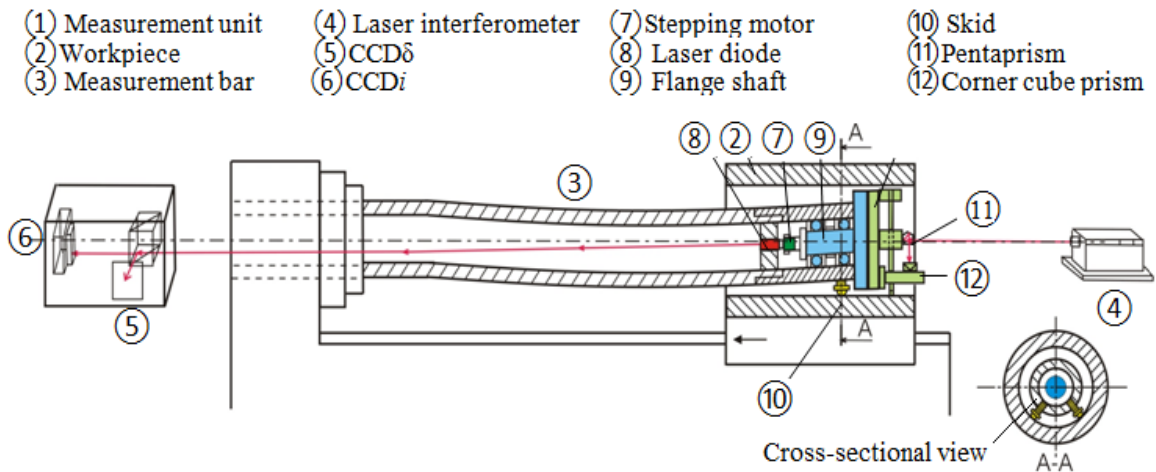


Fig. 4. 18 Laser-guided deep-hole measurement system without actuators

Figure 4.18 shows a deep-hole measurement system with long measurement bar which has no actuator attached to it. It indicates possible bending of the long measurement bar (3) during measurement.

4.8.1.2 Integrated measurement system with actuator

Figure 4.19 shows integrated measurement system for measuring roundness profile. The system consists of various important components and each component is dependent to

another one. The laser interferometer is set on a table and the table can be rotated or moved in 3 directions such as x, y and θ . Another very important apparatus is the measurement table where the workpiece is set to measure and behind the table the measurement long bar is attached to the measurement head or unit. This table is fed by the servo motor in order to measure various depth of the workpiece. Behind the table; there is a black box where the important camera system is integrated. Two CCD cameras are set inside the box in order to detect rear attitude of the measurement probe. The PSD sensor is also necessary in order to set laser interferometer's axis. All analog data is converted in terms of digital values. For this purpose, A/D and D/A converters are used with the system. A rotary encoder is set with the measurement table in order to count the travelling distance of the table. All controls are done through integrated CPU. As the overall system is automatic, human intervention is not required with this system during measurement. But, human monitoring is necessary for the complete system so that unexpected error or accident can be avoided during measurement. Finally; as we can see from the figure and above discussion that the system is automatic and it works as a closed- loop system or feed-back control system in general.

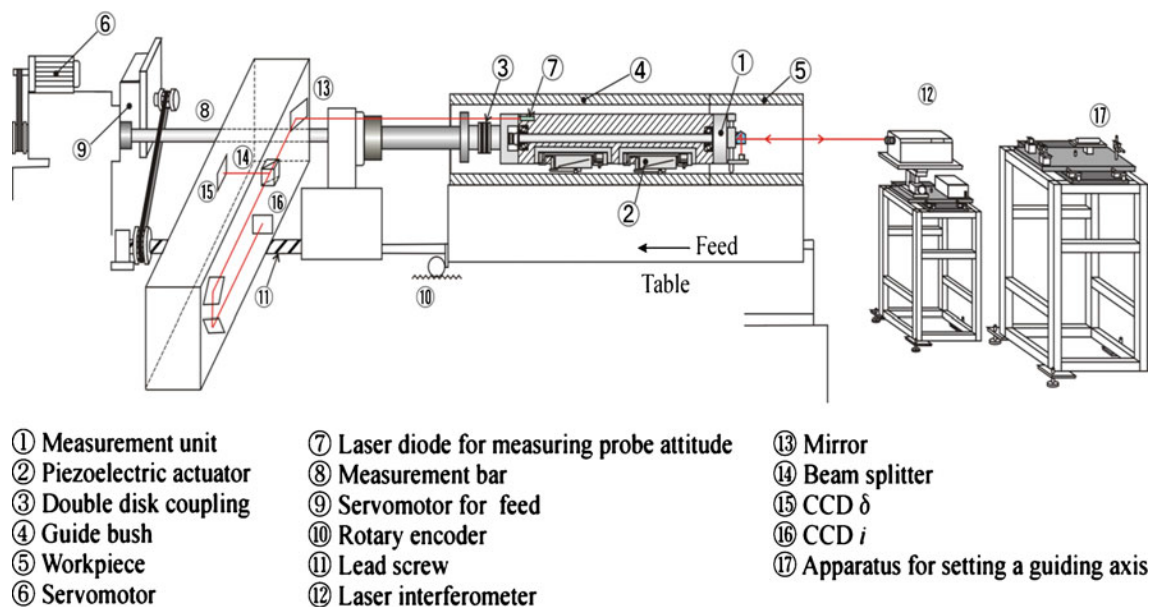


Fig. 4. 19 Integrated experimental set up

4.8.2 Editing program

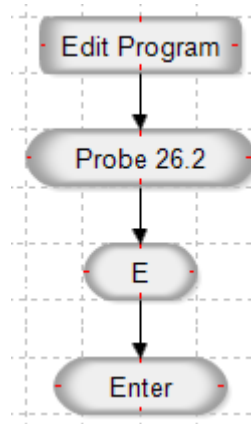


Fig. 4. 20 Flow chart for editing the program

4.8.3 Saving program after editing

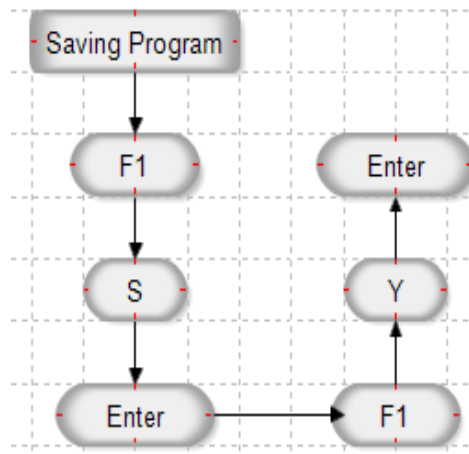


Fig. 4. 21 Flow chart for saving the program after editing

Figures 4.20 and 4.21 show the editing steps of the program and saving the edited program in the desired folder. To carry out the experiment successful; the steps should be followed accordingly.

4.8.4 Compiling program

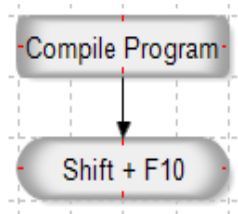


Fig. 4. 22 Flow chart for compiling the program

4.8.5 Table feed

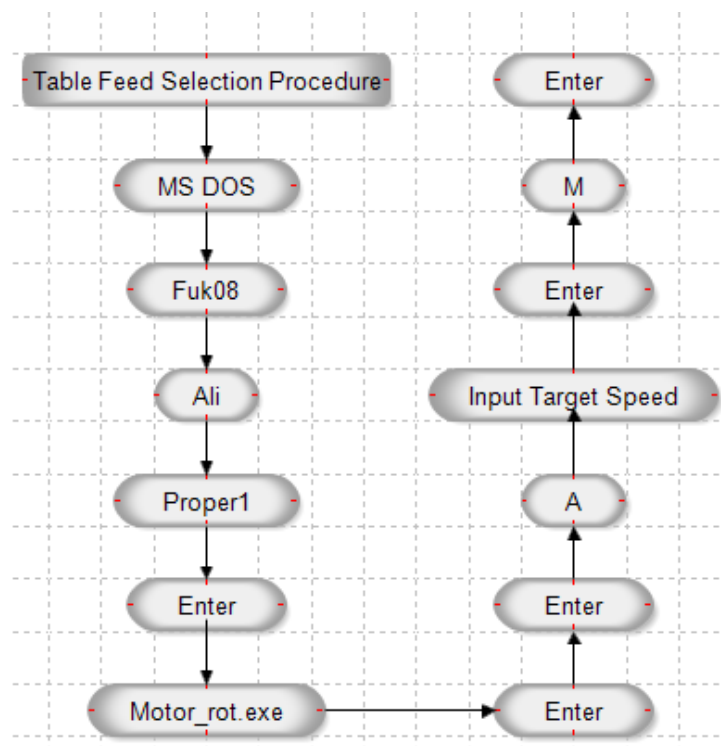


Fig. 4. 23 Flow chart for moving the table

Figures 4.22 and 4.23 show the flow charts of compiling the program as well as the table feed during deep-hole measurement. Some important parameters are: a = Speed change (Max speed = 320000, Min speed = 0), q = quit program, m = moving distance of the workpiece table in mm.

4.8.6 Roundness measurement

Figure 4.24 shows a roundness measurement program flowchart below.

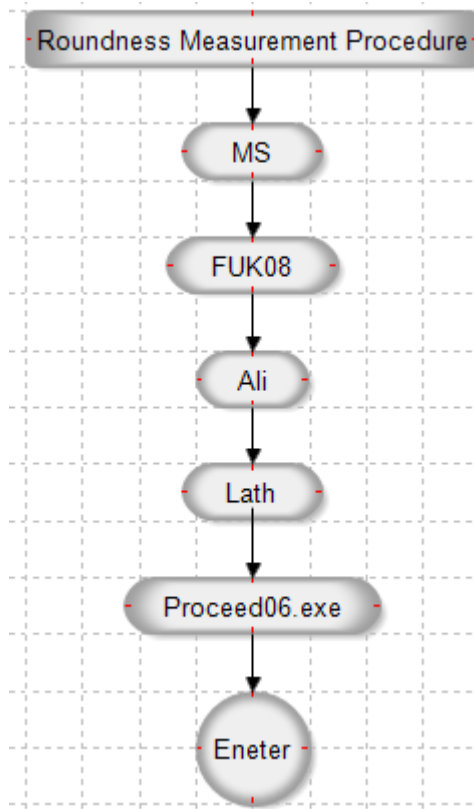


Fig. 4. 24 Flow chart for roundness measurement

4.9 Summary

This chapter discussed the principle of roundness measurement system for deep-holes that have small diameters. The working principles should be followed strictly in order to acquire proper experimental data with high accuracy.

CHAPTER 5

RESULTS AND DISCUSSION

5.1 Introduction

This chapter presents experimental results of the developed system. It analyzes results acquired under various experimental conditions. The results have been analyzed from three perspectives. Firstly, results of a roundness curve are drawn. Secondly, results of 3d spiral graph of the inner hole shapes are drawn. Finally, the rear position of the probe is shown from the acquired CCD camera data. In addition to these, the experimental conditions are mentioned in order to clarify the experimental overall situation.

5.2 Experimental results

Experimental results are discussed below in details.

5.2.1 Experiment # 1: Hole depth = 40 mm

Experimental conditions:

- All lights were switched off
- After 32mm laser was blinking and was unstable
- The table feed was 0.5 mm per minute
- Total travelling distance was 40 mm
- Total measurement time = 30 minutes

The experiment has been conducted under the above experimental conditions. **Figure 5.1** shows the roundness of a measured hole for a length of 40 mm and having a diameter of 17.6 mm. Axis is shown in $\pm X$ and $\pm Y$ directions. One division is equal to 4 micron. **Figure 5.2** shows 3D spiral graph for the complete measured hole up to a

length of 40 mm. In **Fig.5.1**, the drawn circle refers to 1 rotation data only while **Fig. 5.2** refers to the complete measurement data for all rotations of the total length.

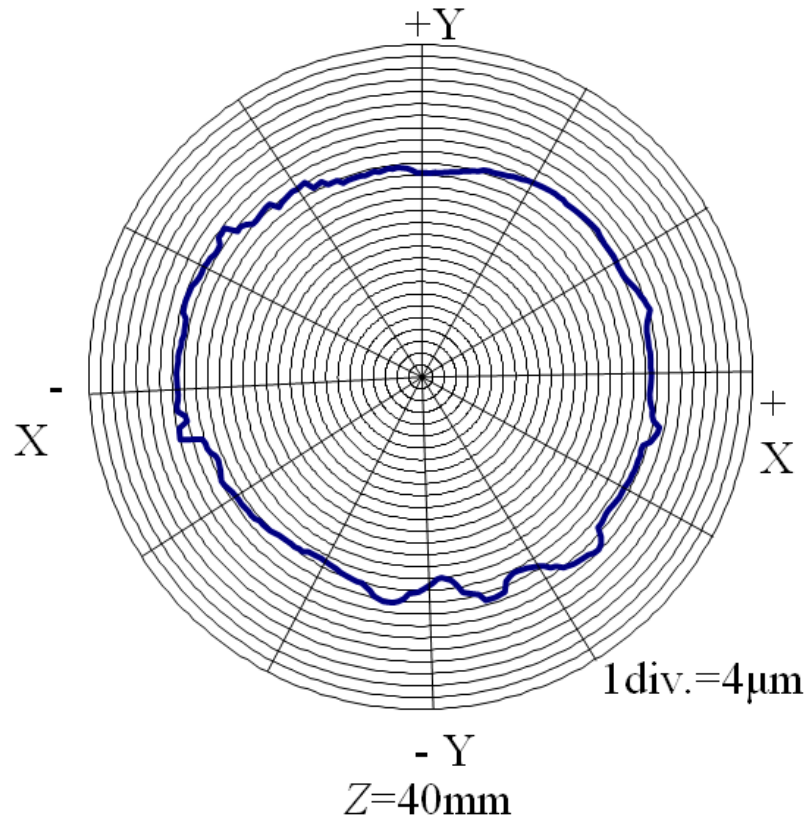


Fig. 5. 1 Measured roundness curve of the hole

Figure 5.3 refers to CCD1 and CCD2 camera acquired data that are recorded during experiment. x_1 and y_1 are the data from CCD1 and x_2 and y_2 are the acquired data from CCD2. Data from rear camera shows that the rear side of the probe was stable in all directions except that the deviation occurred in y_2 direction. The deviation occurred in y_2 direction is ± 0.15 mm. The deviation found after measuring almost half of the target distance. This deviation has very negligible effect over the measured roundness data which is acquired by the front optical system.

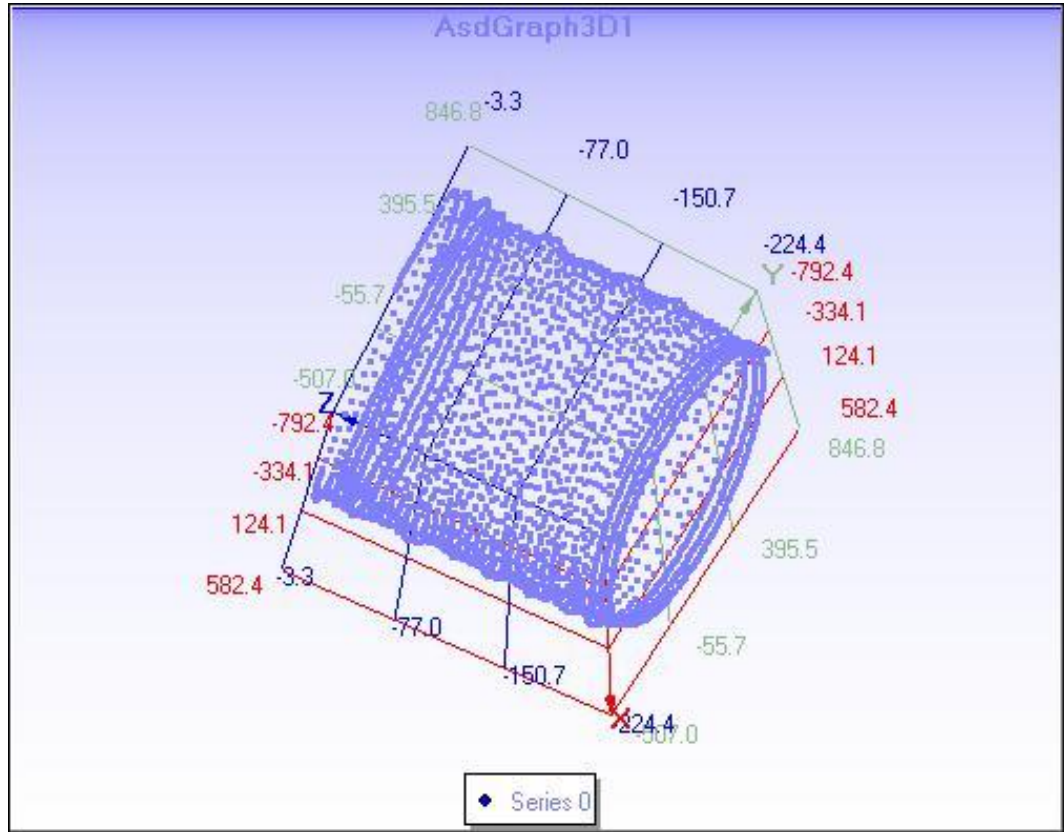


Fig. 5. 2 3d inner shape of the measured deep-hole

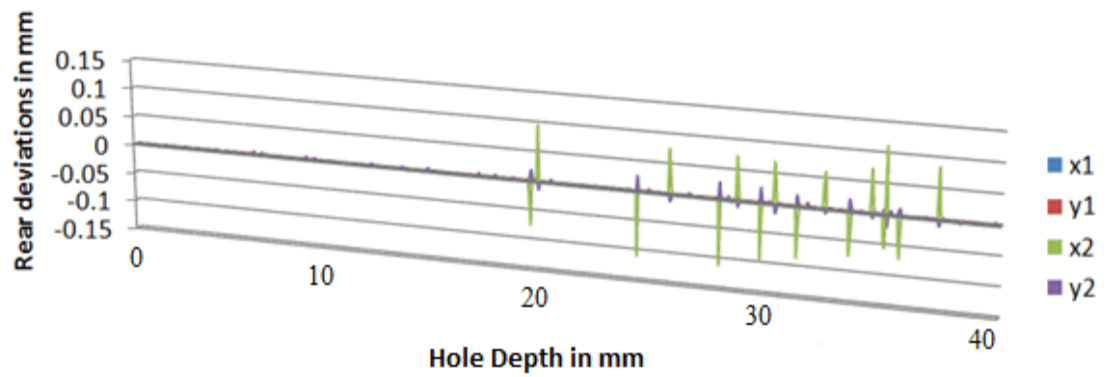


Fig. 5. 3 Rear view obtained from CCD camera

5.2.2 Experiment # 2: Hole depth = 50 mm

Experimental conditions:

- Hole depth = 50 mm
- Rotational speed of the measurement unit, $N = 6 \text{ min}^{-1}$
- Table feed, $f = 0.5 \text{ mm/rev}$
- Measurement time, $t = 33 \text{ min}$

In this experiment, it is examined whether measurement can be performed accurately. **Figures 5.4, 5.5 and 5.6** show the generated experimental result for the above conditions. In **Fig. 5.4**, a roundness error is found due to inappropriate data sampling.

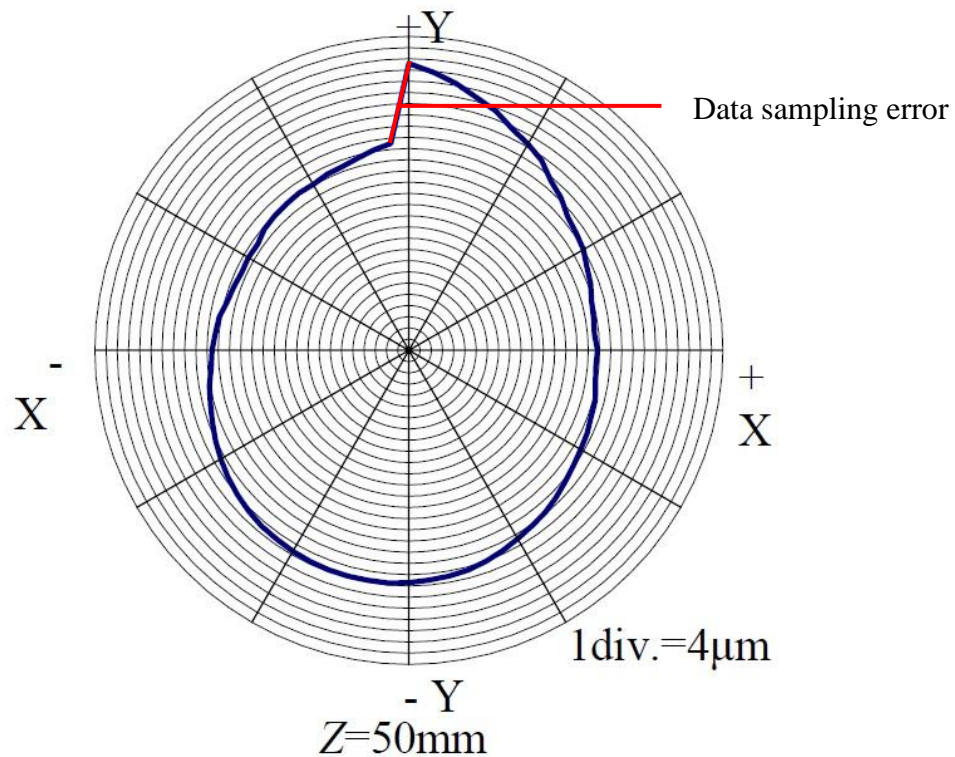


Fig. 5. 4 Measured roundness curve of the hole

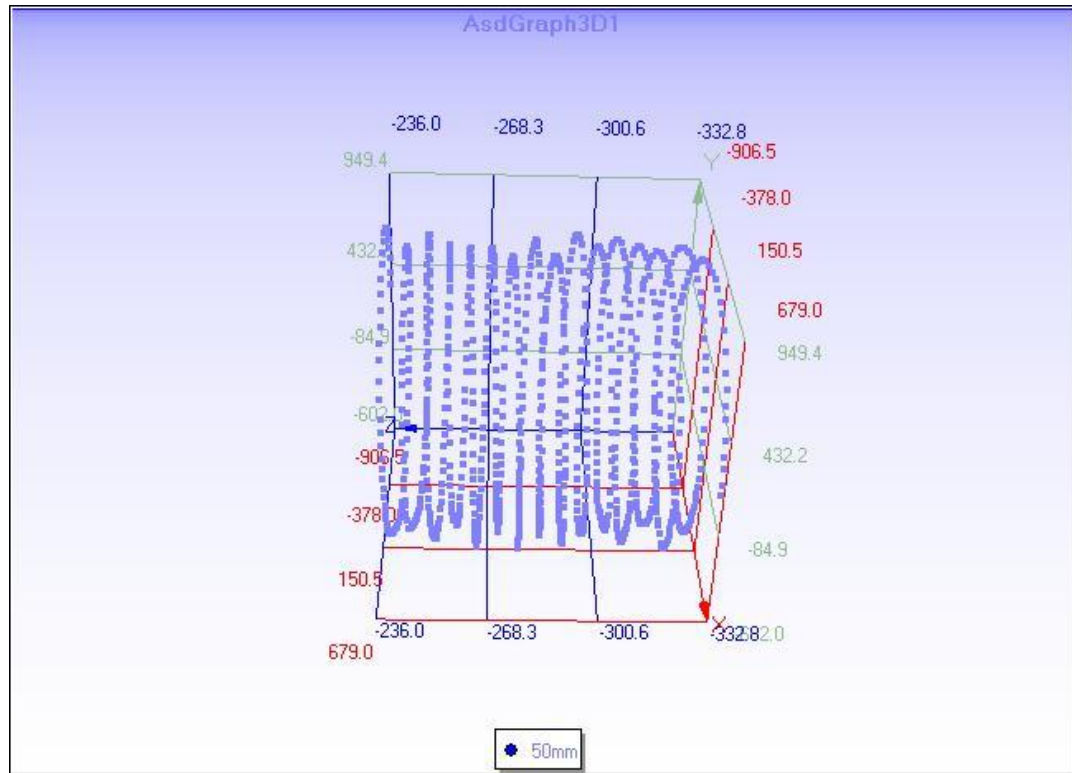


Fig. 5. 5 Measured 3d shape of the inner hole surface

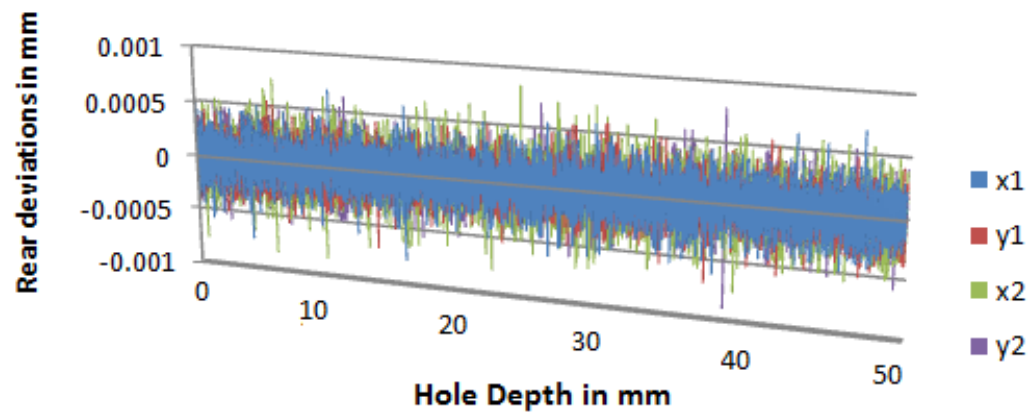


Fig. 5. 6 Rear CCD camera data for 50mm

5.2.3 Experiment # 3: Hole depth = 60 mm

(1) Trial # 1

Experimental conditions:

- All lights were switched off
- Total measured length = - 60 mm (negative sign indicates the direction of table movement)
- The table feed was 2 mm per minute
- Total travelling time = 11 minutes.

This experiment has been conducted under the above experimental conditions. **Figure 5.7** shows the roundness of a measured hole for a length of 60 mm and having a diameter of 17.6 mm. Axis is shown in $\pm X$ and $\pm Y$ directions. One division is equal to 4 micron. The figure shows that the axis is deviated from its original position due to the error occurred in acquiring measurement data. **Figure 5.8** shows 3D spiral graph for the complete measured hole up to a length of 60 mm. In **Fig. 5.7** the drawn circle refers to 1 rotation data only while **Fig. 5.8** refers to the complete measurement data for all rotations of the total length. From this 3d graph it can be seen that the inner hole shape has slight deviation from its original shape and it generates a wavy shape. **Figure 5.9** refers to CCD1 and CCD2 camera data recorded during experiment. x_1 and y_1 are the data from CCD1 and x_2 and y_2 are the acquired data from CCD2. Data from rear camera shows that the rear side of the probe was stable in x_1 and y_1 directions except minor deviations occurred in x_2 and y_2 directions throughout the experiment. The maximum deviation was ± 0.11 mm. This deviation has very insignificant effect to the roundness curve.

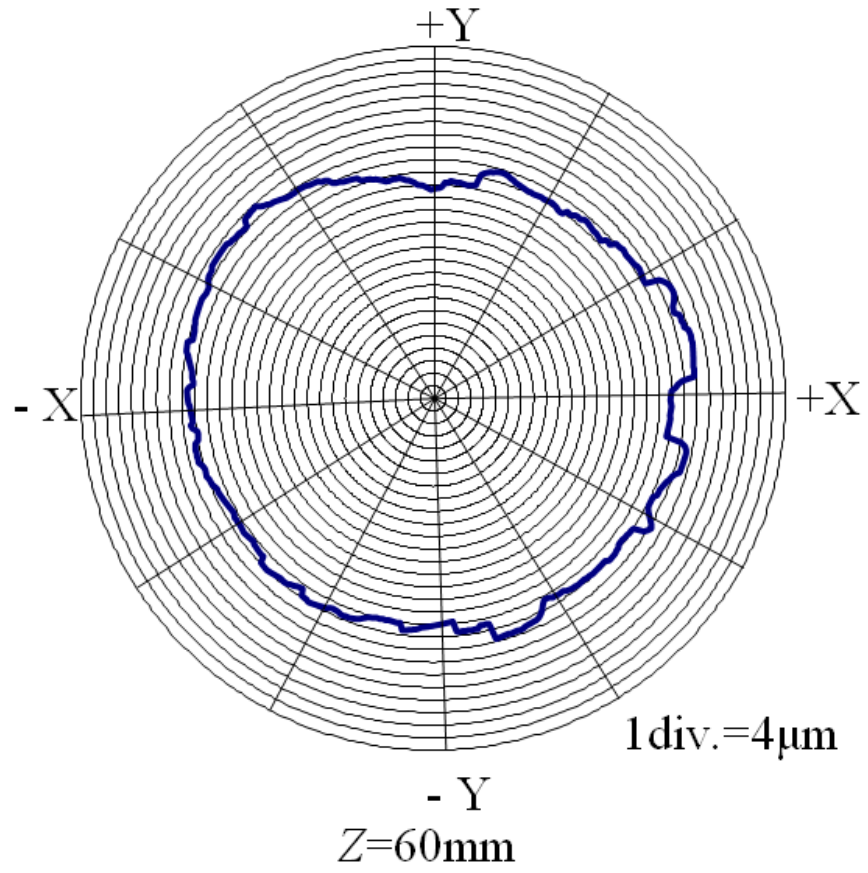


Fig. 5. 7 Measured roundness curve

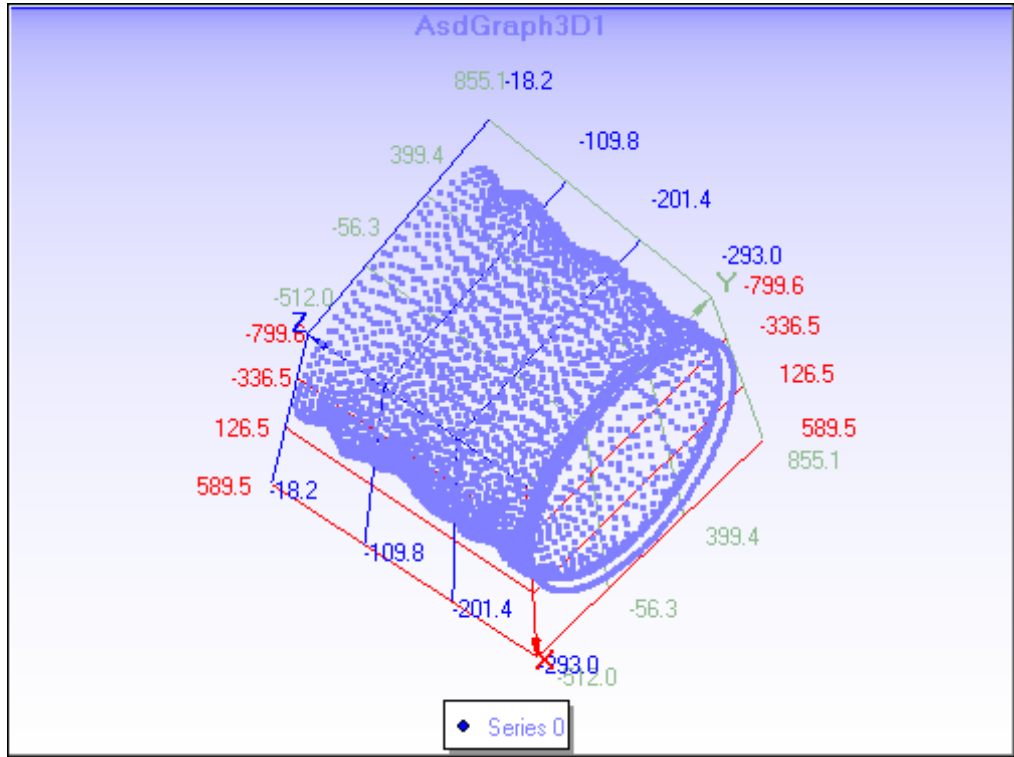


Fig. 5. 8 3d inner shape of the measured deep-hole

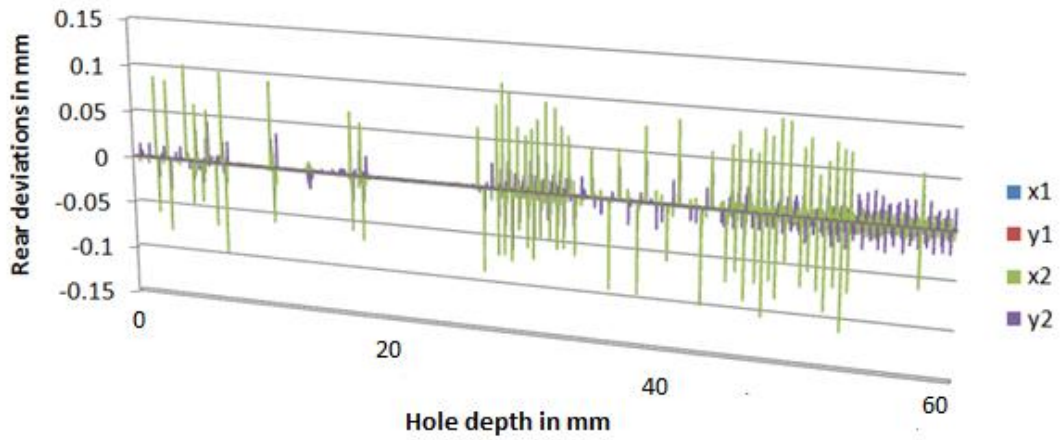


Fig. 5. 9 Rear view obtained from CCD camera

(2) Trial # 2

Experimental conditions:

- All lights were switched off
- Total travel distance = -60 mm
- The table feed was 3 mm per minute
- Total travelling time = 9 minutes
- Very good result was acquired without any laser blinking or disturbance

The experiment has been conducted under the above experimental conditions. **Figure 5.10** shows the roundness of a measured hole for a length of 60 mm and having a diameter of 17.6 mm. Axis is shown in $\pm X$ and $\pm Y$ directions. One division is equal to 4 micron. The figure shows that the axis has been deviated from its original position due to the error occurred in acquiring the measurement data. **Figure 5.11** shows 3D spiral graph for the complete measured hole up to a length of 60 mm. In **Fig. 5.10** the drawn circle refers to 1 rotation data only while **Fig.5.11** refers to the complete measurement data for all rotations of the total length. From this 3d graph it can be seen that the inner hole shape has slight deviation from its original shape and it generates visible wavy shape. **Figure 5.12** refers to CCD1 and CCD2 camera data recorded during experiment. x_1 and y_1 are the data from CCD1 and x_2 and y_2 are the acquired data from CCD2. Data from rear camera shows that the rear side of the probe was unstable in all directions. The deviation was ± 0.00081 mm. This deviation has no major effect to the roundness curve obtained by the front optical system.

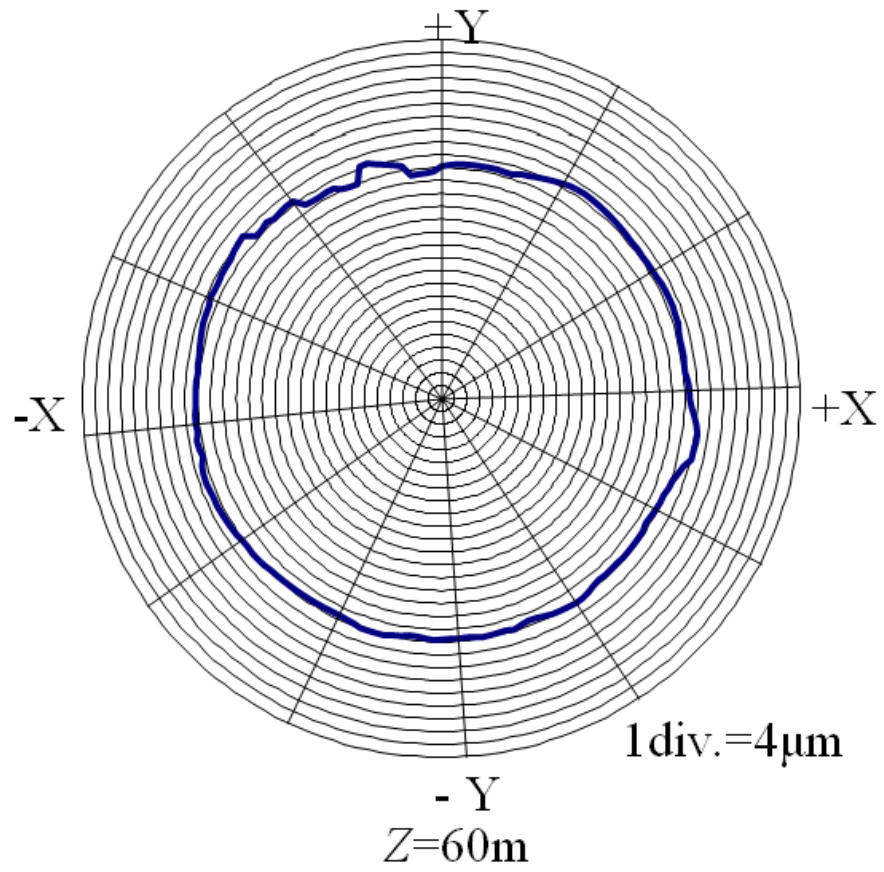


Fig. 5. 10 Measured roundness curve of the hole

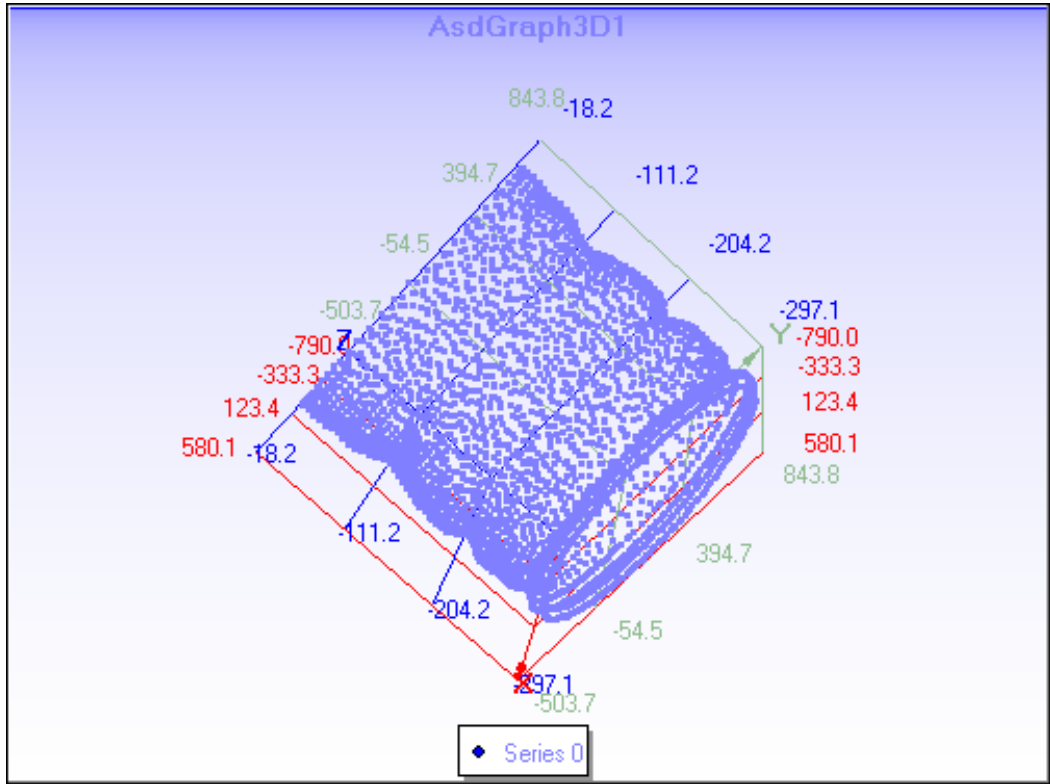


Fig. 5. 11 3d inner shape of the measured deep-hole

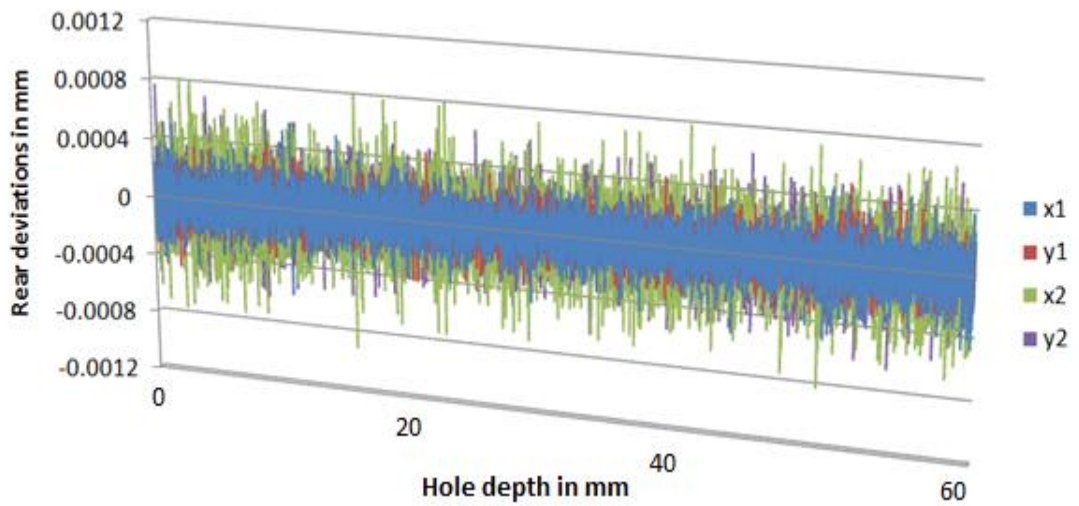


Fig. 5. 12 Rear view obtained from CCD camera

(3) Trial # 3

Experimental conditions:

- All lights were switched off
- Total travel distance was = - 60 mm
- The table feed was 4 mm per minute
- Total travelling time = 5.25 minutes
- Data recorded without laser blinking

The experiment has been conducted under the above experimental conditions. **Figure 5.13** shows the roundness of a measured hole for a length of 60 mm and having a diameter of 17.6 mm. Axis is shown in $\pm X$ and $\pm Y$ directions. One division is equal to 4 micron. From the drawn figure we know that the error can be easily calculated. **Figure 5.14** shows 3D spiral graph for the complete measured hole up to a length of 60 mm. In **Fig. 5.13** the drawn circle refers to 1 rotation data only while **Fig. 5.14** refers to the complete measurement data for all rotations of the total length. From this 3d graph it can be seen that the inner hole shape has slight deviation from its original shape and it generates visible wavy shape in the middle of the graph. **Figure 5.15** refers to CCD1 and CCD2 camera data recorded during experiment. x_1 and y_1 are the data from CCD1 and x_2 and y_2 are the acquired data from CCD2. Data from rear camera shows that the rear side of the probe deviated in x_2 and y_2 directions. The deviation was ± 0.053 mm in x_2 direction and ± 0.01 mm in y_2 direction. This deviation has very negligible effect to the roundness curve obtained by the front optical system.

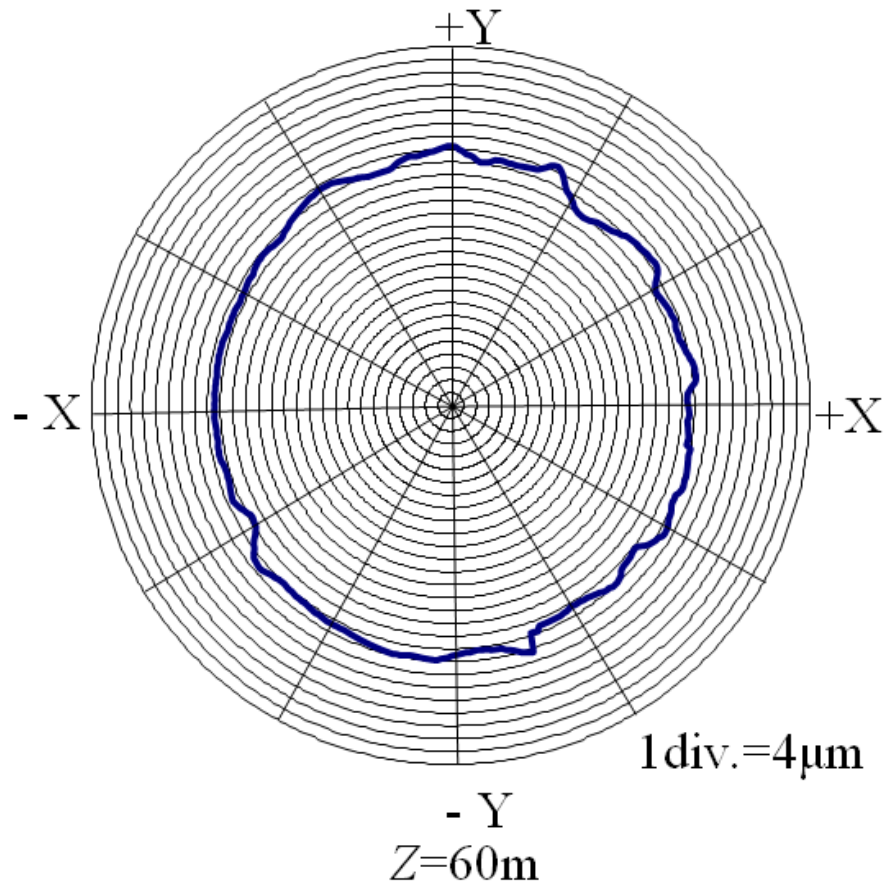


Fig. 5. 13 Measured roundness curve of the hole

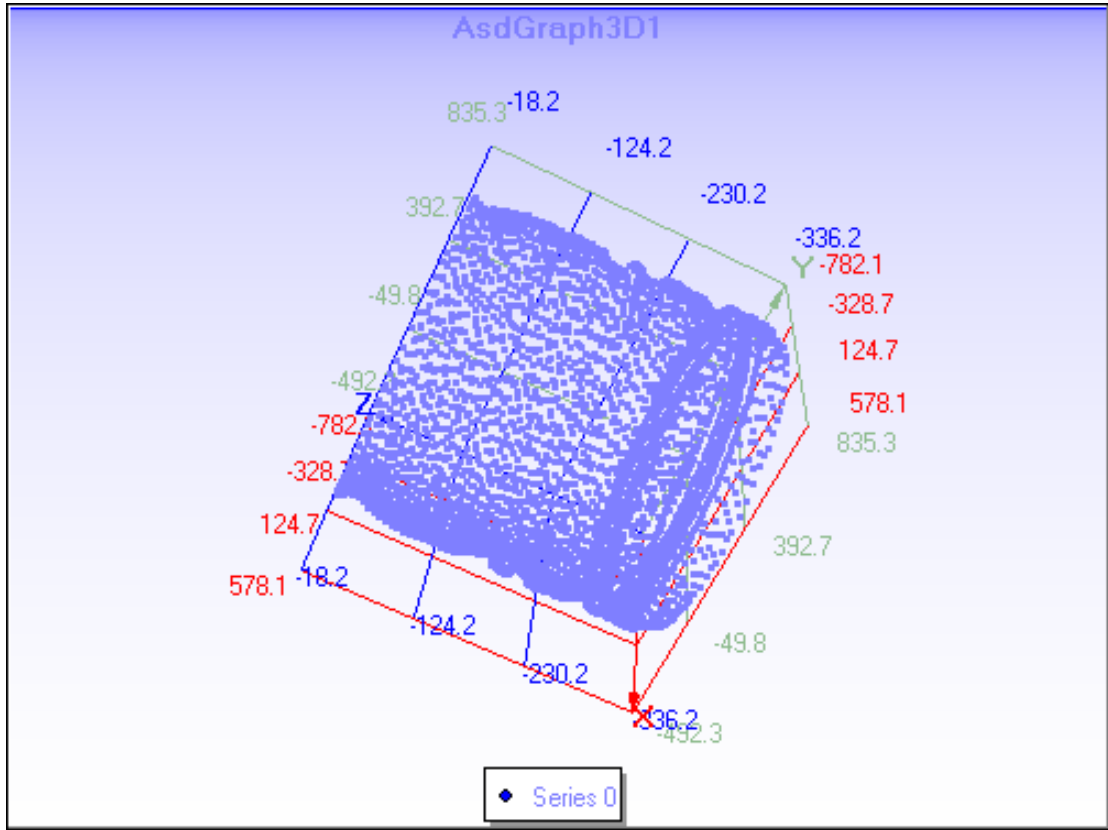


Fig. 5. 14 3d inner shape of the measured deep-hole

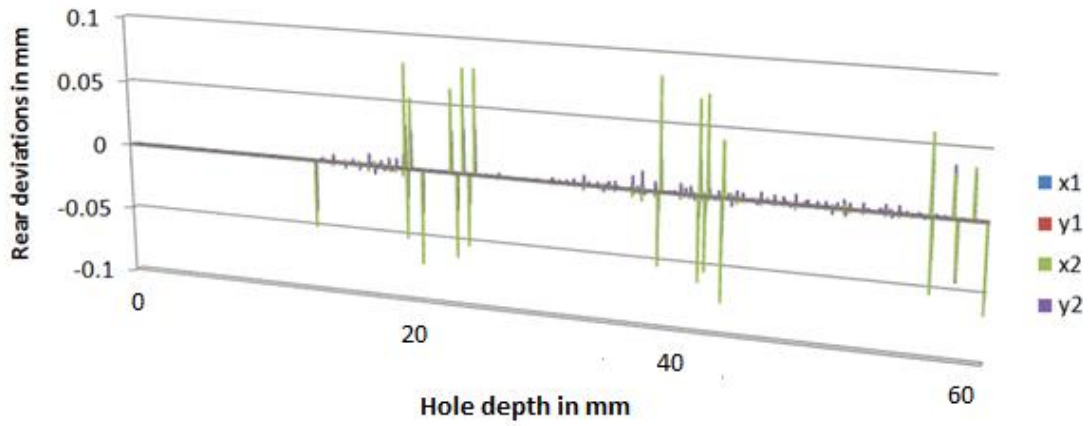


Fig. 5. 15 Rear view obtained from CCD camera

(4) Trial # 4

Experimental Conditions:

- All lights were switched off
- Total travel distance = - 60 mm
- The table feed was 10 mm per minute
- Measurement head's rotational speed, $N = 45 \text{ min}^{-1}$
- Data acquired without any laser alarm

The experiment has been conducted under the above experimental conditions. **Figure 5.16** shows the roundness of a measured hole for a length of 60 mm and having a diameter of 17.6 mm. Axis is shown in $\pm X$ and $\pm Y$ directions. One division is equal to 4 micron. From the drawn figure we can see that the error can be easily calculated. The deviation occurred more in this circle due to some obstacle such as not reaching the laser beam to the pentaprism and corner cube prism properly. **Figure 5.17** shows 3D spiral graph for the complete measured hole up to a length of 60 mm. The smooth shape could be acquired for this experiment. In **Fig. 5.16** the drawn circle refers to 1 rotation data only while **Fig. 5.17** refers to the complete measurement data for all rotations of the total length. The graph shows the smooth shape of the inner hole surface except a very minor fluctuation after the mid-point. **Figure 5.18** refers to CCD1 and CCD2 camera data recorded during experiment. x_1 and y_1 are the data from CCD1 and x_2 and y_2 are the acquired data from CCD2. Data from rear CCD cameras show that the rear side of the probe deviated in x_2 and y_2 directions. From CCD2 we can see the deviations as $\pm 0.075 \text{ mm}$ in x_2 direction and $\pm 0.02 \text{ mm}$ in y_2 direction. These errors have very negligible effect on the roundness figure obtained from the front optical system.

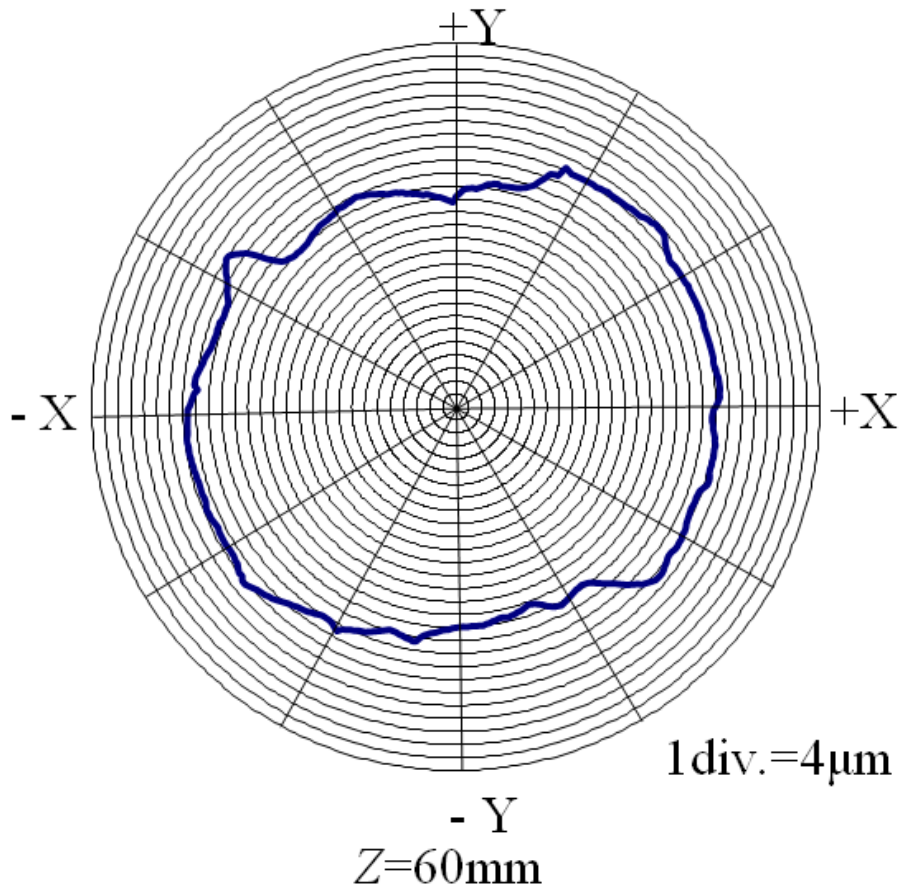


Fig. 5. 16 Measured roundness curve of the hole

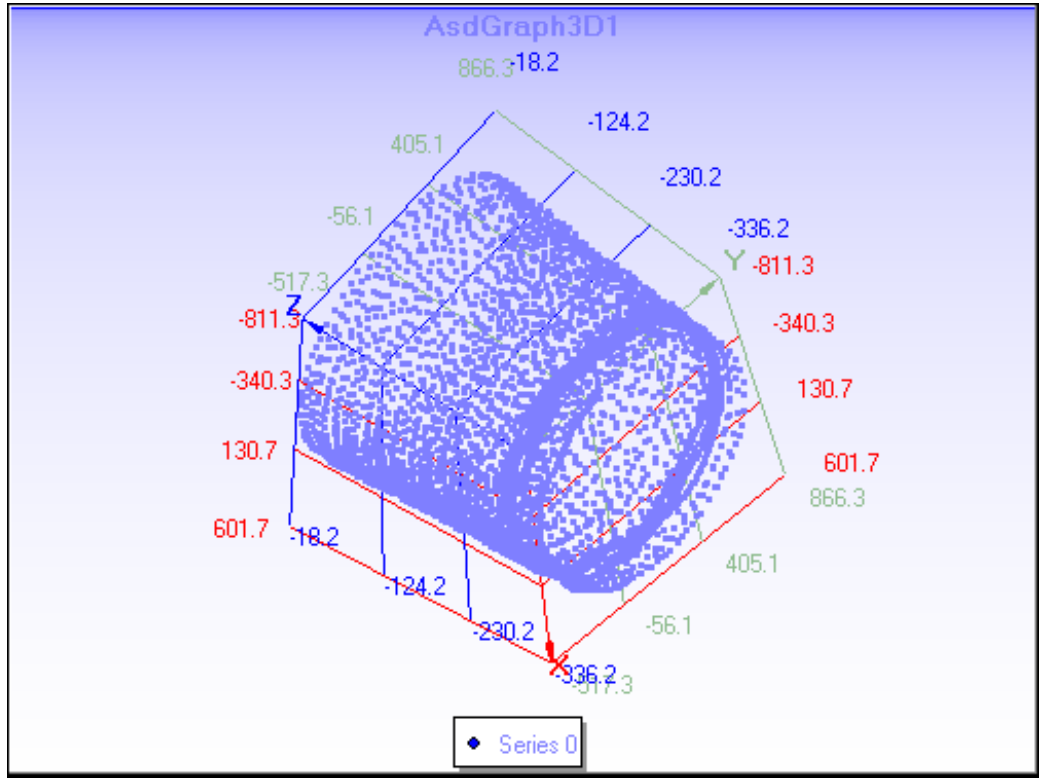


Fig. 5. 17 3d inner shape of the measured deep-hole

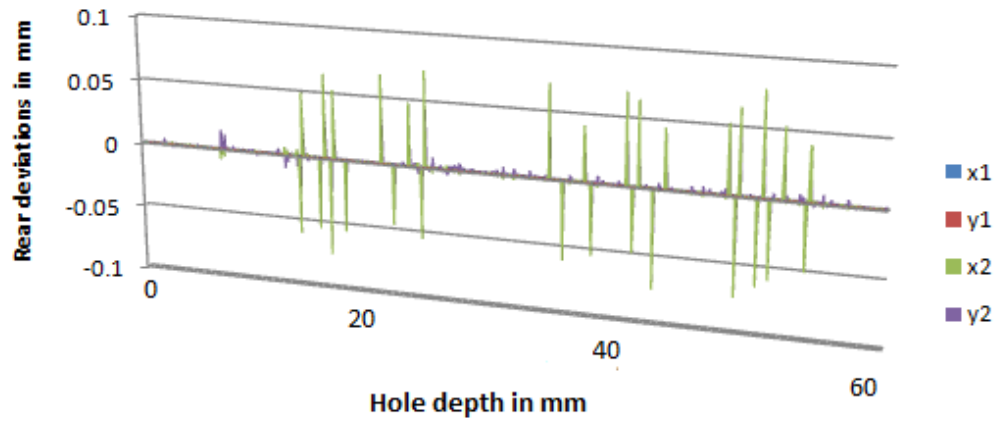


Fig. 5. 18 Rear view obtained from CCD camera

5.2.4 Experiment # 4: Hole depth = 100 mm

Experimental conditions:

- Hole depth = 100 mm
- Rotational speed of the measurement unit, $N = 45 \text{ min}^{-1}$
- Table feed, $f = 0.5 \text{ mm/rev}$
- Measurement time, $t = 33 \text{ min}$

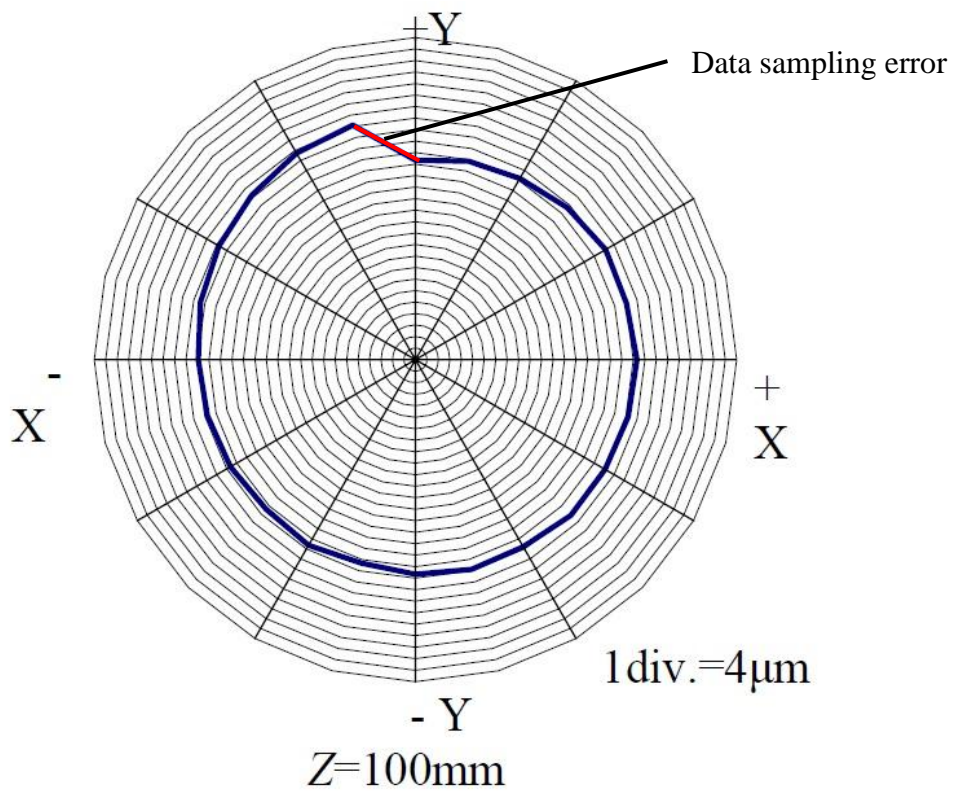


Fig. 5. 19 Measured roundness curve of the hole

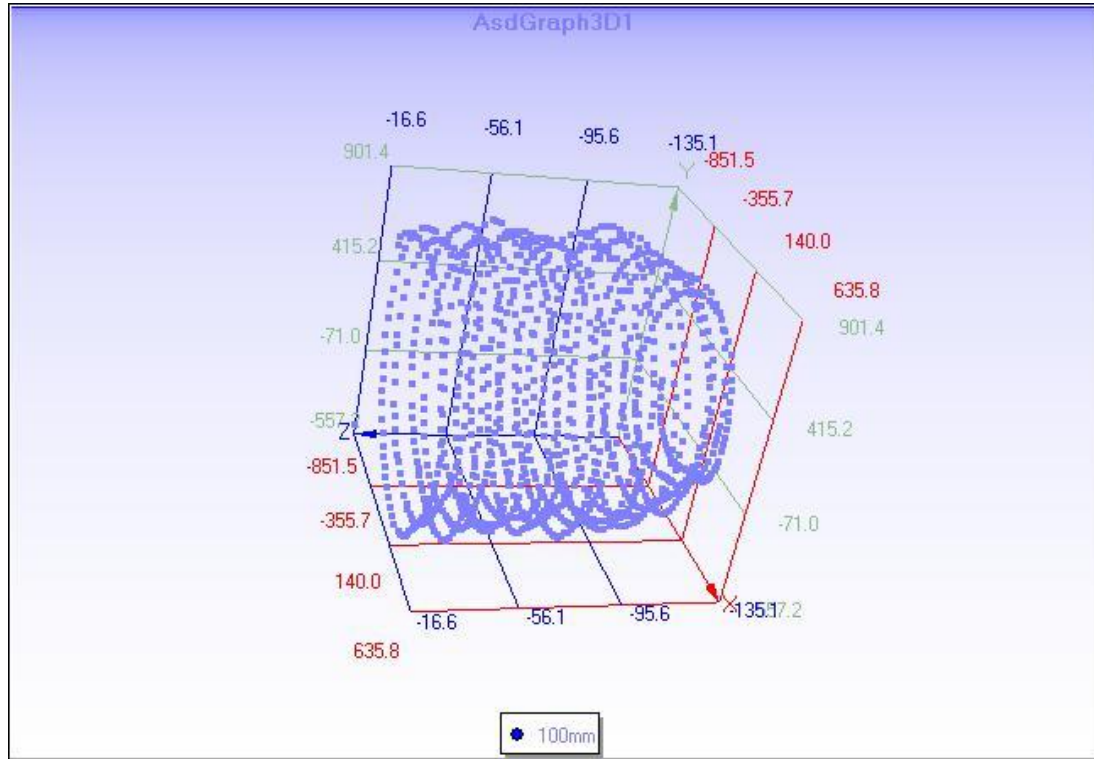


Fig. 5. 20 3d shape of the inner hole surface

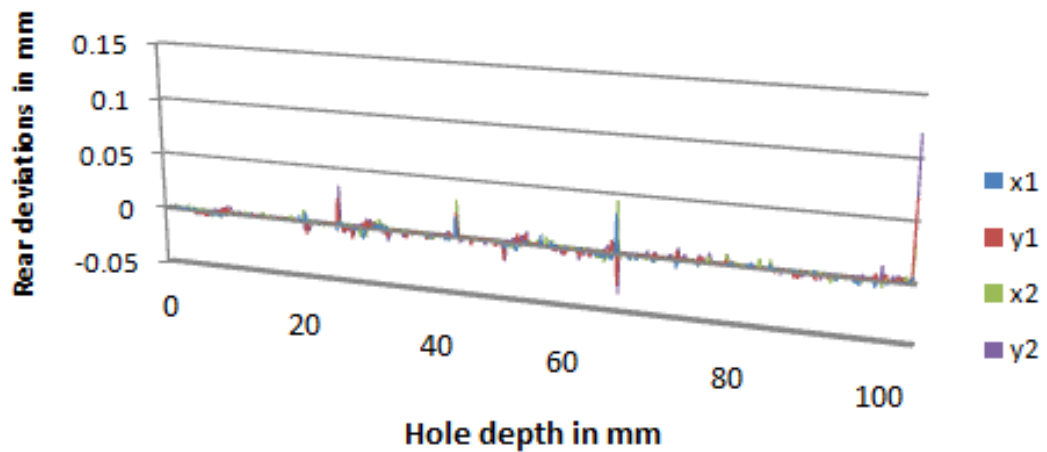


Fig. 5. 21 Rear CCD camera data for 100mm

In this experiment, it is examined whether measurement can be performed accurately. **Figures 5.19, 5.20 and 5.21** show experimental results acquired on the above mentioned conditions.

5.2.5 Experiment # 5: Hole depth = 200 mm

Experimental conditions:

- Hole depth = 200 mm
- Rotational speed of the measurement unit, $N = 45 \text{ min}^{-1}$
- Table feed, $f = 5 \text{ mm/rev}$
- Total measurement time, $t = 27 \text{ min}$

In this experiment, it is examined whether measurement can be well performed even if a hole length becomes large. **Figure 5.22, 5.23 and 5.24** show resulted graph for the above experimental conditions. **Figure 5.22** shows a generated step error which occurred due to improper data sampling.

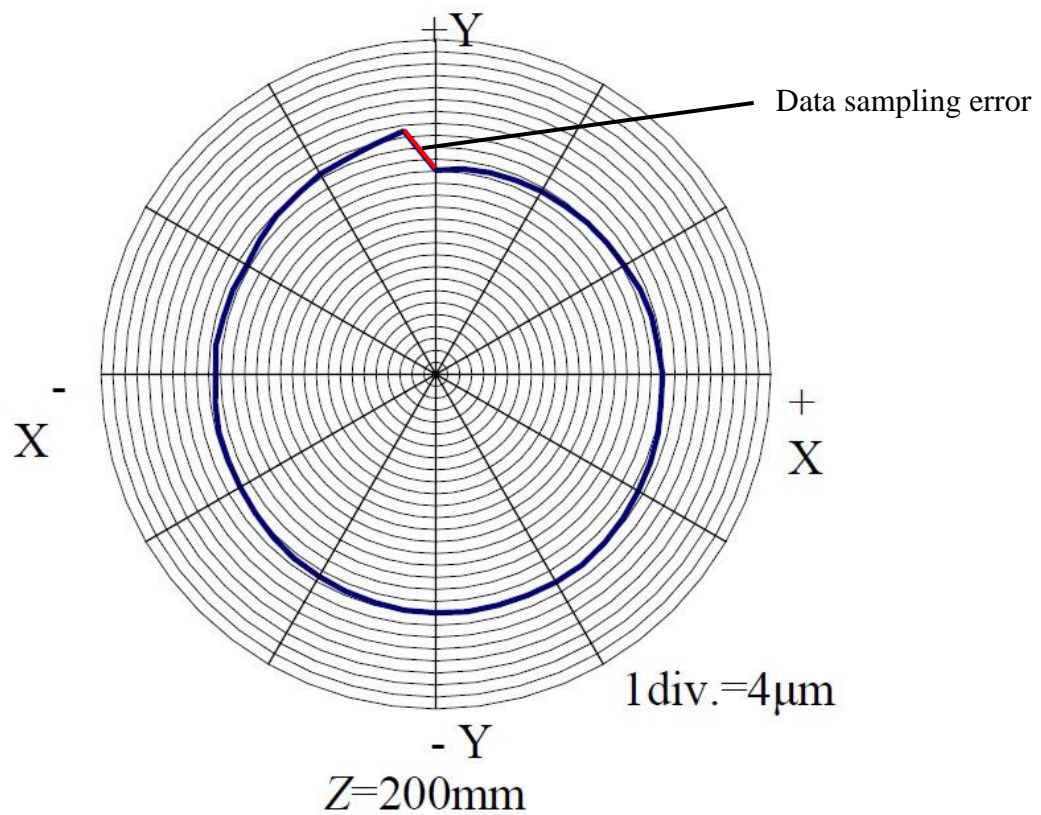


Fig. 5. 22 Measured roundness curve of the hole

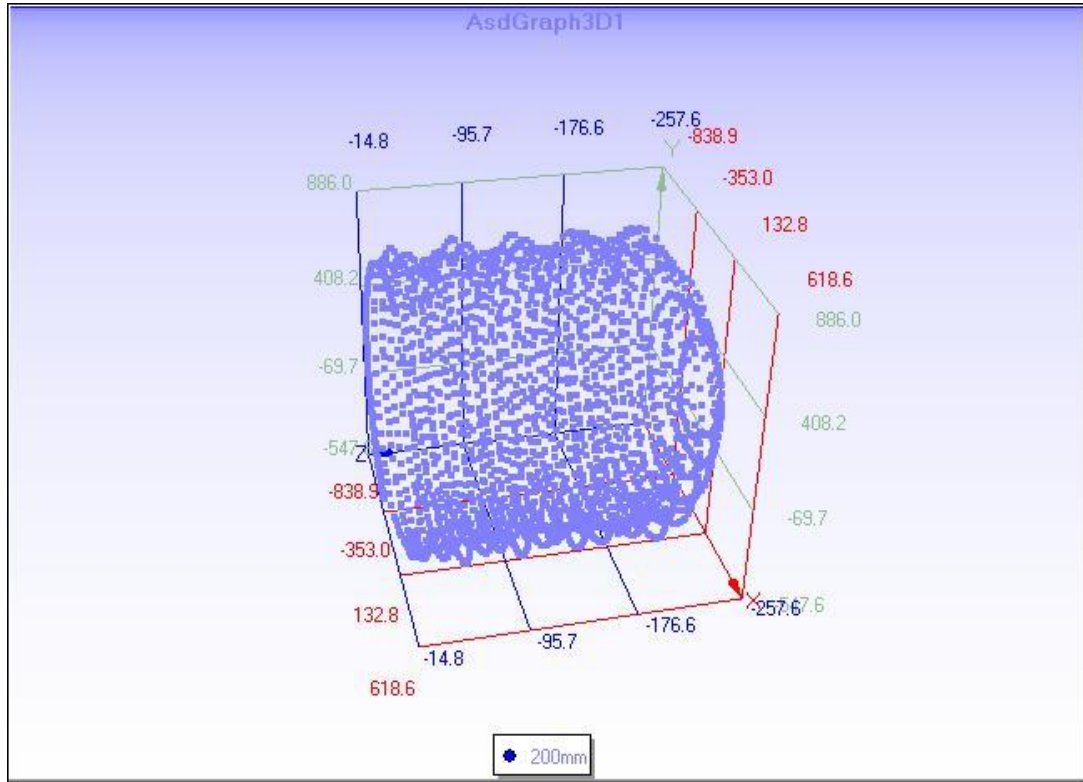


Fig. 5. 23 Measured 3d shape of the inner hole surface

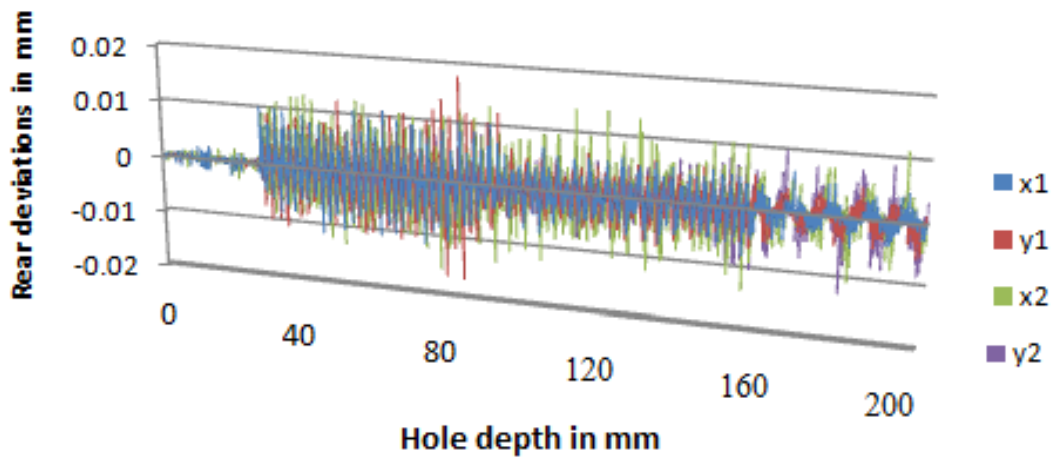


Fig. 5. 24 Rear CCD camera data for 200mm

5.2.6 Experiment # 6: Hole depth = 300 mm

Experimental conditions:

- Hole depth = 300 mm,
- Rotational speed of the measurement unit, $N = 45 \text{ min}^{-1}$
- Table feed, $f = 5 \text{ mm/rev}$
- Total measurement time, $t = 27 \text{ min}$

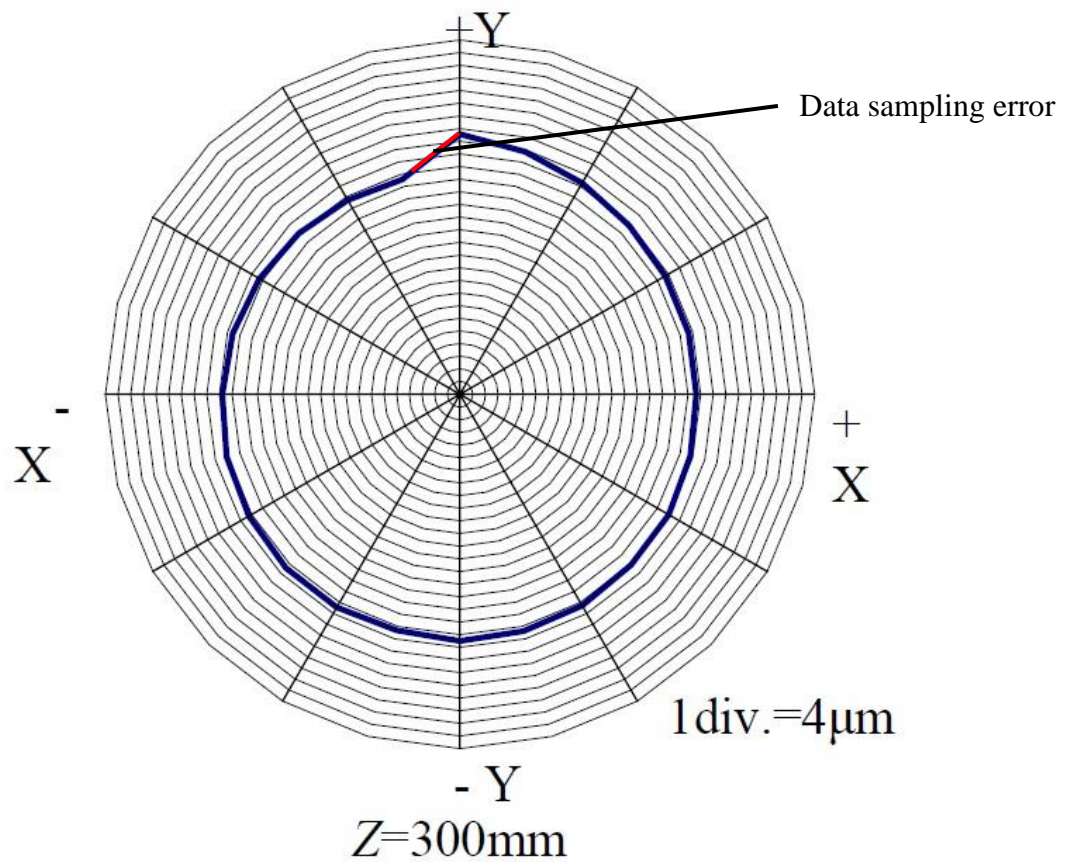


Fig. 5. 25 Measured roundness curve of the hole

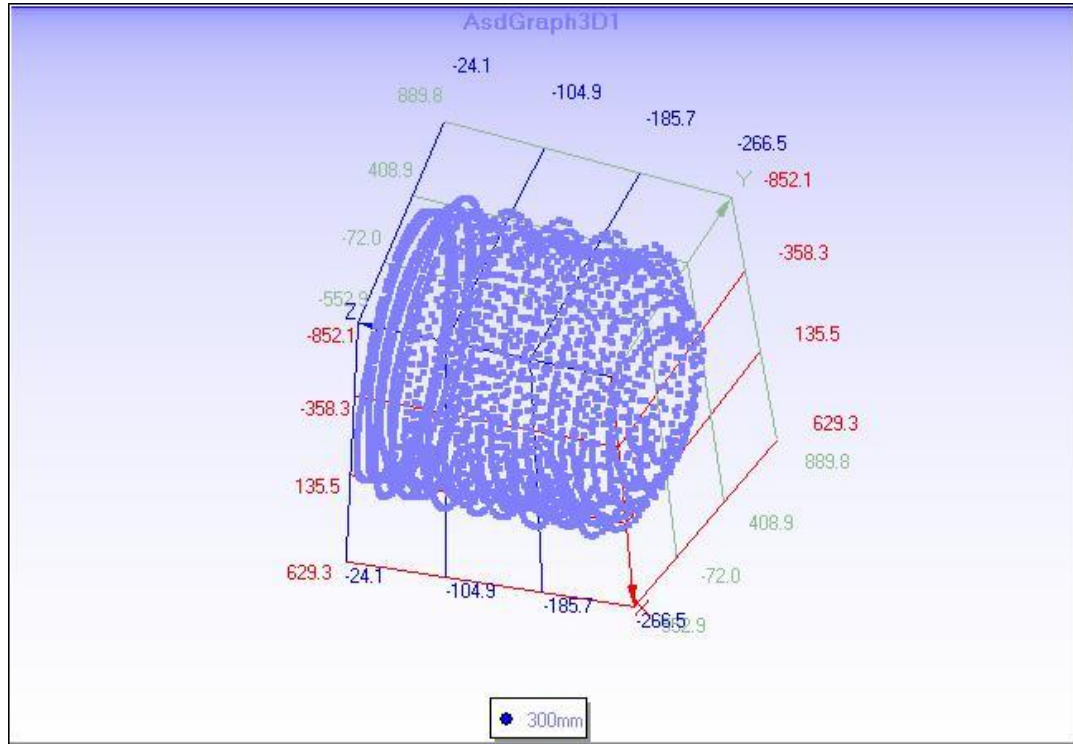


Fig. 5. 26 Measured 3d shape of the inner hole surface

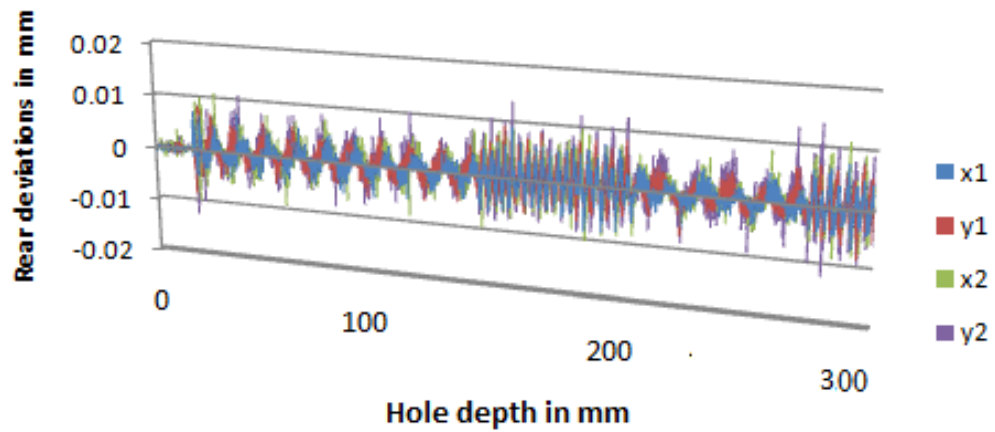


Fig. 5. 27 Rear CCD camera data for 300mm

Figures 5.25, 5.26 and 5.27 show experimental results acquired during experiments applying the above conditions. Figure 5.25 shows a generated error which occurred due to improper data sampling.

5.2.7 Experiment # 7: Hole depth = 400 mm

Experimental conditions:

The experimental conditions remain same as with the experiment # 6 except that the hole depth is 400 mm. Measurement starts at a longitudinal position where two skids enter a hole. Theoretically a guide bush having a hole with a smaller diameter than workpiece is set on the entrance of measured hole. After that, measurement starts at the hole of the guide bush. Probe center is put on the hole center by two skids which move radial direction by their screws.

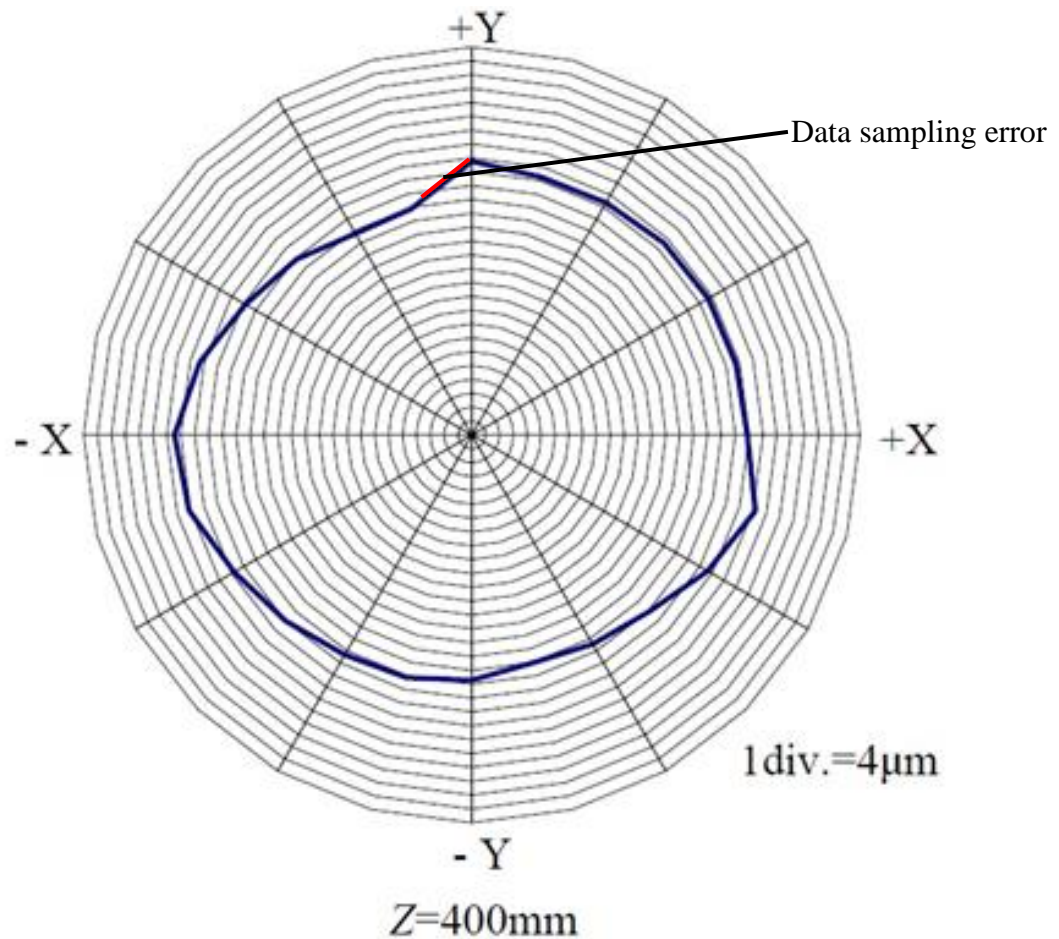


Fig. 5. 28 Measured roundness curve of the hole

Figures 5.28, 5.29 and 5.30 are the experimental results acquired during experiment. Figure 5.28 shows a generated error which occurred due to improper data sampling.

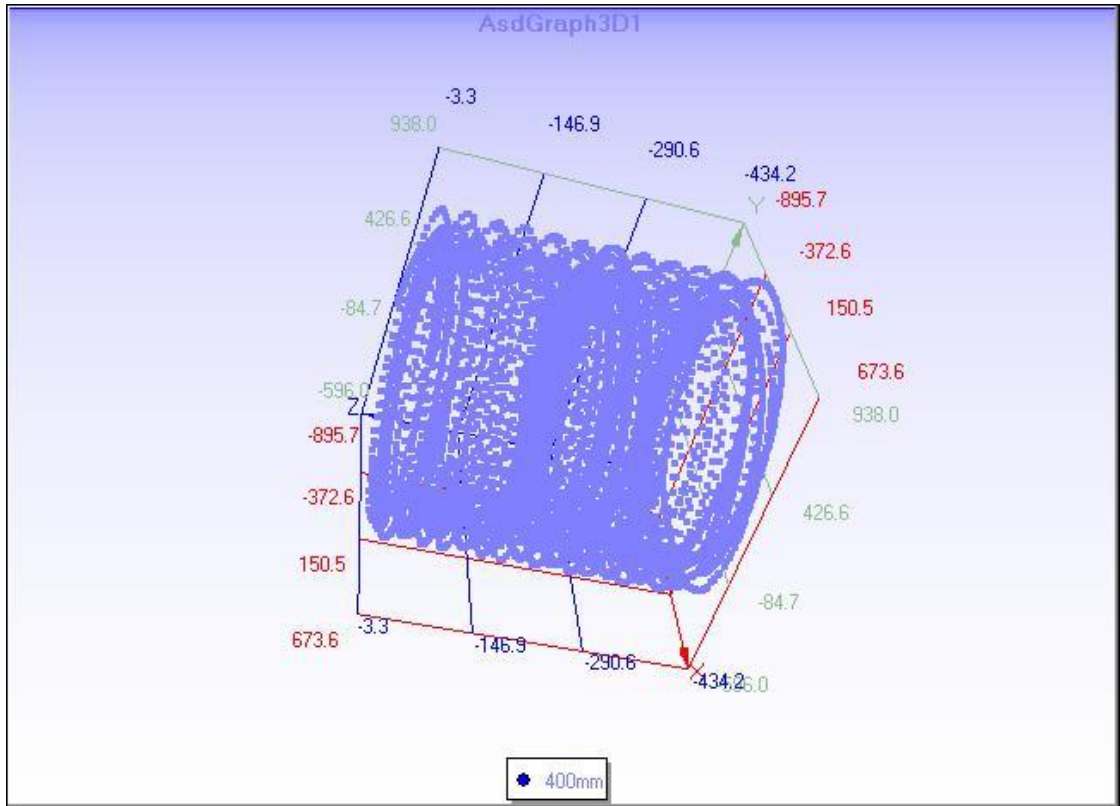


Fig. 5. 29 Measured 3d shape of the inner hole surface

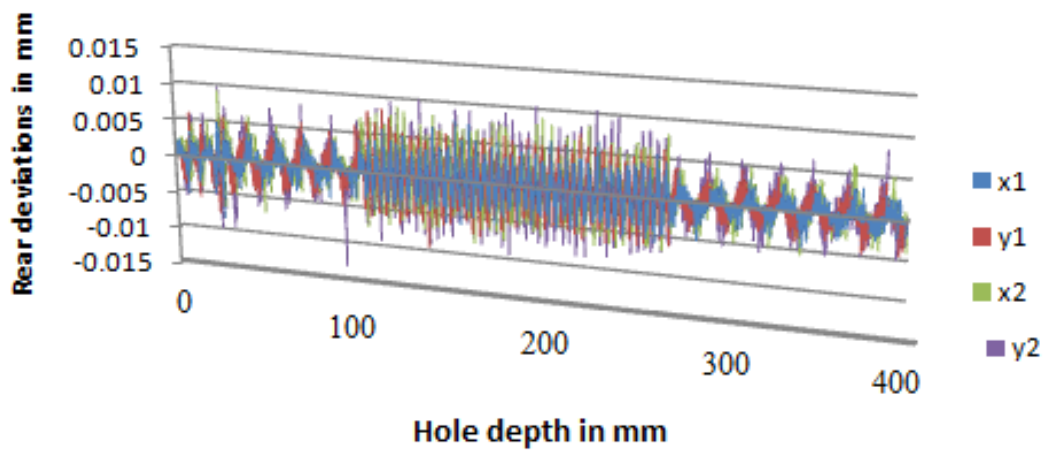


Fig. 5. 30 Rear CCD camera data for 400 mm

5.2.8 Experiment # 8: Hole depth = 800 mm

Experimental conditions:

- Rotational speed of the measurement unit, $N = 6 \text{ min}^{-1}$
- Hole depth = 800 mm
- Table feed, $f = 5 \text{ mm/rev}$
- Measurement time, $t = 27 \text{ min}$

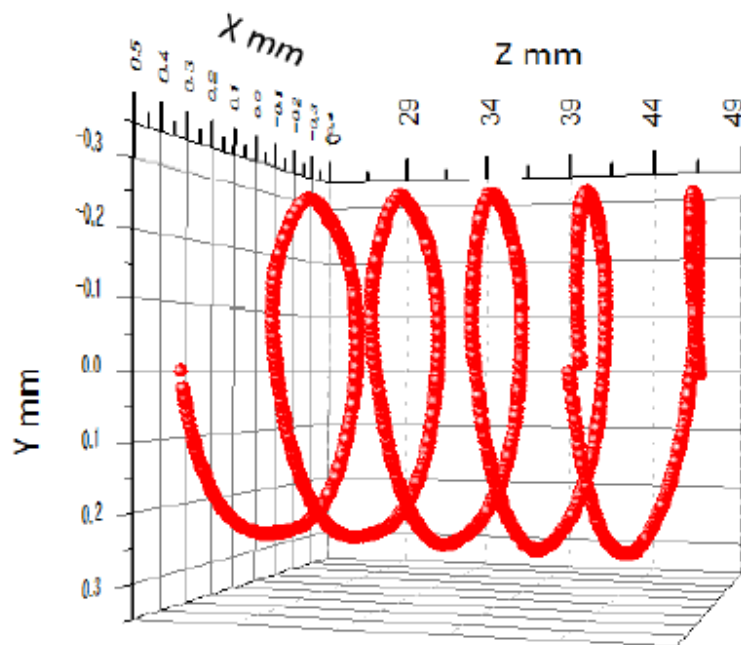


Fig. 5. 31 Spirally scanned hole shape measured by the laser interferometer

Figure 5.31 shows spirally scanned hole wall from a depth of 24 mm to 49 mm. Influence of probe displacement in the hole is removed for this measurement.

5.2.8.1 Intermediate feed and circumferential scanning

First roundness measurement starts at a depth of 24 mm where two supporting pads enter inside the hole. Then, measurement is performed at a hole depth of every 50 mm. Table feed, $f = 120 \text{ mm/min}$. Rotational speed of the measurement unit, $N = 6 \text{ min}^{-1}$. The workpiece table was static during measurement.

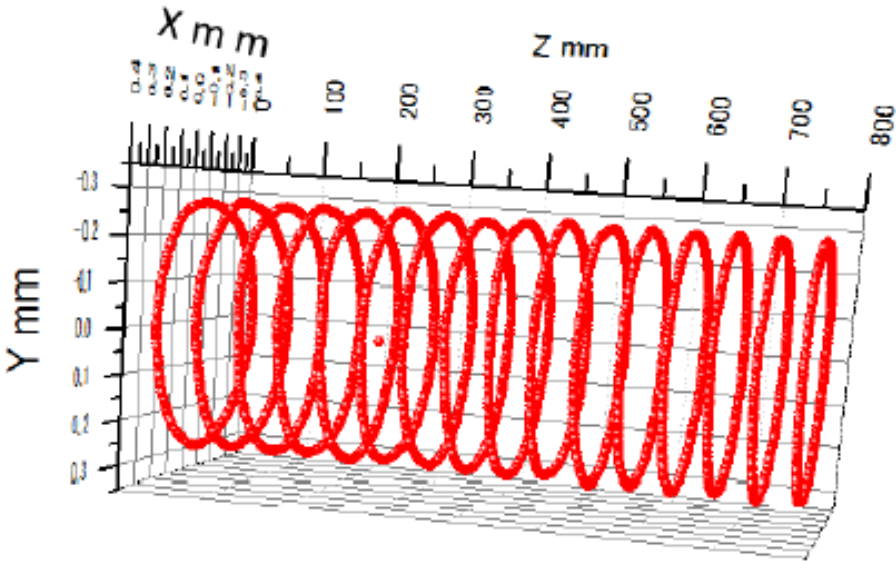
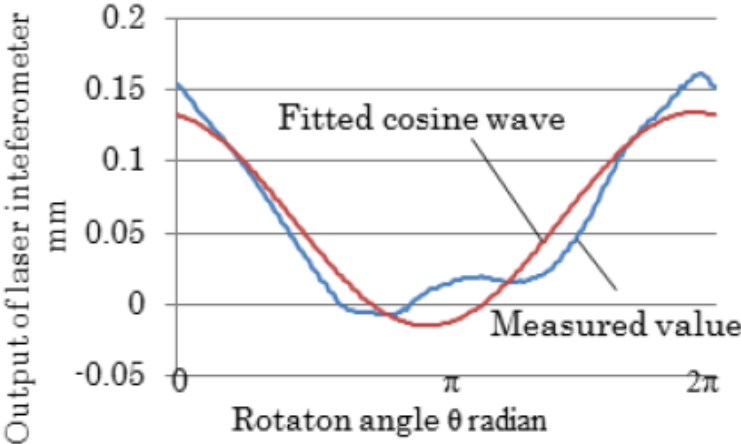
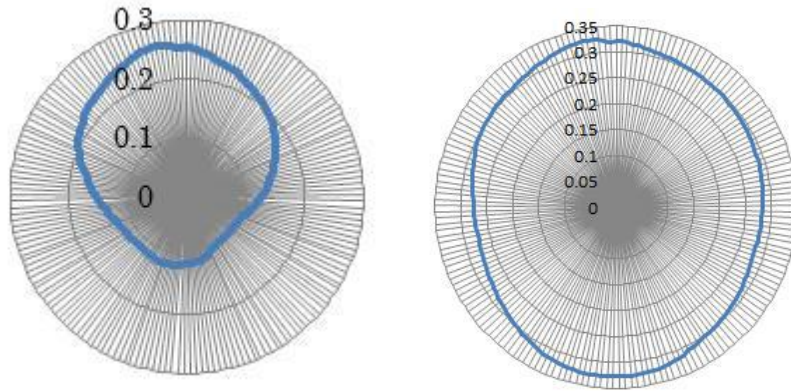


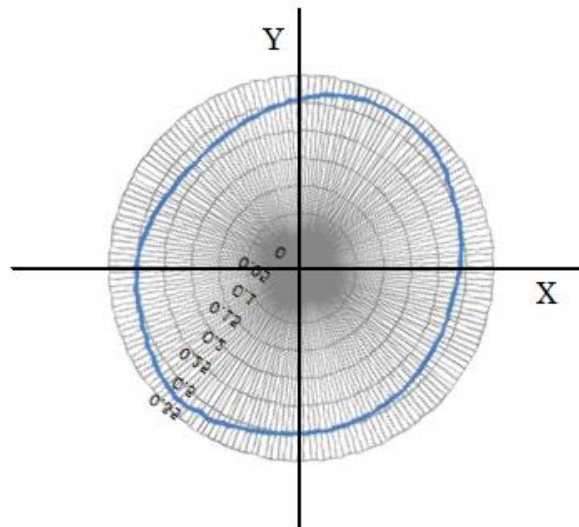
Fig. 5. 32 Circumferentially scanned hole shape: measured every hole depth of 50 mm by the laser interferometer



(a) Fitting to measured value



(b) Roundness profile before correction (c) Roundness profile after correction



(d) Coordinate correction of rotation detection sensor

Fig. 5. 33 Corrections of measured roundness profile using fitting method, and locational delay of rotation-detection sensor

Figure 5.32 shows circumferentially scanned hole shape at a hole depth of every 50 mm measured by the laser interferometer as shown in **Fig. 5.32**. Influence of probe displacement in the hole is removed. **Figure 5.33** shows roundness profile obtained at a depth of 24 mm. This figure is that of a depth of 24 mm in **Fig. 5.31**. **Figure 5.33 (a)** shows the measured value and fitted cosine wave where, $a = 0.07466$ mm and $\varphi = 2.924$

rad. **Figure 5.33 (b)** is an original roundness profile. The roundness profile displaces upward due to the probe displacement. In **Fig. 5.33 (c)**, the influence of the displacement is removed. In **Fig. 5.33 (d)**, roundness is corrected as shown in the workpiece coordinate of **Fig. 4.3**. The stylus is located at an angle of 57° rear position from the magnet which works with the hall element sensor or rotation detector for detecting rotation of the measurement unit. If the stylus, the magnet and the hall element sensor are placed on +X axis at the beginning of measurement; the final correction is unnecessary in this condition.

5.3 Experimental results at different conditions

Measurement starts at a depth of 24 mm under the condition where skids enter with the measurement unit inside the workpiece. Various experimental results are discussed below.

5.3.1 Case 1: $N=6 \text{ min}^{-1}$, $f=0.5 \text{ mm/rev}$, distance 100 mm

Figure 5.19 shows the hole shape of spirally scanned hole wall near a depth of 100 mm and a roundness curve at a depth of 100 mm. Step is observed at the top of the roundness curve.

5.3.2 Case 2: $N=6 \text{ min}^{-1}$, $f=0.5 \text{ mm/rev}$, distance 200 mm and 400 mm

In this experiment, hole wall of a length of 800 mm could be scanned. However laser interferometer could not acquire the complete data after a depth of 400 mm. Diameter of the laser beam is 2 mm. Radiated beam and returning beam did not interfere, it means it receives the data successfully. If the beam diameter is 3 mm, whole length of 800 mm can be measured. **Figure 5.22** the shows the hole shape of spirally scanned hole wall having a depth of 200 mm. **Figure 5.28** shows the hole shape of spirally scanned hole wall having a depth of 400 mm. **Figure 5.34** shows hole deviations obtained from $\text{CCD}\delta$ and $\text{CCD}i$. Hole does not deviate toward Y-direction but it deviates by 0.6 mm toward X-direction.

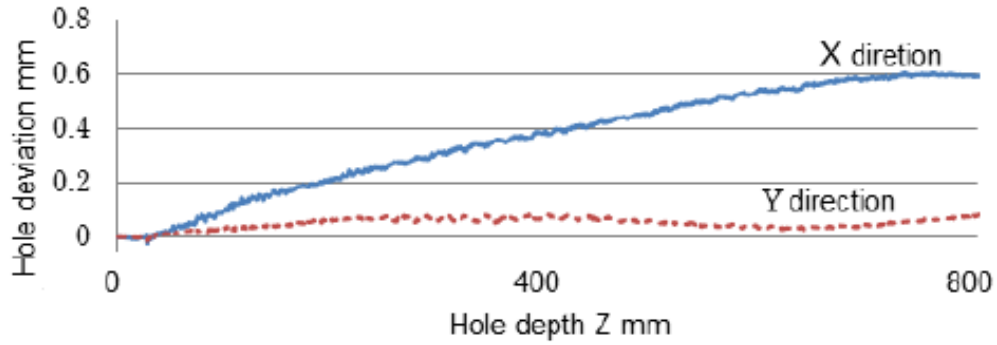


Fig. 5. 34 Hole deviation obtained from CCD δ and CCD i

5.4 Experimental results for longitudinal scanning

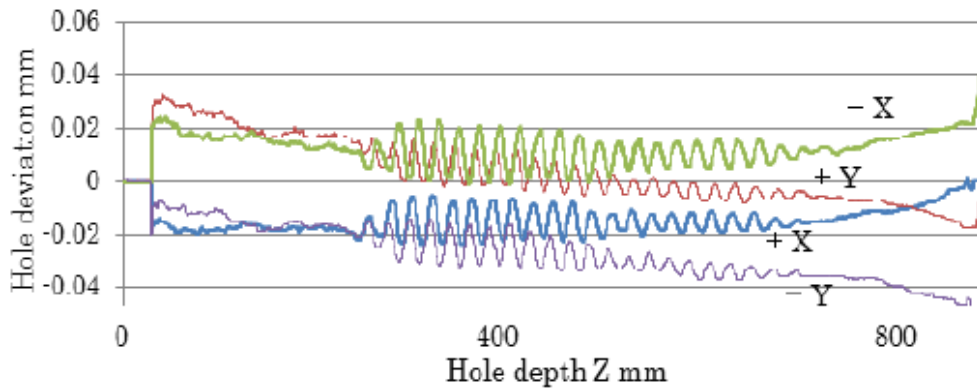


Fig. 5. 35 Longitudinal scanning of four hole walls

Figure 5.35 shows longitudinal scanning results of four hole walls in the directions of $\pm X$ and $\pm Y$. The figures can be obtained from the Y-Z sectional view and X-Z sectional view of the hole shape as shown in **Fig. 5.32**.

5.5 Key achievements

A measurement probe which can measure a small hole with a range of diameters between 17 to 21 mm and a length between 0 to 800 mm is developed. After the measurement system is constructed, the performance test is carried out using a workpiece having a hole of 800 mm long. As a result; following key results are obtained:

- The measurement system can measure accuracy of a deep-hole up to a depth of 800 mm. Further improvement will make the system able to measure deep-holes up to 1000 mm long.
- Measurement accuracy is in μm level based on the accuracy acquired from the laser interferometer, CCD camera and dial gage.
- Deep-hole accuracy (roundness, cylindricity, hole deviation, etc.) can be measured by scanning the hole wall with the developed measurement system.

5.6 Performance analysis of the developed deep-hole measurement system

The system performances are summarized from the obtained results as below.

5.6.1 Performance evaluation of roundness measurement

Measured hole diameter is between 18 to 21 mm. **Figure 5.1** shows very reasonable result of the roundness shape of the workpiece. **Figure 5.4** highlights a roundness curve where the deviation is seen in +Y direction. The deviation observed due to acquired improper experimental data. **Figures 5.7, 5.10, 5.19, 5.22** and **5.25** give better experimental results whereas **Fig 5.13** generates acceptable result. On the other hand, **Figs 5.16** and **5.28** show the resulted roundness figures that are not acceptable due to the range of generated errors.

5.6.2 Performance evaluation of 3d shape measurement

Figures 5.2, 5.8, 5.11, 5.14, 5.17 and **5.29** show very smooth 3d spiral graphs that are drawn from the acquired experimental data. **Figure 5.5** shows a 3d spiral graph which highlights an acceptable 3d graph from the experimental data with minor error. On the other hand, **Figs. 5.23, 5.23** and **5.26** are drawn from the experimental results that have errors at the beginning of the graph. These errors are due to the incorrect data acquisition

during experiment. One of the main possible errors is the cause of deviation of the laser beam from its original axis due to environmental noise such as; light, sound etc.

5.6.3 Performance evaluation of CCD data measurement

From the rear CCD cameras we obtained the data for rear position of the measurement probe during measurement. **Figure 5.3** generates an error of ± 0.15 mm for the rear probe position whereas **Figs 5.6** and **5.9** generates errors of ± 0.001 mm and ± 0.11 mm respectively whereas **Fig. 5.12** shows an error of ± 0.00081 mm which is very smooth data obtained during measurement. **Figures 5.15, 5.18, 5.21, 5.24, 5.27** and **5.30** generate errors of ± 0.0053 mm, ± 0.075 mm, ± 0.13 mm, ± 0.02 mm, ± 0.015 mm and ± 0.013 mm respectively. The errors are shown in four directions in the figures such as x1, y1, x2 and y2. These errors have very insignificant effect on the roundness data acquired by the front optical system.

5.7 Summary

This chapter presented experimental results with detail explanation for each and every experiment. The chapter shows very impressive results with the implementation of the new developed measurement unit and probe. From the results we can easily find the optimum conditions for the experiments in order to acquire the best experimental results from this automatic developed deep-hole system.

CHAPTER 6

CONCLUSION AND FUTURE WORKS

6.1 Introduction

This chapter summarizes the dissertation focusing the achievement of the new system and gives recommendations for future works to develop a further enhanced system.

6.2 Conclusion

The manufacturing of deep-hole is characterized by some difficult problems that do not exist in case of shallow one. Considering these difficulties and problems, a laser-guided deep-hole measurement system is developed on the continuity of previous successfully developed system that applied for larger holes. The developed automatic hole parameter measurement system is elaborated in details in this study. It has been observed that the developed system can measure the hole accurately without manual control. It can measure as well as record data automatically during the experiment. A target measurement system that can measure a small hole with a diameter of 17-21 mm and a length of 0-800 mm is developed. As a result of the performance test, it is observed that the system can be used to measure the hole accuracy of such small holes.

From the discussion in chapter 5; it can be seen that the monitoring system is very important for hole accuracy measurement. Without proper monitoring system, the successful measurement is not possible to be accomplished. Specially; workpiece having small diameter based holes and long length is unable to measure without all steps of proper monitoring. Monitoring system works here like a closed-loop system or feed-back control system. The more the feedback is accurate, the more the system is capable to acquire successful measurement data. During the accomplished measurements; when an error was shown in the display monitor, immediately the machine was stopped and corrected the error before the next measurement was continued. All important measurement sub-systems have separate monitoring system in the developed system such as laser data monitor, CCD camera monitor, motor

travelling distance monitor, measurement head monitor and measurement data display monitor that improved the efficiency of the developed deep-hole measurement system. Following results are obtained from the developed new measurement system:

- The developed system can measure the accuracy of a hole with a length between 0 to 800 mm and a diameter between 17 to 21 mm.
- Influence of changing attitude of the measurement probe can be calculated.
- The complete developed system works as a feed-back control system. Thus; automatic control will further enhance the reliability and safety of the measurement system.

6.3 Future works

In future, we will focus on the implementation of this method for measuring accuracy of a hole having a few meters length with the similar hole diameters. The problem may occur in using long measurement bar where it requires support for the long measurement bar. The main challenge here is to prevent the measurement bar from the deviation during measurement. As far the experiment have been accomplished, it is found that the bending in measuring one meter long-length hole is negligible but more than this length the bending will affect the measurement system unless the anti-bending system is applied on it. This problem can be solved easily if we can use skids to prevent bending.

In future the system can be improved by upgrading the attitude control system by using more precise CCD camera at the rear side of the probe which is attached to the optical device. Once it is implemented successfully the measurement system will generate more accurate output and thus; enhances overall performance of the developed system.

6.4 Mechanical actuator for the measurement system

Mechanical actuator consists of various parts that are designed and made separately and finally assembled them together. **Figure 6.1** shows the middle connector of the actuator.

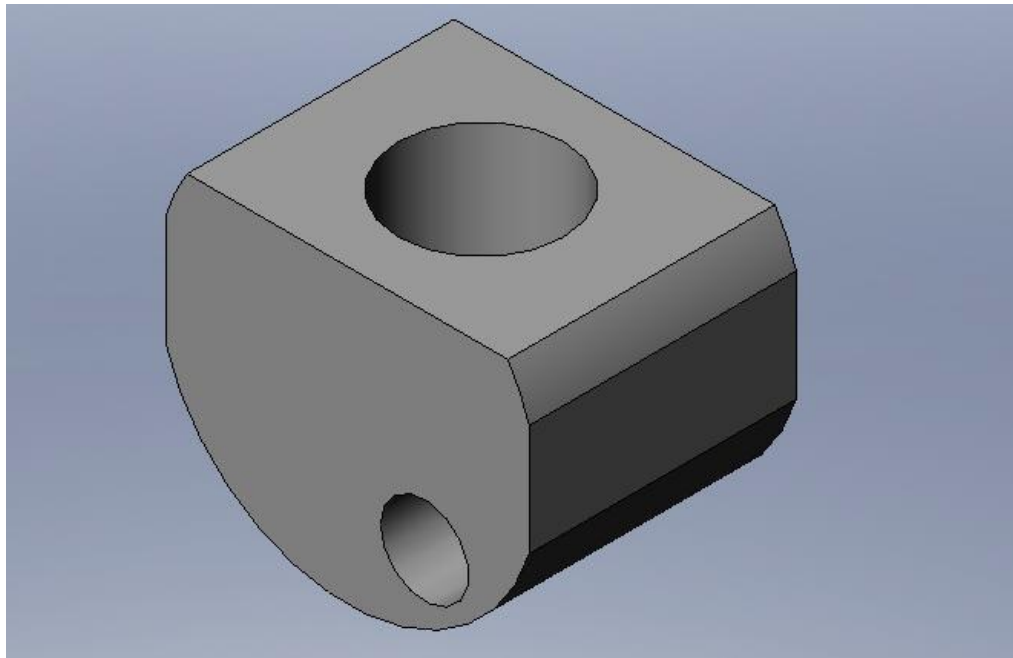


Fig. 6. 1 Middle part of the actuator

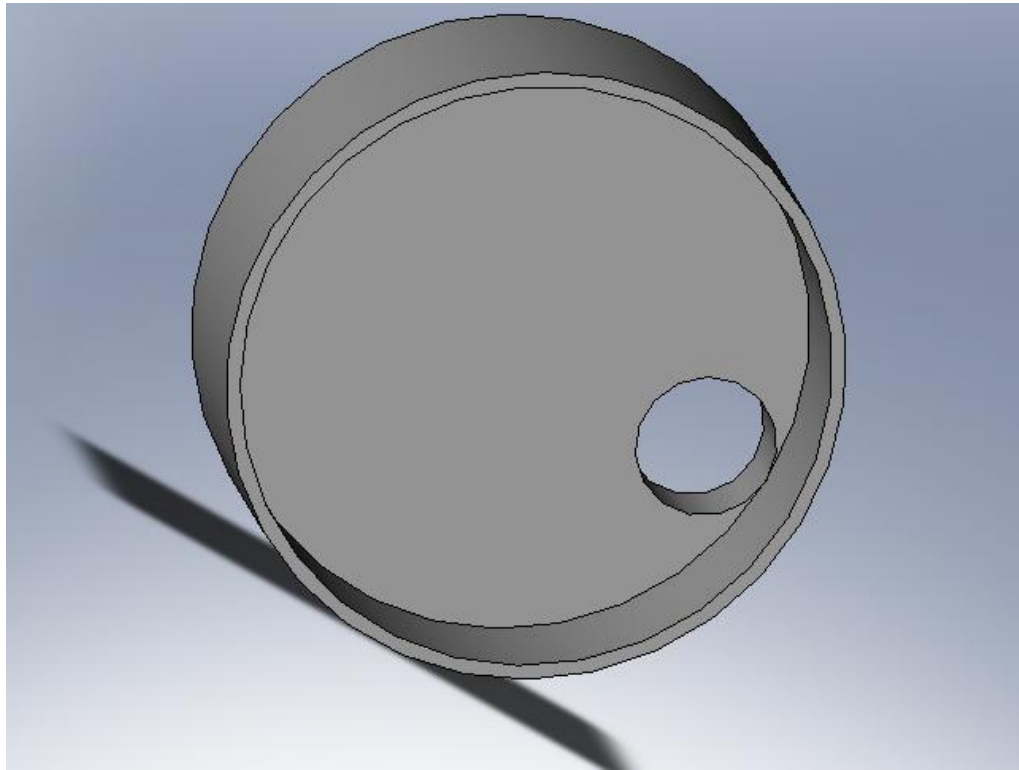


Fig. 6. 2 Connecting part of the actuator

Figure 6.2 shows the connector of the inner part of the actuator. It also shows the front view of the actuator. It is very important to see the internal make up of the designed parts before it is made. The actuator is necessary in measuring inner hole profiles accurately. Without actuator the result may have error in its acquired data.

6.5 Assembly design of the mechanical actuator

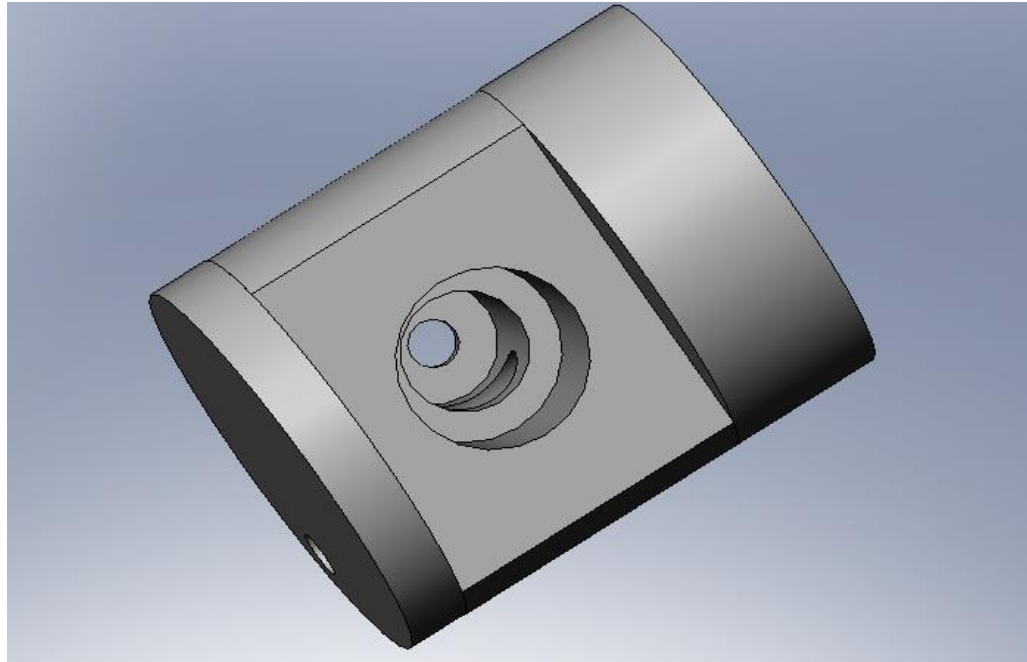


Fig. 6. 3 Assembly design of different parts of the actuator

Assembly design is a process by which products are designed with ease of assembly in mind. If a product contains fewer parts it will take less time to assemble, therefore it reduces assembly costs. In addition, if the parts are provided with features that make it easier to grasp, move, orient and insert them; then this will also reduce assembly time and production costs. The reduction of the number of parts in an assembly has the added benefit of generally reducing the total cost of parts in the assembly. **Figure 6.3** shows assembly views of connected separate parts that are designed to make an assembly for the desired mechanical actuator.

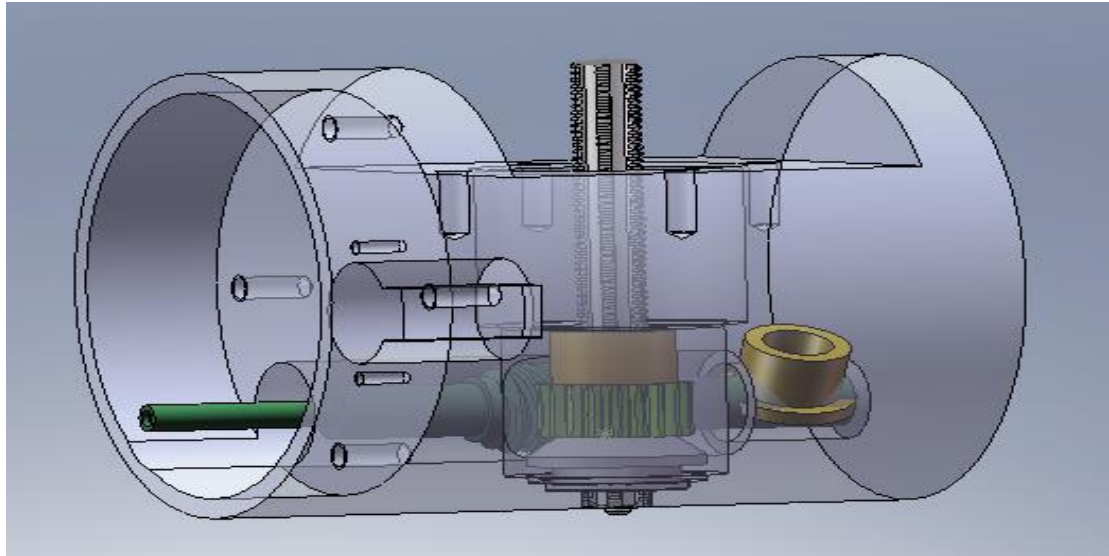


Fig. 6. 4 Assembly drawing with integrated worm gear

Figure 6.4 shows more detail design of the integrated actuator with the highlighted inner parts. The inner parts connected to the actuator are also visible in this figure. Stepper motor is connected to the worm wheel system to drive the linear shaft so that it can carry the loads linearly which works on it during measurement.

REFERENCES

- [1] A. Katsuki, H. Onikura, T. Sajima, M. Rikimaru, "Development of a High Performance Deep-Hole Laser-Guided Boring Tool: Guiding Characteristics." *Annals of the CIRP*. 1997; Vol.46 (1), pp.319-323.
- [2] A. Katsuki, H. Murakami, H. Onikura, T. Sajima "Development of a Laser-Guided Deep-Hole Measuring System: Measurements of Roundness, Cylindricity and Straightness" , *Proceedings of the 4th International Conference on Leading Edge Manufacturing in 21st Century (LEM21)*, (2007), pp.887-892.
- [3] A. Katsuki, H. Onikura, T. Sajima, H. Murakami, T. Sato, H. Nishi, "High-Accuracy On-Machine Measurement of Deep Hole with Diameter Varying at Millimeter-Scale", *Proceedings of the 4th CIRP International Conference on High Performance Cutting (2010)*, pp.239-242.
- [4] A. Katsuki, H. Onikura, T. Sajima, A. Mohri, T. Moriyama, Y. Hamano, H. Murakami, "Development of a practical high-performance laser-guided deep-hole boring tool", *Precision Engineering*, Vol 35(2011), pp.221-227.
- [5] A. Katsuki, H. Onikura, T. Sajima, H. Murakami, T. Sato, Thomas CAETANO, MD. Hazrat ALI and Osamu OHNISHI, "Study on high-speed on-machine measurement of deep-hole accuracy". *Journal of the Japan Society for Precision Engineering*. 2011; 77/7: 681-687.
- [6] A. Katsuki, H. Onikura, T. Sajima, H. Murakami, T. Doi, T. Sato, H. Nishi, Valentine PIETRI and MD. Hazrat Ali. "Development of a laser-guided deep-hole evaluating system", *Journal of the Japan Society for Precision Engineering*, 2011; 77/10: 977-984.
- [7] <https://www.llnl.gov/str/Blaedel.html>, Energy and Technology Review, Lawrence Livermore National Laboratory, Livermore, California, UCRL-52000-87-9, Retrieved in September 1987.
- [8] Fachinger, J., 2006. "Behavior of HTR Fuel Elements in Aquatic Phases of Repository Host Rock Formations". *Nuclear Engineering & Design* Vol.236, p. 54.
- [9] <http://www.xpresspe.com/applications.php>. Accessed on 13th November, 2013.
- [10] <http://www.cern2012.euspen.eu/content/News-and-events/euspen-events>. Accessed on 10th November, 2013.
- [11] http://www.butlercc.edu/engineering/en115/en115_accur_vs_prec.cfm. Accessed on 13th November, 2013.

- [12] P.A.Vermeulen, P.C.J.N. Rosielle, P.H.J. Schellekens, “Design of a high-precision 3D coordinate measuring machine”, *Ann CIRP*, Vol.47 (1) (1998), pp. 447–450.
- [13] P.Yang, T.Takamura, S.Takahashi, K.Takamasu, O.Sato, S.Osawa and T.Takatsuji, “Development of high-precision micro-coordinate measuring machine: Multi-probe measurement system for measuring yaw and straightness motion error of XY linear sage”. *Precision Engineering* Volume 35, Issue 3, July 2011, pp.424–430.
- [14]A. Katsuk, H. Onikura, T. Sajima, T. Nakanishi, T. Ookubo,H. Murakami,N. Okada,M. Arita,M. Mitsunag.“Development of a Laser-Guided Deep-Hole Evaluating Probe: For 100 to 600 mm Diameter Hole”. *Proc. of the 4th International Conference on Leading Edge Manufacturing in 21st Century (LEM21)*, pp. 893-896, 2007.
- [15]IA. Ivan,M.Rakotondrabe,P.Lutz and N.Chaillet. “Study on High-Speed On-Machine Measurement of Deep-Hole Accuracy”. *Signal Measurement and Estimation Techniques for Micro and Nanotechnology*, DOI 10.1007/978-1-4419-9946-7 2
- [16] A. Katsuki, H. Onikura, T. Sajima, H. Murakami, T. Doi, T. Sato, MD.Hazrat Ali, and Alexandre Berjaud, “Development of a Laser-guided Deep-hole Measurement System with High-performance Mechanical Actuators”. The 26th ASPE Annual Meeting, November 13- 18, 2011, Denver, USA.
- [17] A. Katsuki, MD.Hazrat Ali, T. Sajima,H. Murakami, and H. Onikura, “Development of a Laser-guided Deep-hole Measurement System: Usage of Long Measurement Bar”,Mechanical Engineering conference December2011, Chittagong, Bangladesh.
- [18] MD. Hazrat ALI, A.Katsuki, T. Sajima, H. Murakami and S. Kurokawa.Control Strategy of Developed Mechanical Actuator in Measuring Hole-Surface Parameter. *International Journal of Advanced Manufacturing Technology*, Springer, UK, Vol.69, Numbers 5-8, 2013. DOI: 10.1007/s00170-013-5420-0.
- [19] X. Liu, Correlation analysis of surface topography and its mechanical properties at micro and nanometre scales, *Wear*, Volume 305, Issues 1–2, 30 July 2013, Pages 305-311, ISSN 0043-1648, <http://dx.doi.org/10.1016/j.wear.2012.11.033>.
- [20]Wei Gao, Jun Yokoyama, Hidetoshi Kojima, Satoshi Kiyono, Precision measurement of cylinder straightness using a scanning multi-probe system, *Precision Engineering*, Volume 26, Issue 3, July 2002, Pages 279-288, ISSN 0141-6359, [http://dx.doi.org/10.1016/S0141-6359\(02\)00106-X](http://dx.doi.org/10.1016/S0141-6359(02)00106-X).

- [21] A. Janusiewicz, S. Adamczak, W. Makiela, K. Stepień, Determining the theoretical method error during an on-machine roundness measurement, *Measurement*, Volume 44, Issue 9, November 2011, Pages 1761-1767, ISSN 0263-2241, <http://dx.doi.org/10.1016/j.measurement.2011.07.013>.
- [22] A. Katsuki, H. Onikura, T. Sajima, A. Mohri, T. Moriyama, Y. Hamano, H. Murakami: Development of a Practical High-Performance Laser-Guided Deep-Hole Boring Tool: Improvement in Guiding Strategy, *Precision Engineering*, Vol.35 (2) (2011).
- [23] Chen-Chien Hsu, Ming-Chih Lu, Wei-Yen Wang, Yin-Yu Lu, Distance measurement based on pixel variation of CCD images, *ISA Transactions*, Volume 48, Issue 4, October 2009, Pages 389-395, ISSN 0019-0578, <http://dx.doi.org/10.1016/j.isatra.2009.05.005>.
- [24] Xianqing Lei, Chunyang Zhang, Yujun Xue, Jishun Li, Roundness error evaluation algorithm based on polar coordinate transform, *Measurement*, Volume 44, Issue 2, February 2011, Pages 345-350, ISSN 0263-2241, <http://dx.doi.org/10.1016/j.measurement.2010.10.007>.
- [25] O. Horikawa, N. Maruyama, M. Shimada, A low cost, high accuracy roundness measuring system, *Elsevier Journal of the International Societies for Precision Engineering and Nanotechnology* Vol. 25 (2001)pp. 200–205.
- [26] B. Muralikrishnan, S. Venkatachalam, J. Raja, M. Malburg, A note on the three-point method for roundness measurement, *Precision Engineering*, Volume 29, Issue 2, April 2005, Pages 257-260, ISSN 0141-6359, <http://dx.doi.org/10.1016/j.precisioneng.2004.06.007>.
- [27] Zi-qiang Yin, Sheng-yi Li, High accuracy error separation technique for on-machine measuring straightness, *Precision Engineering*, Volume 30, Issue 2, April 2006, Pages 192-200, ISSN 0141-6359, <http://dx.doi.org/10.1016/j.precisioneng.2005.07.006>.
- [28] S. Mekid, K. Vacharanukul, In-process out-of-roundness measurement probe for turned workpieces, *Measurement*, Volume 44, Issue 4, May 2011, Pages 762-766, ISSN 0263-2241, <http://dx.doi.org/10.1016/j.measurement.2011.01.011>.
- [29] Wei Gao, Satoshi Kiyono, High accuracy profile measurement of a machined surface by the combined method, *Measurement*, Volume 19, Issue 1, September 1996, Pages 55-64, ISSN 0263-2241, [http://dx.doi.org/10.1016/S0263-2241\(96\)00066-8](http://dx.doi.org/10.1016/S0263-2241(96)00066-8).

- [30]Wei Gao, Satoshi Kiyono, On-machine roundness measurement of cylindrical workpieces by the combined three-point method, *Measurement*, Volume 21, Issue 4, August 1997, Pages 147-156, ISSN 0263-2241, [http://dx.doi.org/10.1016/S0263-2241\(97\)00060-2](http://dx.doi.org/10.1016/S0263-2241(97)00060-2).
- [31]Qimi Jiang, Hsi-Yung Feng, Daoshan OuYang, Mesay T. Desta, A roundness evaluation algorithm with reduced fitting uncertainty of CMM measurement data, *Journal of Manufacturing Systems*, Volume 25, Issue 3, 2006, Pages 184-195, ISSN 0278-6125, [http://dx.doi.org/10.1016/S0278-6125\(08\)00005-8](http://dx.doi.org/10.1016/S0278-6125(08)00005-8).
- [32]Gi-Bum Jeong, Dong Hwan Kim, Dong Young Jang, Real time monitoring and diagnosis system development in turning through measuring a roundness error based on three-point method, *International Journal of Machine Tools and Manufacture*, Volume 45, Issues 12–13, October 2005, Pages 1494-1503, ISSN 0890-6955, <http://dx.doi.org/10.1016/j.ijmachtools.2005.01.022>.
- [33]MD. Hazrat Ali, Syuhei Kurokawa, Kensuke Uesugi, “Camera based 3d probe control in measuring gear profile”. *Proceedings of IEEE Conference, RVSP, Kitakyushu*, 10-12 December 2013, Japan.
- [34]Leda Villalobos, Sheldon Gruber, Measurement of surface roughness parameter using a neural network and laser scattering, *Industrial Metrology*, Volume 2, Issue 1, December 1991, Pages 33-44.
- [35] Weifeng Wang, Xinping Yan, Helai Huang, Xiumin Chu, Mohamed Abdel-Aty, Design and verification of a laser based device for pavement macrotexture measurement, *Transportation Research Part C: Emerging Technologies*, Volume 19, Issue 4, August 2011, Pages 682-694.
- [36] C.J Tay, S.H Wang, C Quan, H.M Shang, In situ surface roughness measurement using a laser scattering method, *Optics Communications*, Volume 218, Issues 1–3, 15 March 2003, Pages 1-10.
- [37] Su-Ping Fang, Lei-Jie Wang, Masaharu Komori, Aizoh Kubo, Design of laser interferometric system for measurement of gear tooth flank, *Optik- International Journal for Light and Electron Optics*, Volume 122, Issue 14, July 2011, Pages 1301-1304.
- [38] Jinzhong Ling, Junshan Ma, Songlin Zhuang, Experimental research on profile measurement based on laser optical feedback, *Optik - International Journal for Light and Electron Optics*, Volume 124, Issue 14, July 2013, Pages 1770-1772.

- [39] Tung Hsien Hsieh, Wen Yuh Jywe, Hsueh Liang Huang, Shang Liang Chen, Development of a laser-based measurement system for evaluation of the scraping workpiece quality, *Optics and Lasers in Engineering*, Volume 49, Issue 8, August 2011, Pages 1045-1053.
- [40] <http://www.microscopy.olympus.eu/microscopes>. Accessed on 10th November, 2013.
- [41] M.N. Durakbasa, P.H. Osanna, P. Demircioglu, The factors affecting surface roughness measurements of the machined flat and spherical surface structures– The geometry and the precision of the surface, *Measurement*, Volume 44, Issue 10, December 2011, Pages 1986-1999.
- [42] H.Y Kim, Y.F Shen, J.H Ahn, Development of a surface roughness measurement system using reflected laser beam, *Journal of Materials Processing Technology*, Volumes 130–131, 20 December 2002, Pages 662-667.
- [43] Jason Mah, Claire Samson, Stephen D. McKinnon, Denis Thibodeau, 3D laser imaging for surface roughness analysis, *International Journal of Rock Mechanics and Mining Sciences*, Volume 58, February 2013, Pages 111-117.
- [44] <http://www.jrradios.com/Products/Default.aspx?ProdID=JRP03441>. Accessed on 12th November, 2013.

PART II

GEAR PROFILE MEASUREMENT WITH INTEGRATED VISION SYSTEM

Table of Contents

Contents	Page no.
PART II.....	100
Table of Contents.....	101
List of Figures	105
List of Tables	107
CHAPTER 1	108
INTRODUCTION.....	108
1.1 Introduction.....	108
1.2 Previous gear measurement system	109
1.3 Problem statement	109
1.4 Research objectives	110
1.5 Research methodology.....	111
1.6 Thesis organization	112
CHAPTER 2	113
BACKGROUND STUDY	113
2.1 Introduction.....	113
2.2 Conventional gear profile measurement.....	113
2.3 Various methods of gear measurement	115
2.4 Gear profile measurement.....	117
2.5 Summary.....	118
CHAPTER 3	119
METHODOLOGY AND RESULTS OF GEAR MEASUREMENT	119

3.1 Introduction.....	119
3.2 Test gear	122
3.3 Gear measurement systems.....	122
3.3.1 Example of conventional gear measurements.....	123
3.3.2 Developed gear measurement system	124
3.3.2.1 Features of the applied stylus.....	124
3.4 Measurement procedure.....	126
3.5 Whole circumference measurement.....	127
3.6 Tooth flank.....	129
3.7 Measurement results for gear circumference.....	130
3.8 Summary.....	133
CHAPTER 4	135
VISION IN MEASUREMENT	135
4.1 Introduction.....	135
4.2 Camera in measurement	135
4.3 Measurement without camera.....	135
4.4 Camera in gear profile measurement.....	136
4.5 Dynamic tracking in measurement	138
4.6 Proposed static tracking in measurement	138
4.7 Summary.....	139
CHAPTER 5	140
CAMERA BASED STYLUS TRACKING	140
5.1 Introduction.....	140
5.2 Image processing algorithm in proposed system.....	140

5.3 Image processing steps	141
5.3.1 Image acquisition	141
5.3.2 Reference image.....	142
5.3.3 Two frames difference.....	142
5.4 Motion threshold.....	142
5.5 Purpose of Image processing	144
5.6 Apply color filter from the given colors (Euclidean filtering).....	145
5.7 Find objects based on the selected size.....	146
5.8 Find the biggest object.....	146
5.9 Draw object position in bitmap.....	147
5.10 Geometric position of the object in x and y coordinates	147
5.11 Save data in .dat and .rtf formats	147
5.12 Image features.....	148
5.13 Overall gear profile measurement system	149
5.14 Camera system for gear measurement	150
5.15 Stylus tracking based on colors	151
5.16 Controls in precision measurement	154
5.17 Accuracy of the proposed method	155
5.18 Comparison of the result with the existing method	156
5.19 Single camera measurements.....	156
5.20 Multiple camera measurement.....	157
5.21 Summary.....	158
CHAPTER 6	159
CONCLUSION AND FUTURE WORKS.....	159

6.1 Conclusion	159
6.2 Future works	160
ACKNOWLEDGEMENTS	161
REFERENCES	162

List of Figures

Figures	Page no.
Fig. 2. 1 Conventional tooth profile measurement system.....	113
Fig. 3. 1 Front view of gear measuring machine.....	119
Fig. 3. 2 Spur gear	122
Fig. 3. 3 Conventional measurement: scanning of left tooth flank	123
Fig. 3. 4 Conventional measurement: scanning of right tooth flank	123
Fig. 3. 5 Measurement probe with stylus	124
Fig. 3. 6 Developed method for measurement without detaching the probe.....	125
Fig. 3. 7 Developed gear measurement system	127
Fig. 3. 8 Measured whole circumference outline at 3.0 mm/s	128
Fig. 3. 9 Measured whole circumference outline at 5.0 mm/s	128
Fig. 3. 10 Measured surface in discrete point probing	130
Fig. 3. 11 Measured surface in pre-defined path scanning.....	130
Fig. 3. 12 Enlarged view around the tip edge.....	131
Fig. 3. 13 Modified surface in pre-defined path scanning.....	132
Fig. 3. 14 Corrected enlarged image around the tip edge.....	132
Fig. 4. 1 Camera setting to track the stylus	139
Fig. 5. 1 Image after applying two frame differences	142
Fig. 5. 2 Resulted Image when threshold value is 128.....	143

Fig. 5. 3 Stylus tracking.....	144
Fig. 5. 4 Camera setting with the desire color to be tracked	145
Fig. 5. 5 Camera setting to track the purple color	145
Fig. 5. 6 Filtering objects less than the selected range	146
Fig. 5. 7 Video opening with the initial settings.....	147
Fig. 5. 8 Probe's travel directions.....	149
Fig. 5. 9 Experimental apparatus for measuring gear profile	150
Fig. 5. 10 Tracking of various moving pens based on colors in (a), (b), (c) and (d).....	151
Fig. 5. 11 Tracking of a deep red object	152
Fig. 5. 12 Tracking of red object	153
Fig. 5. 13 Simplified feedback control model.....	154

List of Tables

Tables	Page no.
Table 3. 1: Specification of direct drive gear measuring machine	120
Table 3. 2: Specifications of 3D scanning probe.....	121
Table 5. 1: Color based stylus tracking	155
Table 5. 2: Overall accuracy of the system.....	156
Table 5. 3: Comparison between develop and existing methods.....	157

CHAPTER 1

INTRODUCTION

1.1 Introduction

In the variety of industrial products due to the advancement of processing techniques, components and products with free-form surface shapes are made and use in various fields such as vehicles, airplane, ship, mechanical components etc. To meet the requirements of high-precision processing is necessary to get high precise output. To confirm the accuracy in the manufactured parts high -precision measurements is highly necessary. Surface parameters of a mechanical component can be measured into two ways; one is the conventional method and the other is applying Coordinate Measuring Machine (CMM). Conventional machine can measure specified types of surfaces and it cannot apply on various types of components, thus; it does not have measuring flexibility. On the other hand; CMM types of machines can measure various types of mechanical components and has great flexibility.

Surface topography is of great importance in specifying the function of a surface. Gear profile measurement is one of the important issues in mechanical engineering. The correct shape of the gear has great influence in the output of mechanical components. Measuring gear profile within short time is very desirable and useful to improve the total system. The most important parameter describing surface integrity is surface roughness (R_a). In the manufacturing industry, surface must be within certain limits of roughness. Therefore, measuring surface roughness is vital to quality control of machining work piece as well as to enhance performance in general. Improving the versatility of the gear measuring machine is desired in such situation where fatigue occurs specially in tooth root.

1.2 Previous gear measurement system

Analysis of the accuracy of gears at different stages of technological process requires control of geometrical surface parameters with the use of coordinate measuring methods [6-8]. A technique of “Machine Vision Based Identification and Dimensional Measurement of Electronic Components” which is based on color pattern matching approach, that enables identification of an electronic component present in a group and its gauging gives the dimensional measurement of the electronic component [13]. A method for the precise and accurate measurement of part features such as edges require collimated light, careful placement of the part, a telecentric lens, calibration and perhaps optical distortion correction, and computation by the vision system’s computer is proposed [14]. A geometric analysis of laser beam for underwater vehicle in measuring distance is discussed [15]. In this case, the moving object’s distance is calculated by comparing it to a reference object.

A bevel gear measurement system is elaborated in [18]. In another research article [27], a new standard is described for measuring bevel gear with unusual flexibility. In another study [28], a generated hypoid gear tooth flank form is complicated and has a significant influence on the overall performance. In that research a method for analyzing one of the gear dynamics excitations and contact condition of a generated hypoid gear that considers the measured tooth flank form is proposed. Specially optical measuring methods, the inspection of micro gears and alignment problems are discussed broadly. A final section indicates the actual accuracy limits of gear measurements. It highlights that a significant reduction of the measuring uncertainty associated with gears, standards and instruments is an urgent need for the production of high-precision gears [32]. A conventional gear profile measurement system for a shaving gear is shown in [33].

1.3 Problem statement

Measurement technique with high precision and additional information is of utmost necessary in gear measurement. Conventional measurement system for gear profile

measurement is very time consuming and cost effective. It also has limitation of getting extra additional shape data of the measured gear. The system can be used where time and money is not highly considered. But in the real situation; there is no production company where time and money is not considered highly. With the increment of advance technology and its parts; the conventional system should be changed to compete with the world's fast growing industries. Thus; an advance level of gear measurement system is necessary to improve its performance and to reduce production cost. The surface measurement in precision engineering is very essential. Most of the traditional measurement systems do not have integrated camera or vision system. Therefore, application of machine vision in this field is somehow new and interesting. In order to incorporate image processing and machine vision in precision engineering, gear circumference measurement is a good choice to implement. The gear measurement can be monitored through camera based vision system and it can also work as a feed-back control system to control the probe deviation during measurement..

1.4 Research objectives

The research objectives can be summarized in the following ways:

- To synchronize rotational motion with radial motion in the gear measurement system in order to reduce gear measurement time for scanning whole gear outline.
- To acquire data for tooth tips, bottom and root that cannot be measured in traditional system.
- To evaluate performance of the developed system.
- To record video, image and moving coordinate data during measurement.
- To enhance measurement safety and reliability applying vision.

1.5 Research methodology

To achieve the objectives it is very much necessary to develop a new system rather modifying the conventional one. The synchronize movement between measurement probe and spindle rotation is one of the main task to be implemented in order to achieve the goals of this research. Without synchronization; it is very difficult to reduce overall measurement time. As in traditional gear measurement, synchronization between probe and spindle movement is not integrated; it means that each axis has constants speed. Also, to know the shape accuracy of the manufactured gear surface; additional information is necessary from the measurement. For these additional data, conventional gear measurement needs another measurement and it takes extra time to pursue the task.

The important points here is that even the workpiece is required to move to separate machines for measurement due to the constraints of conventional gear measurement system. Indexing is another important issue in conventional measurement. This increased the travelling distance of the stylus during measurement and needs extra time to perform the actions. To solve above problems arises in conventional gear measurement, a new method has been introduced with four axes-movement based gear measurement system which is able to synchronize the movements of the measurement probe and workpiece spindle as well as able to acquire additional data for surface profile and thus; reduces time and production cost by generating additional features in one complete measurement. Finally; for safety and reliability it is important to integrate a camera system that decreases human danger in gear measurement and monitoring. Stylus of the measurement probe is very small and its tip is very sharp and in case of accident; it is easy to break the stylus tip and enter to human eyes or hurt another parts of the body. To avoid this unexpected danger; a camera system will surely enhance the safety and reliability of the whole measurement process.

1.6 Thesis organization

The contents of this dissertation aside from the preliminaries are organized as follows: Chapter 1 comprises of introduction. Chapter 2 contains literature review, where the previous works on measurement systems are discussed in details. Chapter 3 presents gear profile measurement system. Chapter 4 demonstrates camera based gear measurement system. Chapter 5 discusses application of camera in gear measurement with tracking results and evaluates performance. Finally; chapter 6 concludes with future remarks.

CHAPTER 2

BACKGROUND STUDY

2.1 Introduction

The main problem in gear flank measurement is time consuming in conventional measurement system. In order to solve this problem, a new strategy is proposed in this thesis. The new strategy reduces time and can acquire additional information of the gear shape for example; tooth root, tooth tip and tooth bottom profiles. The system can also measure pitch deviations at the same time. Whereas conventional system requires more time in indexing as well as cannot get additional information such as tooth tip, tooth root and bottom profiles.

2.2 Conventional gear profile measurement

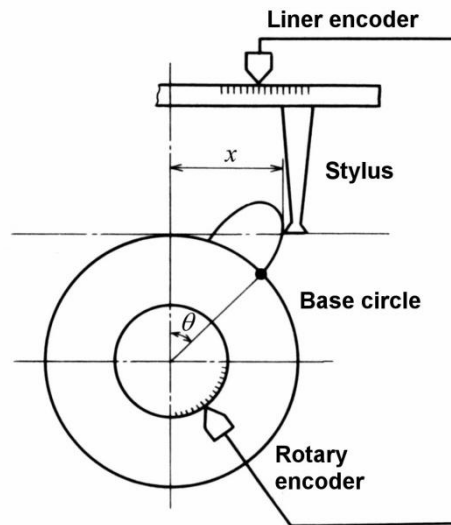


Fig. 2. 1 Conventional tooth profile measurement system

Figure 2.1 introduces a traditional gear measuring machine. This kind of machine is very useful and efficient where high precision and efficiency are necessary. This is usually applied to measure the parameters of involute type of gears. This is only

applicable for measuring tooth flank or pitch deviation at one time. Both of the parameters cannot be acquired at the same time. In addition; indexing time is necessary in conventional gear measurement system. This is a biggest drawback of this system as it requires much more time to accomplish the task. Moreover; it needs indexing time. To solve all the above problems; a rotational movement is integrated with the radial movement so that it generates all the necessary parameters in one measurement without detaching the stylus.

A conventional gear shape measurement system is described in [32]. This article reviews the state-of-the-art of gear metrology, where tactile probing methods dominate almost exclusively. It summarizes new modeling and measuring principles, giving a detail description and inspection of gears. Many of the conventional gear measurement machines are produced for measuring only involute gear profiles. Conventional gear can give precise results and accuracy but only for limited purposes but it takes huge amount of times. In this experimental study [35], width modification of a spur gear was investigated to fix instantaneous pressure effects along the single meshing area on the gear profile. In that gear, variable pressure distribution caused by the single and double teeth meshing and the radius of curvature along the active gear profile was almost kept constant by maintaining a constant ratio of applied load to the tooth width (F/b) on each point. In [37], analytical and experimental investigations of the influence of the deformation and wear on spur gear dynamics have been carried out. These investigations were carried out with the help of geometric and kinematic models, which took into account the reason of gear ratio changes because of the wear of teeth. To justify measurement results, user-friendly auxiliary tools are used in [39], which allows the operator to probe the measurement points according to existing guidelines and standards. Measurements were taken on a robust and highly accurate large involute gear measurement standard of the Physikalisch-Technische Bundesanstalt (PTB) under laboratory conditions. The obtained results of profile, helix and surface measurements are also discussed. In this research finding [42], a gear dynamics test set-up with integrated root strain and dynamic transmission error measurement systems is described. Dynamic factor and dynamic transmission error measurements

from unmodified and modified spur gears are elaborated and their relationship is explained experimentally.

2.3 Various methods of gear measurement

It is discussed in [26] that the use of multiple-coordinate measuring technique and appropriate, problem-oriented software; it is possible to measure manufacturing deviations on bevel gears with great precision. In contrast to the conventional bevel-gear examination, these measurements allow detail analysis of the tooth geometry to be produced. This paper [29] presents a method for measurement of deviation of the real gear tooth surface from the theoretical one with a coordinate measurement machine and compensation of repeatable parts. By investigation of characteristics of distortion of the gear tooth surface along the circle direction, the deviation is derived from distortion, and the definition of deviation with the geometrical invariability is also defined.

This paper shows [34] the results of static deflection tests on spur gear teeth made of acrylic. Also, a method is given for determining the dimensions of tapered cantilever beam to replace the actual gear tooth in deflection analysis as proposed by Timoshenko and Baud. Using the equations which were developed by Timoshenko and Baud for the tapered cantilever beam deflections are calculated and compared with those found from experimental test. In this study [36], methods of wear testing have been compared including direct gear testing and disc testing, together with displacement measurement, weight loss and direct measurement. A new method of characterizing the wear of gears is also presented, which relates actual contact conditions and gear tooth wear.

This research article [38] presents a new noncontact system for measuring pitch errors and tooth profiles. The pitch error measuring system has two optical probes that are equivalent to the fixed probe and measuring probe, respectively, of the pitch variation measuring machine based on the measuring of straight distance. As there is no mechanical interference between the probes and the test gear, high-speed

measurements can be carried out with this system. In another similar study [43], an integrated stereo vision system applied in Coordinate Measuring Machine (CMM) is introduced. That research evaluates the accuracy of different camera calibration and measurement methods used in 3D stereo vision with CCD cameras. These methods are evaluated by means of several precision tests, determining their error limits under specified conditions of operation.

A new type of master gear, the Gauge Block Gear (GBG), was developed for the performance verification of coordinate measuring machines (CMMs) in [44], for the specific task of pitch and chordal tooth thickness measurement. Its main characteristic is the replacement of the teeth with gauge blocks to achieve direct traceability of the chordal tooth thickness. Mathematical models for the geometrical definition of cylindrical gears with involute tooth, data evaluation, and assessment of the task-related uncertainty, were formulated, and measuring strategies for CMMs were designed and implemented in that research. In this paper [46], an indirect measurement based on the virtual gears model (VGM), obtained by NUBS fitting of the surface points measured by CMM is presented. By comparing the VGM with CAD model (soft-master model), various errors such as tooth profile error and tooth trace error can be automatically measured with this proposed method.

This paper [47] presents a new system of measuring cutting errors of flexspline (FS) gears of harmonic speed reducers for quality control of the hobbing machine used to cut the gear. Two laser displacement probes are used in this research in order to replace the conventional measurement method that employs a combination of Van-Kuven wires and a micrometer. The presented [48] novel micro gear standard uses cylinders to model the involute tooth flanks. The approach describes the estimation of the uncertainty of measurement for measurements of the profile, helix, pitch and tooth flank deviations. Furthermore, initial measurement results of a prototypical standard are provided in the above article. To the problem of gear parameters measurement, this paper [50] has presented a system design method based on machine vision. Firstly, gear image was captured by CCD and input into computer for processing. Then, gray image processing methods such as noise removal, binary conversion and mathematical

morphology have been conducted. After that, a method for gear center location and gear teeth number counting is proposed and the other parameters can be obtained by calculating. In this research [52], the technique of conventional photoelasticity has been reviewed to explore the possibility of using it as a supplementary technique to experimentally measure the variation of gear mesh stiffness. In addition to that an attempt has been made to calculate the variation of mesh stiffness for a pinion having a cracked tooth and a gear tooth with no crack of a spur gear pair.

2.4 Gear profile measurement

A scanning measurement of tooth flank form of generated face mill applying 2 axes measurement system with sensor is explained in [15]. In another study [30], a laser interferometric system (LIS) based on oblique incidence and phase shifting technique has been designed for the measurement of gear tooth flank. A spur involute gear has been selected with a module of 2.0, 60 teeth, and a 20-mm face width, some calculated critical parameters of the LIS are considered, the oblique incidence angle is 84.5° , the beam diameter is 20 mm, and the focal length of imaging lens is 100 mm. In separate article [31]; a numerical simulation of the wear sustained by the surface of a Forschungsstelle fuer Zahnrad und Getriebebau (FZG) pinion during a gear micropitting test was performed. Underlying the simulation on a mixed lubrication model that takes into account surface roughness and lubricant properties, as well as a wear model based on Archard's wear equation. The adequacy of the models was ascertained by comparing simulated and measured roughness profiles at the end of each stage in that study. As there is no mechanical interference between the probes and the test gear, high-speed measurements are possible with this system [38]. In that system, a measuring time of 3 to 4 seconds was required to measure the pitch errors of a spur gear with a module of 0.8 and 48 teeth. Apart from that, modern bevel gear inspections with CMMs only measure the pitch deviations on both flanks and subsequently estimate runout deviation based on explicitly less information than the classical (direct) runout measurement. This paper [40] presents a new approach for

this evaluation problem and compares theoretical and experimental runout results carried out with several CMMs. In another study, roundness measurement for discontinuous perimeters via machine visions is also discussed [41].

2.5 Summary

This chapter presented various types of existing gear measurement systems; difference between conventional and advance level of gear measurement; gear parameters measurement and the improvement of the gear measurement systems up to the latest development.

CHAPTER 3

METHODOLOGY AND RESULTS OF GEAR MEASUREMENT

3.1 Introduction

Measuring gear circumference and saving its data and information are useful for improving measurement performance and reliability. **Figure 3.1** shows a 3D gear measurement machine. **Table 3.1** indicates the specification of a direct drive gear measuring machine which is used to measure gear circumference. There are three motors for the probe movement. One controls the linear motion of the probe and two other control axial and radial movement of the probe.

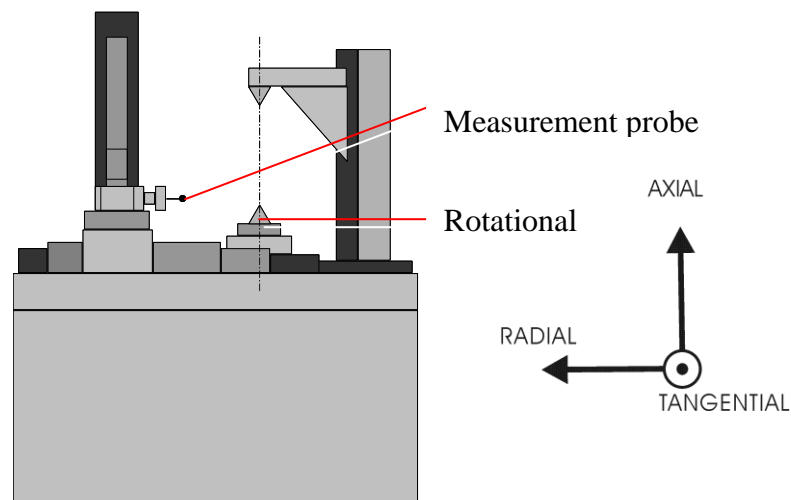


Fig. 3. 1 Front view of gear measuring machine

In addition; rotary spindle for mounting a workpiece (Spindle axis) is applied to shorten the scanning time. The position detection of each axis is done by the linear scale, the minimum resolution, $0.1 \mu\text{m}$. Tangential axis has a resolution of $0.05 \mu\text{m}$ and axial axis $0.1 \mu\text{m}$. The meaning of resolution for each motor here is that; the motor can detect the minimum displacement based on the specified division in micro

meter level. Furthermore; all axes apply closed-loop control system. Scanning results are obtained by a voltage value at the same time through the displacement of the three mutually perpendicular axial directions. Measuring range of the scanning probe can be displaced up to 1 mm. In conjunction; the stylus tip attached to the probe measurement is made by artificial ruby ball of 2 mm nominal diameter. The detail features of the measurement machine are given in **Table 3.1**.

Table 3. 1: Specification of direct drive gear measuring machine

	Tangential axis	Axial axis	Radial axis
Motor	Linear motor	Servo motor	Servo motor
Guide	Roller guide	Casting guide	Roller guide
Drive shaft	Direct drive	Ball screw	Ball screw
Position detection device	Linear scale	Linear scale	Linear scale
Position detection resolution	0.05 μm	0.1 μm	0.1 μm
Control	Full closed loop	Semi closed loop	Semi closed loop

Table 3.2 shows the specifications of the 3D scanning probe for the developed gear measuring system. All the motors are controlled applying either the closed loop control method or semi-closed loop control method.

Table 3. 2: Specifications of 3D scanning probe

Three-dimensional probe	
Probe attribute	3axis measurement(X,Y,Z) Linear and parallel motion in all axes
Measurement range	± 1 mm in all axes and orientaions with a 50mm, 4.6g stylus
Overtravel range	X,Y and -Z protected by a kinematic joint
Resolution	0.1 μ m
Spring rate	120mgf/mm nominal (X,Y,Z)
Damping	20% (X,Y,Z) typical
Weight	299g
Power supply	12V to -12V, 5V (± 10 V)
Outputs(X,Y,Z)	Analogue propotional Voltage Output scaling : 4V to 8.5V/mm
Mounting	mounted directly

3.2 Test gear



Fig. 3. 2 Spur gear

Figure 3.2 shows a test spur gear which is tested for justifying the output from the developed method. As shown in this figure; this is an involute cylindrical spur gear, whose module is 6, the number of teeth is 21, the pressure angle is 20° and the face width is 15 mm. Gear working tooth flank, root, bottom and tip edge profiles are geometrically regarded as unknown profiles depending on cutter paths.

3.3 Gear measurement systems

Gears are normally measure in both traditional and advance ways. Both the ways have their own advantages and disadvantages. Based on our requirements; proper machine can be selected but compared to the conventional measurement system; the output of the developed measurement system has much more scanning data information and it saves time about 95% as well as it is 20 times faster than the conventional gear measurement system. For the above mentioned reason, developed gear measurement system has greater advantages over traditional gear measurement system.

3.3.1 Example of conventional gear measurements



Fig. 3. 3 Conventional measurement: scanning of left tooth flank



Fig. 3. 4 Conventional measurement: scanning of right tooth flank

Figures 3.3 and 3.4 show a measurement of the test gear using conventional measurement machine. **Fig. 3.3** shows the measurement of the left tooth flank whereas **Fig. 3.4** shows the measurement of the right tooth flank by the traditional gear

measurement machine. It requires two opposite directional rotations for the spindle to perform the action where as the radial movement is on the same axis. Probe moves linearly forward and backward during measurement, thus; index motion is necessary.

3.3.2 Developed gear measurement system

The probe based gear measurement system is described below in details.

3.3.2.1 Features of the applied stylus

Figure 3.5 shows the stylus which is attached to the measurement probe. It has the following characteristics:

- Stylus materials = Ruby
- Stylus tip diameter = 2 mm
- Dimension tolerance of stylus tip = $\pm 5.63 \mu\text{m}$
- Sphericity (Spherical shape of the tip) = $0.13 \mu\text{m}$
- Voltage changes based on the displacement of measuring range = ± 1 mm.



Fig. 3. 5 Measurement probe with stylus

Figure 3.6 shows the developed measurement system for gear profile which can solve all the above problems at one time by saving a huge amount of time during experiment. The proposed measurement system has advantages to overcome long-time consuming measurement procedure because the developed technique is to scan whole circumference of a cylindrical gear circumference including gear tooth flanks, tooth tip, root and bottom profiles without detaching the stylus tip from the gear surface. It can also be done with two axes movement; the first axis for the linear stylus movement in radial direction of a target gear and the second axis for the rotational motion of the target gear.

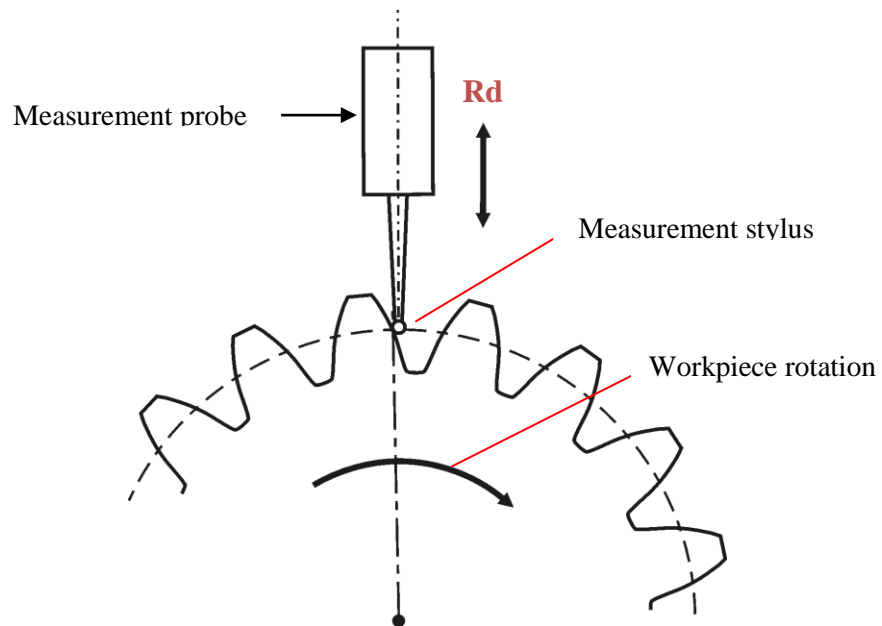


Fig. 3. 6 Developed method for measurement without detaching the probe

The movement of the stylus is reciprocal along the radial direction during one tooth space measurement. The distance of stylus movement in this method is shorter than that in the conventional one. However; the scanning speed is not constant. The rotational speed of the workpeice is not constant either. Therefore; the synchronized movement control of both axes is the key issue in order to achieve the constant scanning speed in complete measurement.

3.4 Measurement procedure

Applying the developed method; the measurement procedures are described below. Discrete-point probing (DPP) is applied at first as this technique is more reliable to measure unknown gear profiles than direct scanning measurement. Applying the resulted data of DPP as nominal data for pre-defined path scanning (PPS), scanning measurement is finally carried out. Not only the tooth root and bottom profiles but also the working tooth flank profiles and tip edges are measured at the same time. For the test spur gear; at first, the stylus tip touches 10 points on a single gear tooth space in the radial direction. Next, the intervals between the 10 points were interpolated by spline interpolation. The stylus tip approaches the interpolated point along the normal vector of the spline curve. Total numbers of DPP data for the above test spur gear were 91. One tooth's nominal data is enough for the PPS to be performed. The total number of DPP is obtained by multiplying with the total number of tooth of the whole gear. PPS follows the calculated path by DPP and perform the necessary action. This way; additional time and information are not required for gear profile measurement. It also avoids the repetition of the same process. **Figure 3.7** shows the image of gear measurement of the developed system. Here we can see that the stylus is scanning tooth bottom which is impossible to measure by the conventional gear measurement machines.

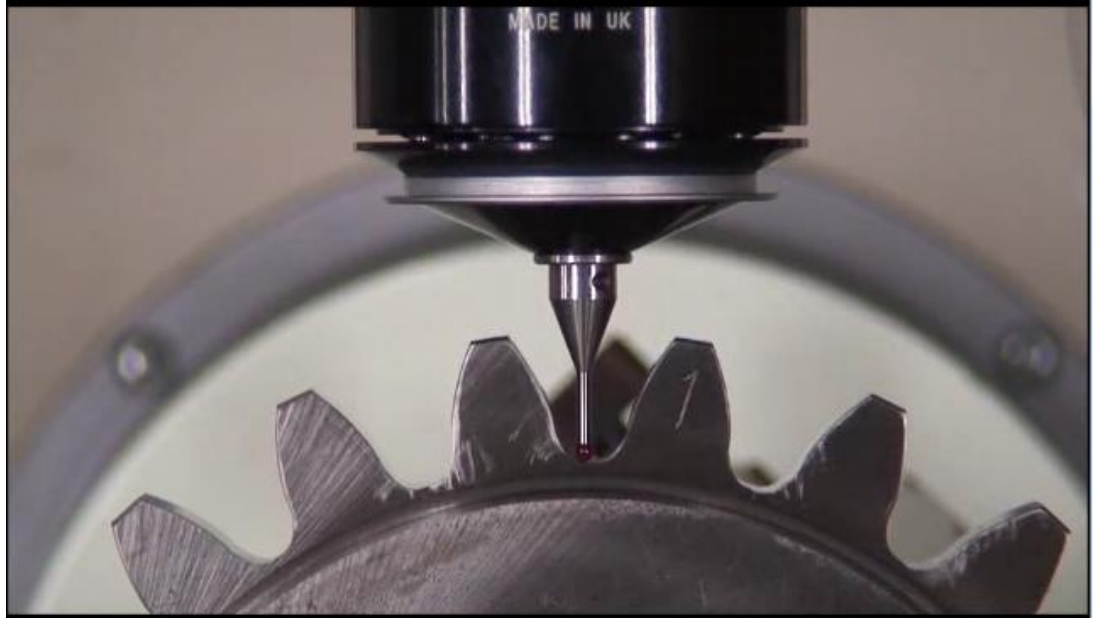


Fig. 3. 7 Developed gear measurement system

3.5 Whole circumference measurement

All tooth spaces are successfully measured and root, bottom as well as tip profiles have generated expected shape as shown in **Fig. 3.8**. At a speed of 5.0 mm/s, the outline shapes are completely the same. PPS measurement at the scanning speed of 7.0 mm/s was also carried out and the measurement itself has been succeeded, however; the outline at the tip edge had slight overshoot in its shape. It is due to the servo-control limitation. To eliminate this problem; servo motor with expected properties and further intelligent control is necessary.

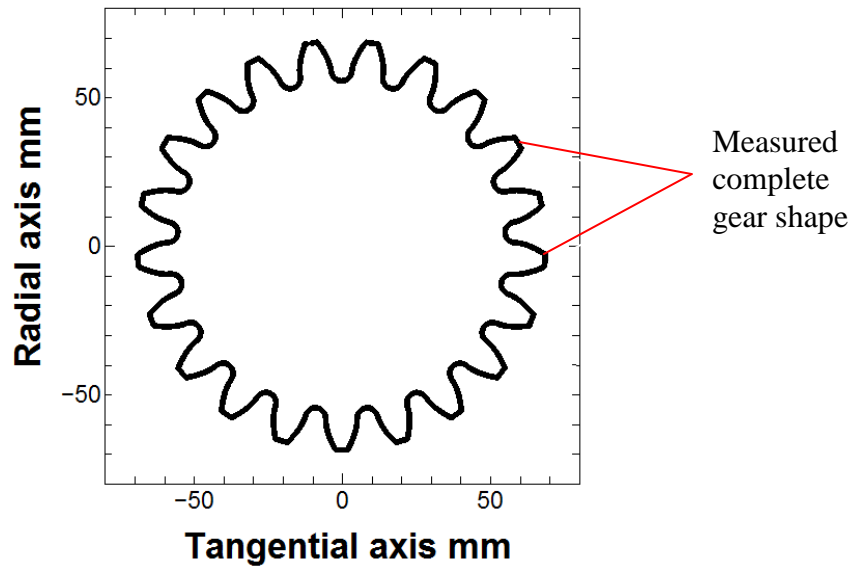


Fig. 3. 8 Measured whole circumference outline at 3.0 mm/s

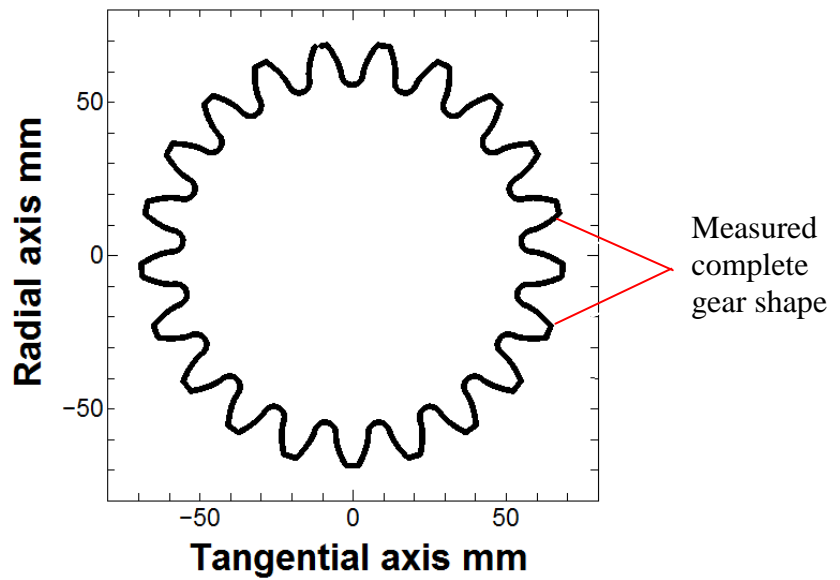


Fig. 3. 9 Measured whole circumference outline at 5.0 mm/s

In overall; PPS has great advantage because it can get more than 6,000 data points in a single tooth space and it takes only 9s, while DPP takes about 200s. Only in a twentieth time interval, more than 80 times data points are obtained by PPS.

Figures 3.8 and 3.9 show the resulting shapes of the gear profile at the scanning speeds of 3 mm/s and 5 mm/s respectively. In addition; the proposed method has better performance as it measures whole data generating information of tooth profiles of both working tooth flanks of all teeth, tip diameter, the edge shapes of tooth tips, root and bottom profiles of all teeth as well as pitch deviations. One of the interesting applications is 3D evaluation of tooth spaces. Using the same nominal data, different cross sections can be scanned on a single tooth space. A radius of tooth root is conventionally evaluated by a profile projector but it is quite hard to achieve the accuracy up to 0.01 mm order applying conventional methods. Applying PPS, different cross sections are measured in a short time and highly accurate 3D evaluation can be carried out easily.

3.6 Tooth flank

Tooth flank measurement by conventional as well as by the developed gear measurement system is similar but differs from each other by the scanning speed and total scanning time. In addition; conventional measurement system needs extra indexing time. From the experiments that are conducted in the laboratory; it is observed that both the left tooth flank and right tooth flank can be measured by the conventional and developed systems. Conventional measurement system generates higher peak values compare to the developed one. In case of the developed measurement system; the generated micro deviation can be avoided by correcting the spline shape during DPP measurement. As a result; it improves the measurement accuracy.

3.7 Measurement results for gear circumference

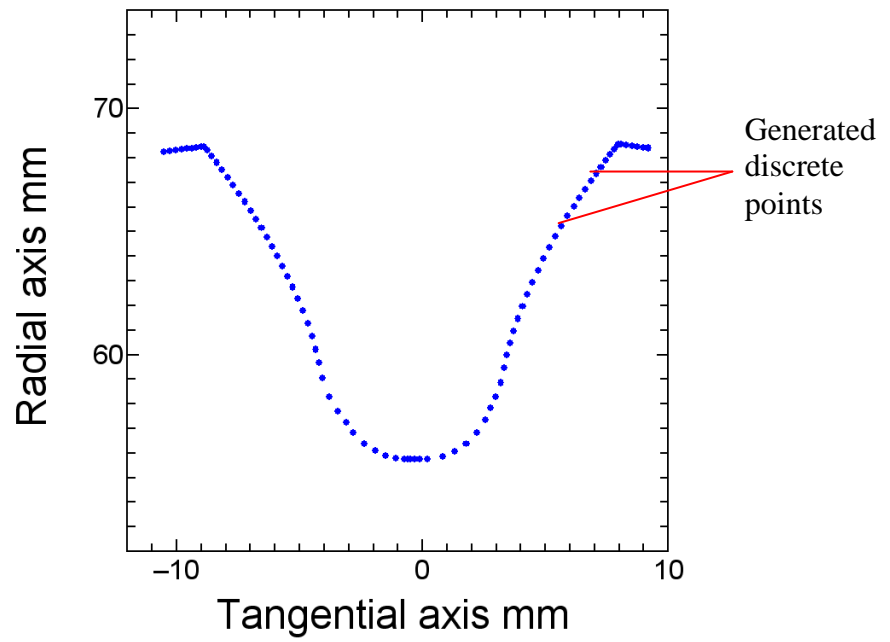


Fig. 3. 10 Measured surface in discrete point probing

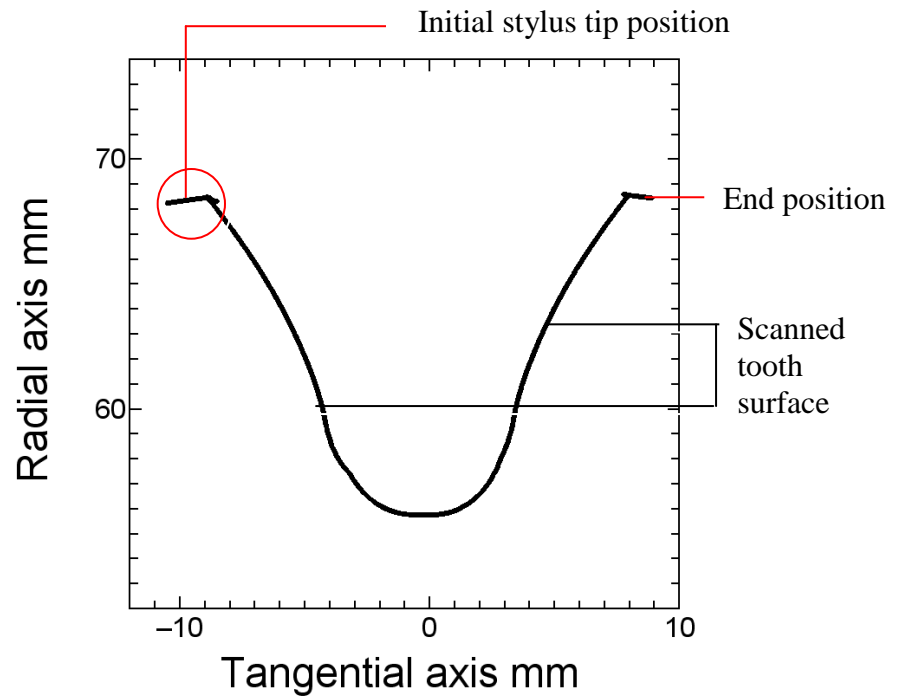


Fig. 3. 11 Measured surface in pre-defined path scanning

The result of DPP measurement is shown in **Fig. 3.10**. Regarding the DPP data as target point for PPS, scanning measurement was made at a scanning speed of 3.0 mm/s. Initial position of stylus tip is shown in **Fig. 3.11**.

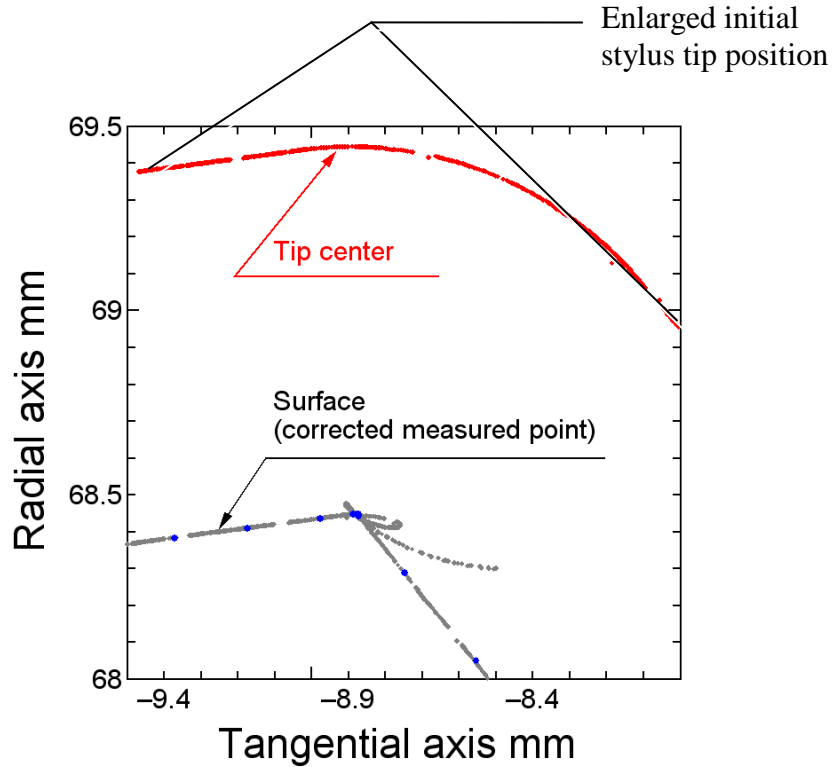


Fig. 3. 12 Enlarged view around the tip edge

Working tooth flanks and root as well as bottom profiles are measured correctly, however; the obtained tip edge profile contained some errors in corrected measured points. An enlarged view around the left tooth tip edge is shown in **Fig. 3.12**. Since the loci of the stylus tip center are obtained correctly, the compensation procedure of the radius of the stylus tip seems to be incorrect. The reason why the surface data have some errors is that the normal vectors for radius compensation are calculated from the measured curve of the stylus tip center. The curve of the stylus tip center has slight

fluctuation because the actual surface has surface roughness and some other vibration influence on the stylus tip during measurement.

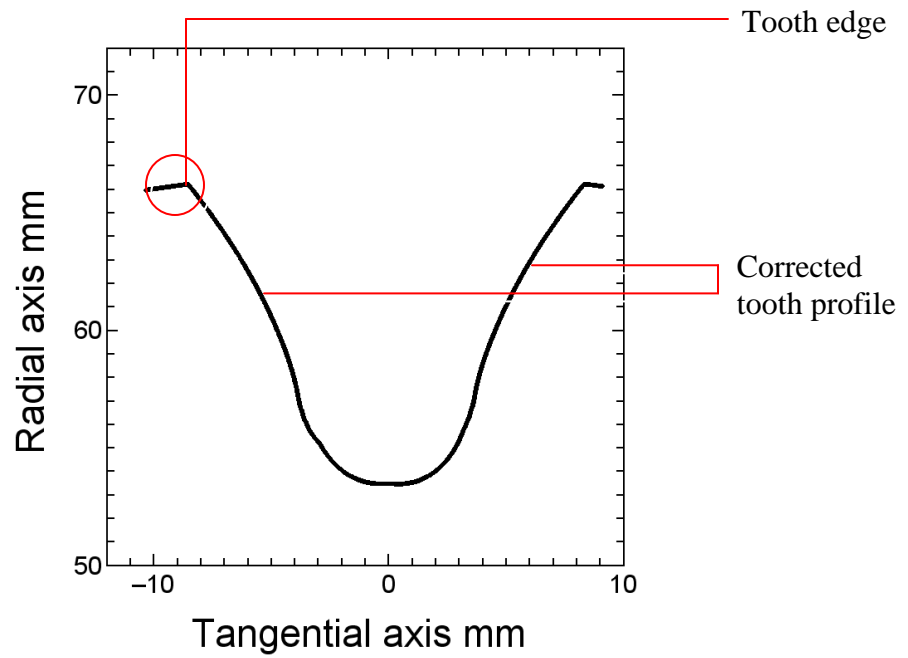


Fig. 3. 13 Modified surface in pre-defined path scanning

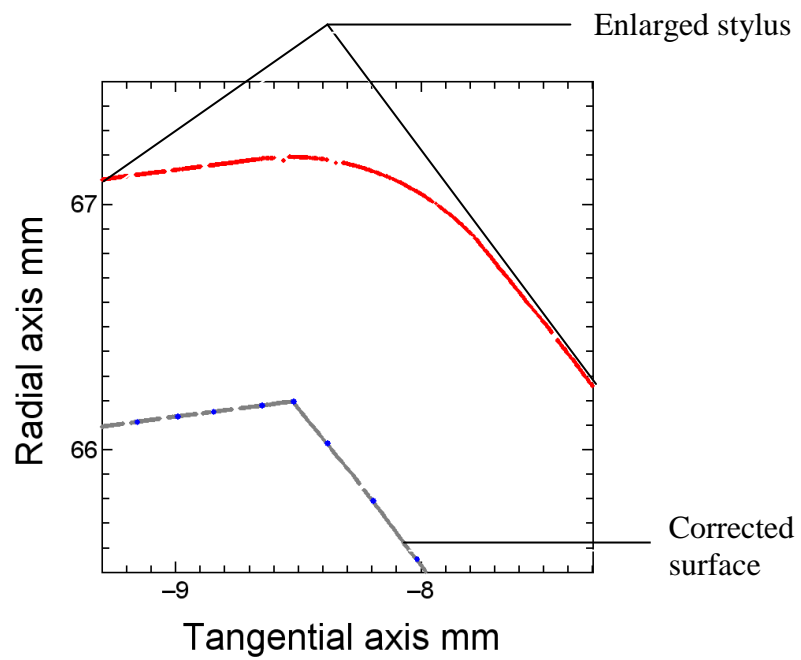


Fig. 3. 14 Corrected enlarged image around the tip edge

Since fluctuation of the normal vectors must be excluded, the modified normal vectors to be used are calculated from the interpolation curve of measured DPP data. Intervals of DPP data are larger than those of PPS. For this reason; it is predicted that the interpolated curve and resulting normal vectors do not have fluctuation. By applying modified normal vectors and removal method of close-spaced points, a single tooth space is measured and corrected measured points are calculated as shown in **Fig. 3.13**. The tip edge profile seems to be improved. A corrected shape of the enlarged image view around the left tooth tip edge is shown in **Fig. 3.14**.

The profile of corrected measured points is very clear and there is no unexpected error. In this case, there is an assumption that the tip profile consists of sharp edge but in actual tip profile there is a certain roundness or chamfer. It is necessary to consider the tip roundness and chamfer in the future development. Since the PPS measurement is successfully carried out for a single tooth space, DPP target points are copied for every pitch of all other tooth spaces and the set of copied target points is regarded as the nominal data for whole circumference of the gear profile after acquiring DPP data for a representative single tooth space. The measurement procedure is completely the same as that for a single tooth space after the nominal data is applied in PPS measurement.

3.8 Summary

The aim of this research is to develop a high-functional Gear Measuring Machine (GMM) and a 3D scanning probe is integrated with GMM in order to analyze gear measurement in various patterns. The proposed measurement strategy is necessary to scan whole circumference of a cylindrical gear circumference including working tooth flanks, tooth tip, root and bottom profiles without detaching the stylus tip from the gear surface that are impossible to measure by the conventional GMMs. Applying Pre-defined Path Scanning (PPS) method with a highest scanning speed of 7.0 mm/s was successfully carried out. In addition; different cross sections were also measured by PPS within short time. The profile acquired from the measurement data, generates

similar shape with the real photograph of the gear profile. The tip edge is one of the challenging shapes to be measured, but it was also obtained with better accuracy by adjusting the nominal data. The developed method has greater advantage over the existing CMMSs as it gives complete measured data information of tooth profiles of both tooth flanks of all teeth, tip diameter, the edge shapes of tooth tips, root and bottom profiles of all teeth as well as pitch deviations in one complete measurement. As the useful deviation parameters can be obtained by only one complete scanning for a target gear, it is very useful in terms of applications for mass production industries.

CHAPTER 4

VISION IN MEASUREMENT

4.1 Introduction

Camera and vision is very important in precision engineering specially in surface measurement and evaluation process. The application of machine vision or camera enhances safety and reliability of the system. The existing applications of machine vision show the importance of the camera system in precision measurement.

4.2 Camera in measurement

A camera based gear tooth measurement system is proposed in [5]. There are two cameras integrated to the projector and both are controlled through computer. This system has some limitations as well. In this system; camera needs to have reasonable frame per second (fps) to process the require data. In addition; turn table should move accordingly during measurement in order to measure whole gear teeth.

4.3 Measurement without camera

This system [18] is similar to the developed system in our laboratory. The main difference between this one [18] and the developed one is the implementation of the rotational movement into the measurement; as well as integrated vision system. In the developed vision based measurement system, we use cameras and one stylus attached to the probe in order to measure the gear profile. Due to the integration of camera with the system, the safety and reliability increases with the increment of overall performance such as reducing measurement time by the developed system. Another system [17] is used to measure the space of circular rings, and comparison with the results measured by universal tool microscope shows the maximum absolute measurement error of this system is below $8\mu\text{m}$. The measurement of image itself is often a principal method for acquiring scientific data and generally requires that features or structure be well defined, either by edges or unique color, texture, or some

combination of these factors. In our previous research, a vision based measurement system is presented [1-2]. To investigate mechanical damage of the apple, a vision based detection system is discussed in [3]. Based on image processing application, the apple's skin damage checking was accomplished here [3]. RGB is often considered as the standard in many programming languages, and it is used in many important color image data formats, such as JPEG, TIFF, etc. True color consists of 24 bits of RGB color, 1 byte per color channel for 24 bits. In order to enhance performance, a 32-bit or 4-byte representation is often used because various commands are optimized for groups of 4 bytes or more [4]. Another important issue described is the impact of measurement performance in automatic mode on the quality of performance in case of the numerical image of scanned surface, from the standpoint of accuracy and number of collected data points within the shortest time. The discussion includes an analysis of conditions related to the measurement works, such as the process of preparing the model and measurement equipment as well as the data processing capacity [5].

4.4 Camera in gear profile measurement

A vision based non-contact gear profile measurement system is discussed in this research [20]. It consists of two main parts, developed hardware and developed software. The hardware consists of three items. The first item is the backlighting table (1), which is a lighting box with diffusing surface at its front, and it is used to produce a back lighting for the gear to be measured (2). The second item is a CCD color video camera (3) and a set of lenses with different focal lengths. The camera is carried by a camera holder (4). The third item is a 24 bit per pixel (ELF VGA) frame grabber video card (5), which is installed inside the PC computer (6) and connected to the CCD camera. Capturing software (7) is provided with the frame grabber to acquire images and save it to files with various types of file formats [20]. In another case, a low-quality frame grabber results in poor performance and instability of the entire system. For this reason, one commercial frame grabber called myVision USB is used to perform the desire activities in [9]. In 2009, Fukuda and others have presented a cost-

effective (a term previously introduced by Lee and Shinozuka [10]) vision based displacement measurement system applied to large-size civil engineering structures, such as bridges and buildings [11]. They also implemented a TCP/IP (transmission control protocol/Internet protocol) for communications and carried out time synchronization for the time synchronization of the system.

More recently, in 2011, Choi and others have introduced a vision based structural dynamic displacement system using an economical hand-held digital camera. In this case, a recorded video containing dynamic information of target panel attached directly to the civil structure was processed with image resizing method, and mm/pixel coefficient updating process, then the structure displacement was successfully determined by calculating the target position in each frame [12]. Another evaluation based on Minimum Zone Circle (MZC) method as to comply with the definition of roundness error given by Y14.5M-1994 and ISO 1001 is discussed and highlighted the advantage of applying machine vision in the non contact nature of the measurement process which can be implemented in-process of making the cylindrical part [16]. A bore scope measurement system based on machine vision, which was composed of a bore scope, a CCD camera, an industrial computer, and a precision linear stage mounted with an optical linear encoder, was developed. The image processing algorithm was developed based on IMAQ Vision [17]. The types of measurements that can be performed on entire scenes or on individual features are important in determining the appropriate processing steps [18]. A computer vision algorithm for measurement and inspection of spur gears using multiple available software is proposed in order to increase the accuracy only limited to a maximum outer gear diameter of 156 mm [20].

Similarly, computer-aided inspection using a machine vision system is one of the many new technologies adding to the efficiency of manufacturing processes and metrology in [44]. An algorithm for line segment measurement is developed to improve edge orientation detection in general edge detectors. In addition, a way to explicitly determine the measurement loss for a machine vision system is developed in that research. Measurement loss is also studied by the cost caused from measurement

error which is composed of acceptance and rejection errors. In that case, users can evaluate if a machine vision system is feasible for the application.

4.5 Dynamic tracking in measurement

The C-Track dual-camera sensor is a complete portable 3D measurement tracker that offers probing inspection and dynamic measurement capabilities [19]. It is fitted with high-quality optics and special lighting, enabling it to measure all reflectors within its operating distance. The probing stylus is very useful for aligning parts with respect to a referential (calculated using a group of reflectors), which allows movement or deformation monitoring directly on the part's referential [19].

4.6 Proposed static tracking in measurement

Figure 4.1 shows camera setting position for the measurement probe as well as target stylus which is to be tracked during measurement. In this setting condition, camera is placed 30 degree angular inclination from the target stylus tip. The position can be changed based on the desire location and optimum focus point. One of the target points of the camera position is on the top of the measurement stylus. In this situation, the good image and video can be acquired from the camera.



Fig. 4. 1 Camera setting to track the stylus

4.7 Summary

As discussed above that the existing gear measurement machines do not integrate camera for stylus tracking as well as control through camera in precision engineering such as gear circumference measurement. In addition; human safety is also in danger during monitoring this kind of high speed (10 mm/s) measurement probe and stylus. The purpose for the development of this new technique is to implement vision in precision measurement based on the stylus tracking; thus it enhances the safety and reliability during gear measurement. In addition to that; vision based gear measurement system can be applied to monitor the measurement of micro gears where human eyes have great possible danger in monitoring such kind of micro gear measurement specially at a scanning speed higher than 5 mm/s.

CHAPTER 5

CAMERA BASED STYLUS TRACKING

5.1 Introduction

Image processing is a method to convert an image into digital form and perform some operations on it, in order to get an enhanced image or to extract some useful information from it. It is a type of signal dispensation in which input is image, like video frame or photograph and output may be image or characteristics associated with that image. Usually Image Processing system includes treating images as two dimensional signals while applying already set signal processing methods to them. It is among rapidly growing technologies today, with its applications in various aspects of a business. Image Processing forms core research area within engineering and computer science disciplines too [49].

Image processing basically includes the following three steps:

- Capture the image or import the image.
- Analyzing and manipulating the image which includes data compression and image enhancement.
- Finally, acquire desire output of the image.

5.2 Image processing algorithm in proposed system

Image processing has several steps to perform in order to acquire the most accurate image from the source. One of the most common approaches for image processing is to compare the current frame with the previous one. It's useful in video compression when it is necessary to estimate image changes and to save only the changes into the hard disk rather saving the whole frame. But it is not the best one for motion detection applications. There are many other options for motion detection in image processing.

5.3 Image processing steps

The applied image processing method follows the steps in sequence as mentioned below.

5.3.1 Image acquisition

Depending on the field of work, a major factor involved in image acquisition in image processing sometimes is the initial setup and long-term maintenance of the hardware used to capture the images. The actual hardware device can be anything from a desktop scanner to a massive optical telescope. If the hardware is not properly configured and aligned, then visual artifacts can be produced that can complicate the image processing. Improperly setup hardware also may provide images that are of such low quality that they cannot be salvaged even with extensive processing. All of these elements are vital to certain areas, such as comparative image processing, which looks for specific differences between image sets.

One of the forms of image acquisition in image processing is known as real-time image acquisition. This usually involves retrieving images from a source that is automatically capturing images. Real-time image acquisition creates a stream of files that can be automatically processed, queued for later work, or stitched into a single media format. One common technology that is used with real-time image processing is known as background image acquisition, which describes both software and hardware that can quickly preserve the images flooding into a system. There are some advanced methods of image acquisition in image processing that actually use customized hardware. Three-dimensional (3D) image acquisition is one of these methods. This can require the use of two or more cameras that have been aligned at precisely describes points around a target, forming a sequence of images that can be aligned to create a 3D or stereoscopic scene, or to measure distances. Some satellites use 3D image acquisition techniques to build accurate models of different surfaces.

5.3.2 Reference image

Normally reference image is used to compare between two images. The quality of the image is usually estimated by comparison with a known reference image. One of the methods uses simple technique such as mean quadratic difference. The drawback is that it is not possible to distinguish big differences from various small differences. Instead of the mean quadratic difference, the mean absolute difference or simply maximal absolute difference can be used too. Another class measures the resolution of small or proximate objects in this image processing technique.

5.3.3 Two frames difference

Figure 5.1 shows an example of resulted image applying the image processing technique called two frames difference

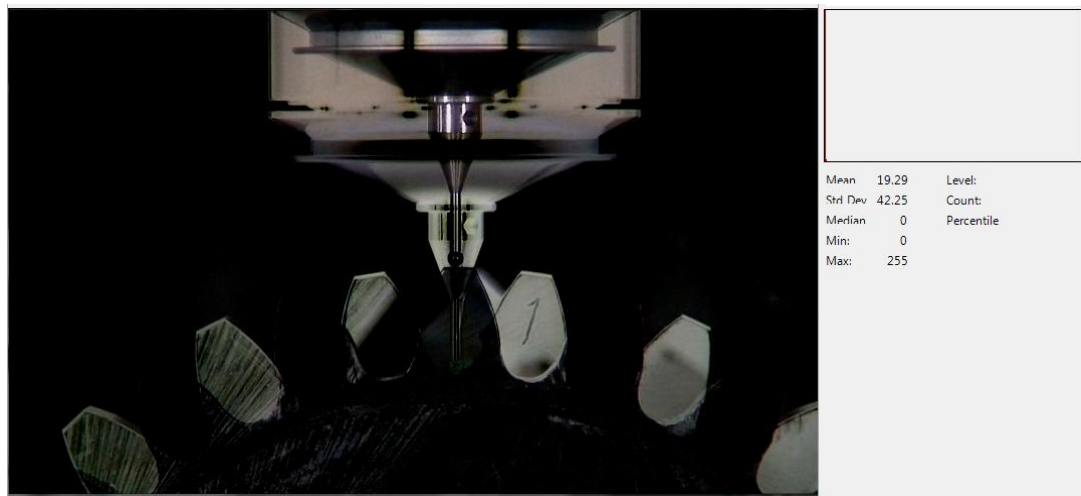


Fig. 5. 1 Image after applying two frame differences

5.4 Motion threshold

Motion threshold is very important in image processing. In motion threshold; the resulting image from opening filter is passed to pixel count. This counts the white pixel in the image. Histogram computation method is used for pixel count. As there

exists binary image; histogram is used to count the value of white pixels applying **Eqn. (5.1)**.

$$h'_f(z) = \frac{1}{2K+1} + \sum_{j=-K}^K h_f(z+j) \quad (5.1)$$

Where k is a constant representing the size of the neighborhood used for smoothing and its value is 128 as in **Fig. 5.2**, z refers to the count 0 to 255, j applies to the pixel values, and h_f refers to the total histogram values for the image function where mean = 0.40 and standard deviation = 10.12. This value of white pixel count is used as motion level. It signifies the magnitude of the motion. Greater magnitude of motion produces more white pixels; thus generates higher motion level. Motion threshold is very important parameter in image processing.

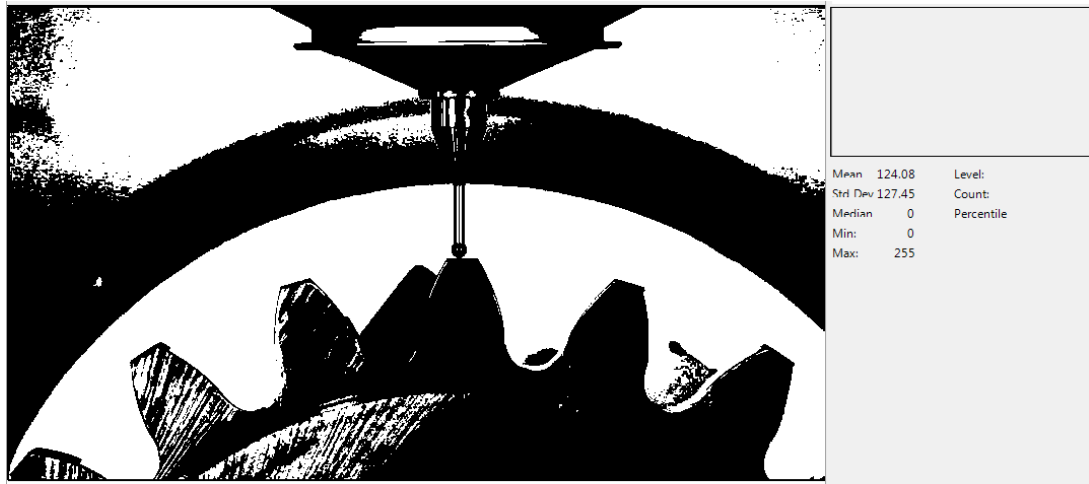


Fig. 5. 2 Resulted Image when threshold value is 128

The background and the images are first converted to gray scale image for simpler processing. Subsequently the image is compared to the background to detect any changes in the image. The algorithm for this process in histogram is given by the threshold value T which consists of a number between 0 and 255. It also creates a T -th frame by replacing all the pixels that have gray level lower than or equal to T with black (0) and the rest with white (1). Generally in threshold graph, axes g and f

indicate the required memory in bytes. Often only 256 bytes of memory needed. Thus; selected threshold values minimize both effects.

5.5 Purpose of Image processing

The purpose of image processing in the developed system is divided into 5 categories. Those are:

- Visualization - Observe the objects that are not visible.
- Image sharpening and restoration - To create a better image.
- Image retrieval - Seek for the image of interest.
- Measurement of target pattern – Measures various target gears based on motion.
- Image recognition based on motion detection – Distinguishes the objects in an image and records videos during measurement.

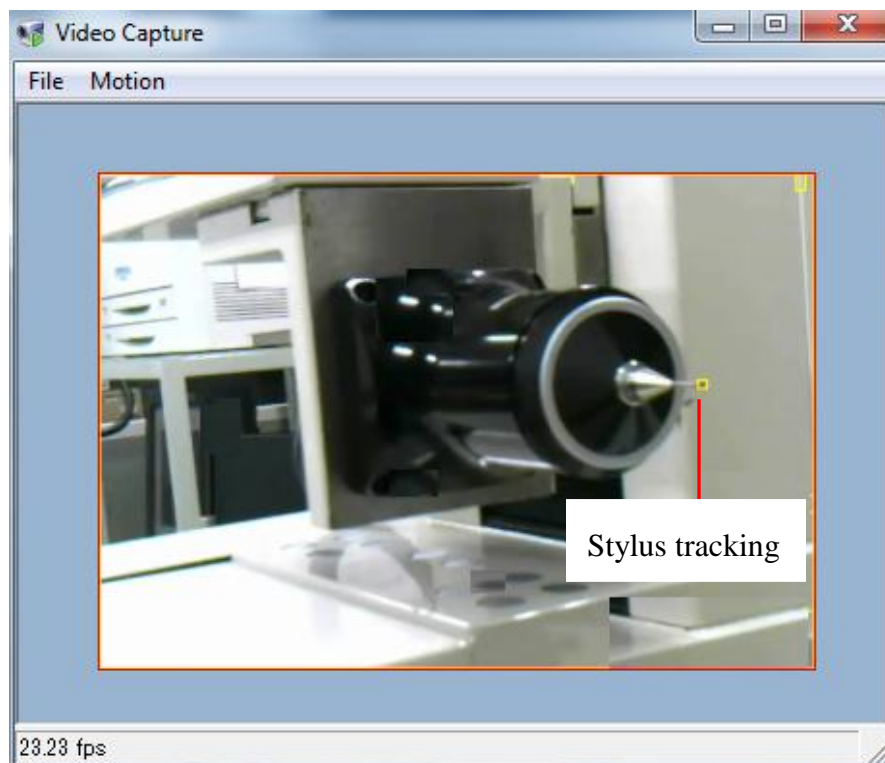


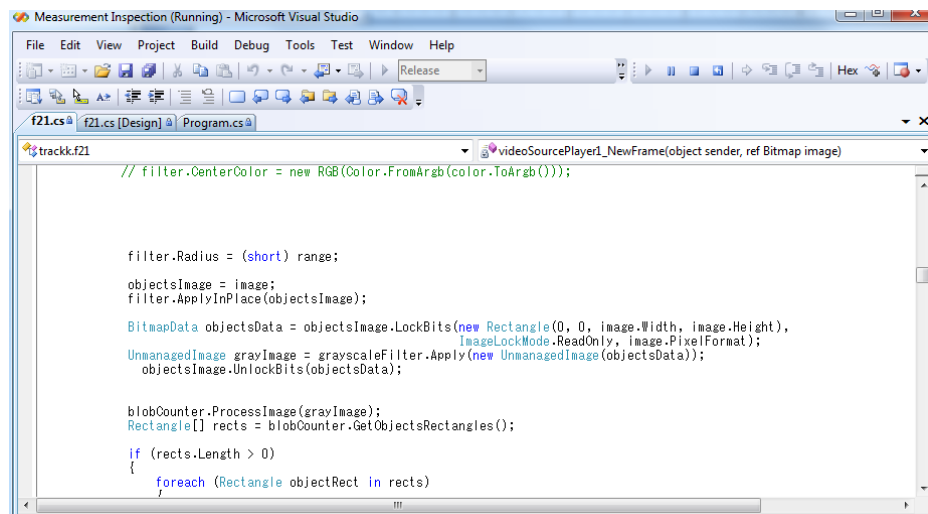
Fig. 5. 3 Stylus tracking

The filter eliminates pixels from the color that are inside RGB sphere with specified center and radius. It keeps pixels with colors inside the specified sphere and fills the rest with specified color. The filter accepts 24 and 32 bit color images for processing. **Figure 5.4** shows a Euclidean color filtering option which can be used to track the specific objects based on colors. **Figure 5.5** highlights a state where a object is tracked based on its target color which is selected through Euclidean filtering option.

5.7 Find objects based on the selected size

Figure 5.5 shows a window where the desire object's dimension can be chosen by selecting the pixel dimension for x and y axes. Also the range of the pixel can be defined in this window. The minimum height and minimum width of the object can be selected in terms of pixel value from this drop down menu.

5.8 Find the biggest object



```
Measurement Inspection (Running) - Microsoft Visual Studio
File Edit View Project Build Debug Tools Test Window Help
f21.cs [Design] | Program.cs
trackk.f21 videoSourcePlayer1_NewFrame(object sender, ref Bitmap image)
// filter.CenterColor = new RGB(Color.FromArgb(color.ToArgb()));

filter.Radius = (short) range;
objectsImage = image;
filter.ApplyInPlace(objectsImage);

BitmapData objectsData = objectsImage.LockBits(new Rectangle(0, 0, image.Width, image.Height),
ImageLockMode.ReadOnly, image.PixelFormat);
UnmanagedImage grayImage = grayscaleFilter.Apply(new UnmanagedImage(objectsData));
objectsImage.UnlockBits(objectsData);

blobCounter.ProcessImage(grayImage);
Rectangle[] rects = blobCounter.GetObjectsRectangles();

if (rects.Length > 0)
{
    foreach (Rectangle objectRect in rects)
    {

```

Fig. 5. 6 Filtering objects less than the selected range

Figure 5.6 shows the program in C # through which the smaller objects are filtered away from the group of detected objects. Objects are detected and marked by the blob or rectangular boundary box to separate from each other. The objects smaller than the defined parameters will be automatically deleted from the final selection and only object with the defined parameters will be visible in the final camera panel.

5.9 Draw object position in bitmap

Figure 5.5 shows above that an object with the position drawn in fourth camera panel where '0' marked is drawn throughout the path following the object's movement. By seeing the initial and final position from the .dat or .rtf file we can easily find the starting and ending point of operation and also can calculate deviation along the stylus movement.

5.10 Geometric position of the object in x and y coordinates

Figure 5.5 also shows the geometric position of the object in terms of pixel value in 'X' and 'Y' coordinates. This pixel value can be converted in terms of millimeter and centimeter values depend on the desirable unit. Beside this; it also has the following two important features. One is for recording videos and another is to record the experimental images. In addition; it can record or save the data in .dat and .rtf format during measurement.

5.11 Save data in .dat and .rtf formats

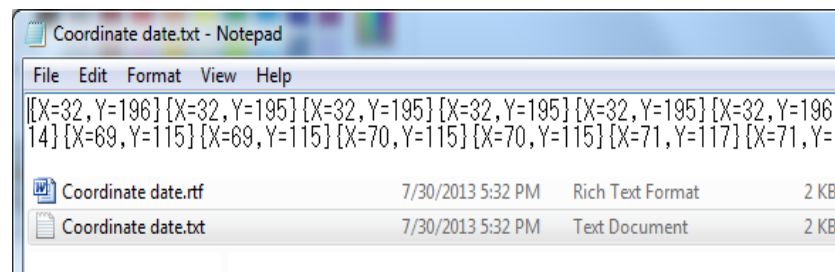


Fig. 5. 7 Video opening with the initial settings

Figure 5.7 shows the data process system during measurement. The data is recorded in .rtf and .dat formats during measurement. In .dat format the data is recorded in horizontal axis whereas in .rtf format the data is recorded in vertical axis. The file takes almost same data space in both formats. The first data is displayed in terms of pixel value of the original position during setting. The next value shows the position changed in terms of pixel value. The developed system is able to save the video files based on detected motion. The system saves the video only when it detects a motion and highlights the image border by the red lines. If there is no motion then the camera is in idle state. Thus it saves the memory too. During measurement once the measurement starts, the camera recording also starts automatically and stops as well when the measurement stops. Video feature has the following options:

- Log in with valid username and password
- Open video file
- Open a live camera
- Close the window
- Start video capture
- Video capture on motion
- Apply image processing

5.12 Image features

The system has another option to save the image frames during measurement. In both cases the capture rate is between 25-30 fps. The image quality is quite good in both cases. Based on the detected motion; the image saves in the destination file. Image feature has the following properties:

- Log in using valid username and password
- Select live camera
- Click start button for image capture

- Click stop button
- View the number of acquired image

5.13 Overall gear profile measurement system

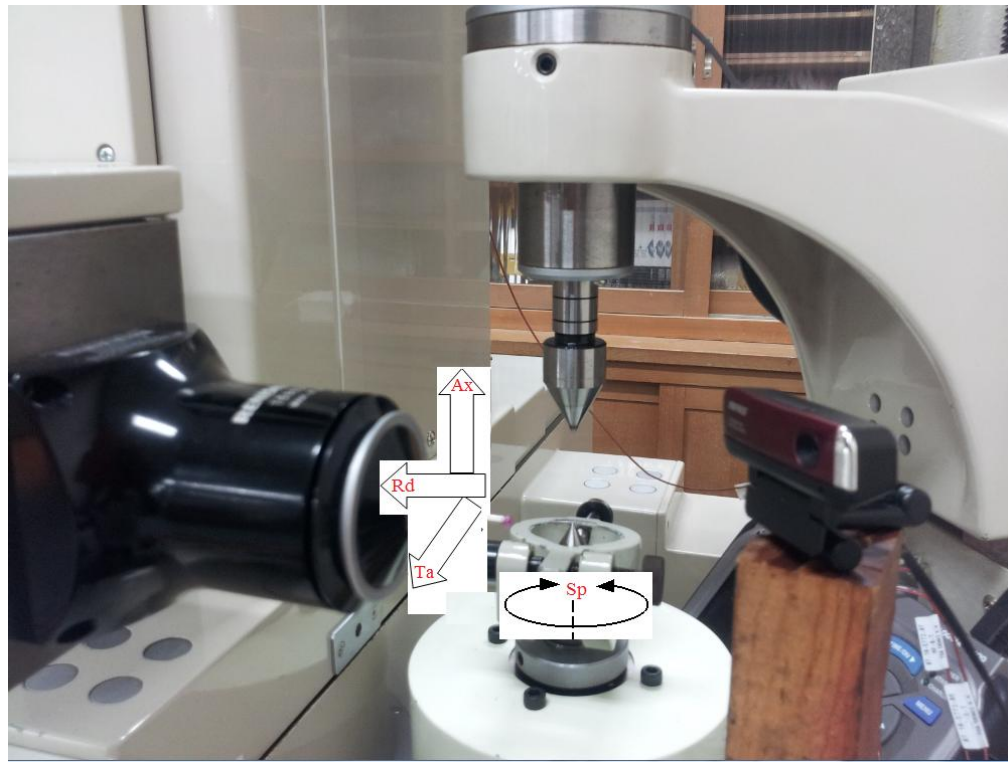


Fig. 5. 8 Probe's travel directions

Figures 5.8 and 5.9 show the system overview of gear profile measurement with the application of vision. The four directional movement of the system is shown in **Fig 5.8**. The camera position may vary depending upon desire results. Best results are acquired at the inclination angle of 45 degree between stylus and cameras. All the controls are done through integrated computer system. The camera data is also acquired through computer programming. The scanning data are saved in the desired folder. During experiment; the result can be viewed through computer monitor. The main purpose for the camera system is to track the stylus, particularly when the measurement is under progress.

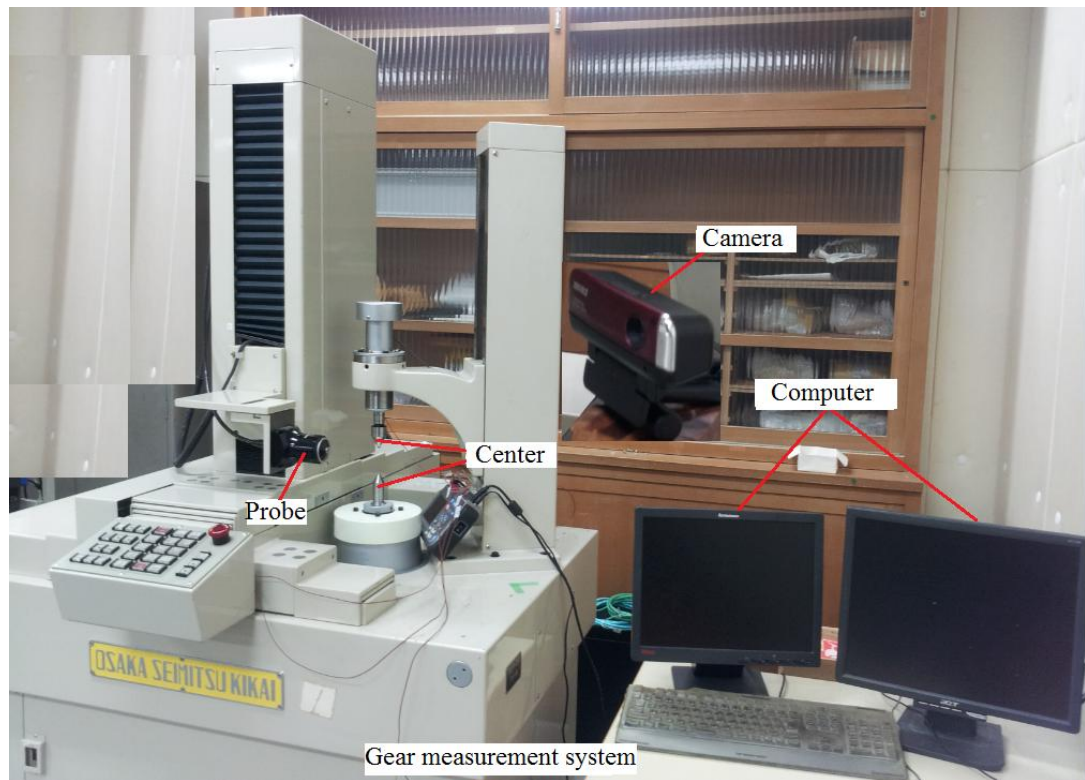


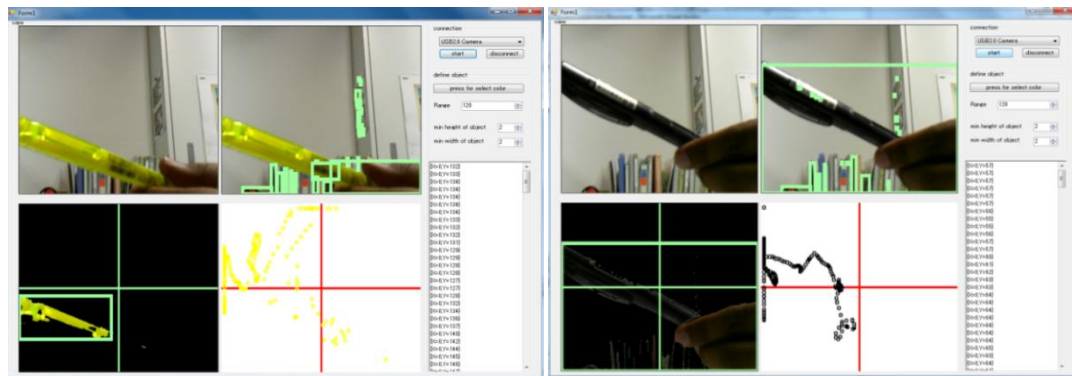
Fig. 5. 9 Experimental apparatus for measuring gear profile

5.14 Camera system for gear measurement

When the program runs, it starts tracking by default color as black and white and color range is 120 but; it can be adjusted according to our needs. In order to change default color it requires to press the color selection option and then a color dialog box will appear, then choose the target color and press OK and the solid color box shows the selected color. There are 4 panels to view, 3 of them are Aforge video source control and another one is a picturebox. The first one shows real video from camera, the second one shows all moving objects in rectangular boxes, the third panel shows only the biggest object and the fourth one just draws a '0' sign in biggest object location. It is also added a richtextbox which shows the pixel of biggest rectangle position.

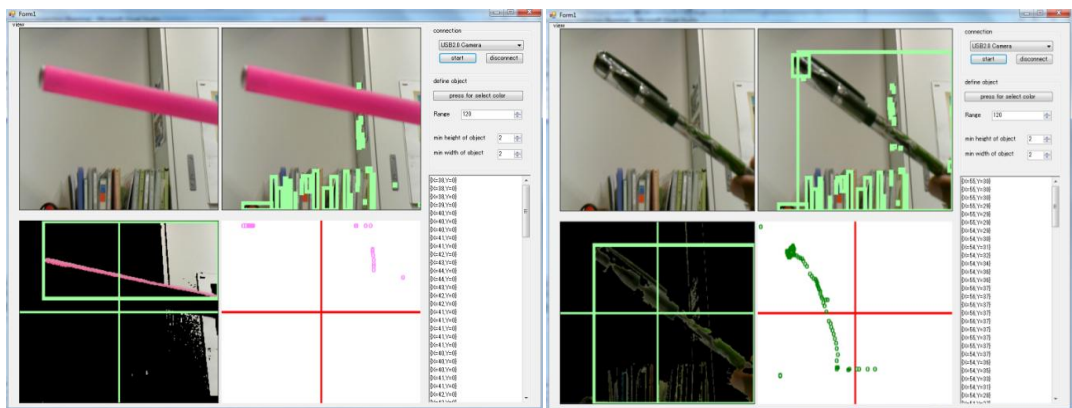
5.15 Stylus tracking based on colors

Figs. 5.10 (a), (b), (c) and (d) show different objects tracking status based on their colors. Based on color selection; the system tracks the objects with the selected color. Yellow, black, pink, green etc. color based moving objects can be tracked by the system. As for example; if the stylus color is black then the selection must be black for the tracking purpose.



(a)

(b)



(c)

(d)

Fig. 5. 10 Tracking of various moving pens based on colors in (a), (b), (c) and (d)

If the probe and stylus have same color then the detected objects area will be bigger than that when the stylus and probe colors are different. Only unique color stylus can be tracked at a time. For the present system; single probe and stylus can be tracked successfully. This tracking has great advantage in controlling the machines during experiment. Thus; it is very useful in precision measurement.

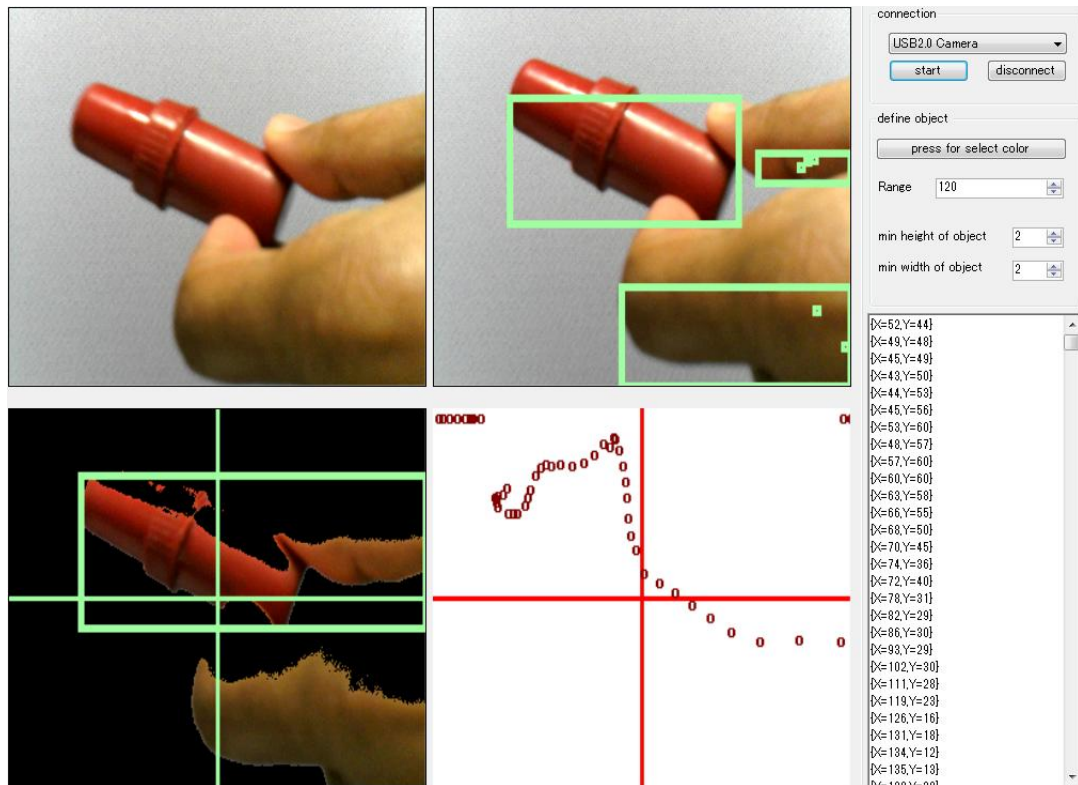


Fig. 5. 11 Tracking of a deep red object

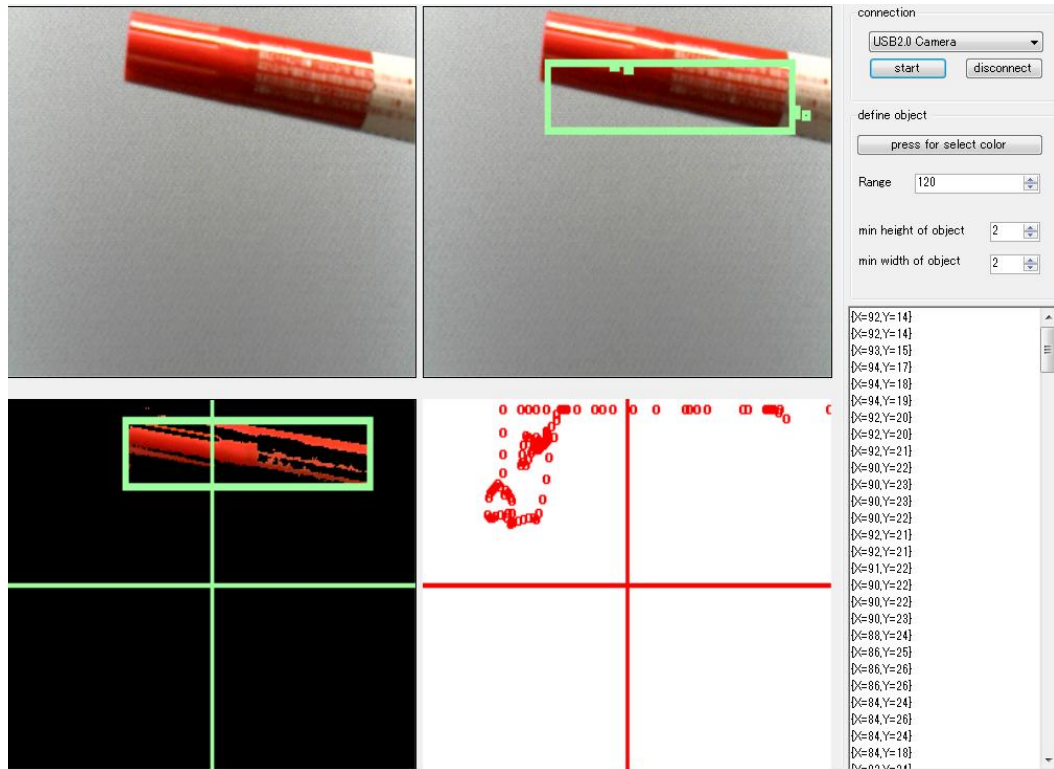


Fig. 5. 12 Tracking of red object

The red point in the below axis indicates the initial position. The system we developed in our lab is based on static tracking. In case of static tracking the camera remains static at all times during measurement and it is fixed on a suitable position where the camera has the ability to track the measurement probe or stylus accurately. In case of dynamic tracking, extra camera movement controlling motors and controllers are necessary to drive the camera. For clarification how this system works in detection and tracking the stylus, it is convenient to use a color code. The user can choose his/her desire color and size. In the developed system; the color detection code is applied here by implementing Euclidean filter and then apply blob counter to extract data. In the top-right corner of **Fig. 3.12**, software application options are shown. The first line selects the color value. As we know, color has a range of values from 0 to 255. From the function Argb (205, 20, 30); here, center color will be a red effected color and value of red is 205, green is 20, blue is 30 and radius = 105 means that all

color values around 105 in the specified color. Applying filter; if the color is inside the RGB sphere with specified center and radius then it keeps pixels with colors inside the specified sphere and fills the rest with specified color. Thus, the rectangle appears in the final detected object with the specified color. And if the color is outside of the RGB sphere without the specified center and radius then the sphere will not be filled by the specified color. **Figures 5.11** and **12** show the status of tracking red objects by the camera. These tracking are very important as the stylus tip's color is generally deep red or red.

5.16 Controls in precision measurement

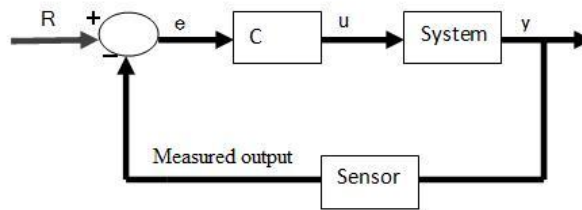


Fig. 5. 13 Simplified feedback control model

Figure 5.13 shows a block diagram of a simplified feedback control system. The system represents the plant which is to be controlled. Its output $y(t)$ is continuously compared to a reference signal $r(t)$ representing the desired output [23]. The difference between the two, called the error signal t is used by a controller device c to generate a control signal $u(t)$ to change the behavior of the plant. **Equations (5.1) and (5.2)** simplify the displacement of the measurement probe.

$$\Delta X_i = X_{i+1} - X_i \quad (5.1)$$

$$\Delta X_f = X_f - X_{f-1} \quad (5.2)$$

Where,

X_i = Initial position of measurement probe

- X_{i+1} = First point of measurement probe
- X_f = Final position of measurement probe
- ΔX_i = First displacement of the probe
- ΔX_f = Final displacement of the probe

After calculating displacement for each position, if the result sends to the probe in order to keep the measurement probe always on its original position then the measurement error will be eliminated easily by the output value. In this case; the probe only travels back to the same distance as it is diverted from its original position. It means the probe will always maintain its original axis during measurement to avoid measurement error. Front position of the measurement probe is determined by the front camera and rear position can be detected by a rear camera. Based on the measured data; the control is performed. Disturbances are the noises that occur during measurement from the inner and outer environment. Controller gain can be both positive and negative based on actuator’s input values. In the first case; if the process gain is positive, an increase in the measurement requires a decrease in the control action through driver. In the second case; if the process gain is negative, an increase in the measurement requires an increase in the control action.

5.17 Accuracy of the proposed method

Table 5. 1: Color based stylus tracking

Color based stylus	Detect	Display Tracking Path	Display and Save Coordinate Data (x, y)
Yellow	Yes	Yes	Yes
Black	Yes	Yes	Yes
Pink	Yes	Yes	Yes
Green	Yes	Yes	Yes
Red	Yes	Yes	Yes

Overall performance for video recording during measurement is very accurate and capturing rate is 100%. On the other hand, image frames saving function generates

some errors during experiment. The error here is not due to false detection rather it's because of missing the detected frames in desire location. Parameterized threading and cross threading improves the performance of this system. The frame rate can be increased by selecting perfect threading technique. Euclidian filter is more suitable than HSL filters or color filtering for this purpose. Color based object detection has a success rate of 100% while color based stylus tracking also has a success rate of 100% in the developed system as shown in **Table 5.1**.

5.18 Comparison of the result with the existing method

Recent, rapid technological improvements in video cameras have improved the utility and accuracy of measurements with such systems as mentioned in [22, 23]. The developed system has a single camera system for this purpose but it is possible to integrate the system together for multi-camera based measurement system. The single camera used in the developed system is iBuffalo, 1.3 Mega Pixel, Real Color CMOS web camera having a resolution of 640x480. The overall accuracy is shown in **Table 5.2** below.

Table 5. 2: Overall accuracy of the system

Parameters	Number of Object	Ratio	Accuracy (%)
Detected	5	5/5	100%
Tracking	5	5/5	100%
Video / Image	5	5/5	100%
File Save (x, y)	5	5/5	100%
Total	5		

5.19 Single camera measurements

For single camera measurements the error and precision varied when camera was rotated to an angle of more than 45 degrees. If measurements were made at angles less than 45 degrees, there were substantial improvements in the accuracy and precision.

5.20 Multiple camera measurement

One of the most significant advantages of stereo-video technology is the ability to make repeat measurements of the length of a particular object. Taking the mean of a set of repeated measurements can substantially improve the accuracy and precision of stereo-video measurements.

Accuracy is defined as the nearness of a measurement to the actual value being measured, while precision referred to the closeness of repeated measurements of the same subject to one another. The accuracy is calculated by subtracting the known length or distance from the observed measurement made from the single and multiple camera systems.

$$C_v = \sigma/\mu \quad (5.3)$$

Table 5. 3: Comparison between develop and existing methods

Parameters	Developed method	Existing methods
Image Save	Yes	No
Video Save	Yes	No
Precision control	Yes	No
Data save(x, y)	Yes	No
Human monitor	Not Necessary	Necessary
Time	Saves time	Time consuming
Cost	Less human monitoring; inexpensive	Human monitoring thus expensive
Safety	Safe	Unsafe

The standard error (SE) of the measurements is also calculated. **Equation (5.3)** is applied to calculate the above mentioned parameters. **Table 5.3** analyzes the merits of the developed method over the existing methods for measurement. Overall parameters

show that this method has great advantages over existing methods in practical application during precision measurement.

5.21 Summary

This chapter has elaborated several tracking results of the proposed color based stylus tracking system. The performance has been analyzed in order to test the feasibility of the developed system in the practical applications.

CHAPTER 6

CONCLUSION AND FUTURE WORKS

6.1 Conclusion

The developed gear measurement system has better performance in terms of reducing time up to 95% and generating additional necessary data from the gear profile measurement. From the comparison of the gear measurement system; it is verified that the developed measurement system is better than the conventional measurement system in terms of the measurement time as it is 20 times faster than the conventional gear measurement system. Besides; it can also generate all the important data for tooth root, tooth tip, tooth bottom and tooth flank in one complete measurement. The additional data enriched the developed gear profile measurement system. Conventional system has significant disadvantage as it requires indexing time for gear profile measurement; thus the stylus needs to travel more distance compare to the developed system. Another big disadvantage is that; in order to get more information, the workpiece needs to mount on another machine and for this reason, it is very inconvenient to use in industry. Based on the performance of the developed system it is obvious that this gives better precision measurement in precision engineering specially for the mechanical components production industries. Moreover; integration of vision with the developed system will further enhance the system in increasing human safety and reliability. It can also be noted that the vision based measurement system has advantages over non-vision based measurement system. Two important image processing applications are applied in order to increase safety for the developed measurement system.

Furthermore; color based stylus tracking and control of the measurement stylus as well as measurement probe is very much necessary for precision machining in manufacturing industries. The overall scanning performance has increased compare to the conventional measurement system as it can be seen below.

- Measurement of pitch deviation takes 9.57 minutes in conventional measurement system.
- Measurement of tooth flank takes 14.55 minutes in conventional system.
- Measurement of tooth trace takes 14.4 minutes in conventional system.
- But in the developed gear measurement system it takes 1.7 minutes only. Thus; within this short time all the above data can be acquired by the developed system.

6.2 Future works

In future two important tasks will further enhance the measurement system. One is to control the probe through vision system and the other is to apply this vision system in micro gear measurement for monitoring purpose. Control the probe will surely make the system more autonomous and will have less interference during measurement. For the purpose of controlling the measurement probe; a feed back or closed-loop control is suitable as it will immediately correct the probe deviation and guide to the right axis during measurement. Feed-back control will eliminate the possibility of accident to be happened during measurement. Several key points are observed during the implementation of vision based gear measurement system. Those are:

- Occlusion handling is necessary in the practical environment due to light variance and shadow.
- Higher camera angle results are not satisfactory.
- False detection varies depending on the camera resolution and target distance.

ACKNOWLEDGEMENTS

Special thanks and deeper respects are given from the author to his both parents for all of their supports, encouragements, advices and prayers.

The author would like to express his sincere thanks and gratitude to Professor Syuhei KUROKAWA, Precision Machining Laboratory, Department of Mechanical Engineering, Kyushu University for all of his kind advices, guidance, supports, encouragements, motivations as well as providing necessary experimental equipments throughout the complete doctoral research.

The author also would like to express his deepest and heartfelt gratitude and thanks to Emiratus Professor Hiromichi Onikura and Professor Yamamoto Motoji for being external examiners for his doctoral thesis. The author is very much grateful to them for their valuable times, efforts and constructive suggestions to make the dissertation a successful one.

Similarly; heartfelt thanks are also given to Assistant Professor Dr. Akio Katsuki, Precision Machining Laboratory, Kyushu University for all of his warm advices, supervisions and great helps concerning all the research stages for this interesting research. His contribution goes beyond appreciations. His great helps enabled me and gave me an opportunity to involve and conduct this advance level of research in precision engineering.

Author's sincere appreciation goes to Assistant Professor Takao Sajima, Precision Machining Laboratory, Kyushu University, for all of his helps, advices and guidance. Additionally; special thanks are also given to all other staff and students of Precision Machining Laboratory, Kyushu University regarding many kinds of supports and helps during his study. Also; sincere thanks to Osaka Seimitsu Kikai Co. Ltd. for providing us the DDS system to continue further research in gear measurement.

Finally; the author is pleased to acknowledge the scholarship granted by The Japanese Ministry of Education, Science and Culture (MEXT), which gave him privilege to study at Kyushu University for his doctoral degree.

REFERENCES

- [1] MD. Hazrat Ali, Syuhei Kurokawa, Kensuke Uesugi, “Vision based measurement system for gear profile”. IEEE International Conference of Informatics, Electronics & Vision, 2013. doi:10.1109/ICIEV.2013.6572652.
- [2] MD. Hazrat Ali, Syuhei Kurokawa, Kensuke Uesugi, Takashi Teraoka, “Camera based 3D probe control in measuring gear profile”, IEEE The second international conference on Robot, Vision and Signal Processing, Dec 10-12, 2013, Kita Kyushu, Japan.
- [3] Beyaz, A., Ozturk, R., Turker, U. (2010). Assessment of Mechanical Damage on Apples with Image Analysis, Journal: Food Agriculture Environment (JFAE), Vol. 8, Issue 3&4, pp. 476-480, Online ISSN: 1459-0263, Publisher: WFL.
- [4] Lukac, R., Plataniotis, K. N. (2007). Colour Image Processing Methods and Applications (Image Processing), ISBN: 13: 978-0-8493-9774-5 (Hardcover), CRC Press, Printed in the Canada.
- [5] Adam Marciniak, Grzegorz Budzik, Tomasz Dziubek, “Automated Measurement of Bevel Gears of the air craft gearbox using GOM”, Journal of KONES Powertrain and Transport, Vol. 18, No. 2 2011.
- [6] Budzik, G., Kozik, B., Pacana, J., Muda, B., Modeling and prototyping of aeronautical planetary gear demonstrator, Journal of KONES Powertrain and Transport, Vol. 17, No. 3, pp. 49-54, 2010.
- [7] Budzik, G., Dziubek, T., Sobolewski, B., Zaborniak, M., Selection measuring strategy for gear wheels produced by RP methods, devices in coordinate Metrology, pp. 407-414, 2010.
- [8] Haertig, F., Lotze, W., 3D Gear Measurement by CMM, Laser Metrology and Machine Performance V, 2001.
- [9] Withrobot Lab, 2012, <http://www.withrobot.com>. Accessed on 21st October, 2013.
- [10] Y. Fukuda, M. Q. Feng, and M. Shinozuka, “Cost-effective vision-based system for monitoring dynamic response of civil engineering structures,” Structural Control and Health Monitoring, vol. 17, no. 8, pp. 918–936, 2010.
- [11] J. J. Lee and M. Shinozuka, “A vision-based system for remote Sensing of bridge displacement, “NDT and International, Vol39, No.5, pp.425-431, 2006”.
- [12] H. S. Choi, J. H. Cheung, S. H. Kim, and J. H. Ahn, “Structural dynamic displacement vision system using image processing ,” NDT and E International, vol. 44, no. 7, pp. 597–608, 2011.

- [13] Jainy S., "Machine Vision Based Identification and Dimensional Measurement of Electronic Components", Master's Thesis, pp.12, June, 2006.
- [14] Dalsa technology, "Precision Measurements with Machine Vision", USA.
<https://www.teledynedalsa.com>.
- [15] R. Takeda and . Komori, "Deelopment of scanning measurement tooth flank form of generated face mill hypoid gear pair". Journal of metrology Society of India, Vol.26, No.1, 2011.55-67.
- [16] Mohamed A., Esa A.H. and Ayub M.A, "Roundness Measurement of Cylindrical Parts by Machine Vision". International Conference on Electrical, Control and Computer Engineering, 2011, pp.486-490.
- [17] Tao Zhang, Yi Luo, Xiaodong Wang and Mixin Wang, "Machine Vision Technology for Measurement of Miniature Parts in Narrow Space Using Borescope". International Conference on Digital manufacturing and Automation (ICDMA), pp.904-907, 2010, China.
- [18] Russ, J. C, The Image Processing Handbook, Fifth Edition (Image Processing Handbook), ISBN 0-8493-7254-2, CRC Press, 2006, Printed in the United States of America.
- [19] Hexagon Metrology. (2009, March 20). Gear Measuring with Leitz CMM Retrieved from <http://www.creaform3d.com/en/ndt-solutions/c-track>.
- [20] Tugrul O'zel, International Journal of Advance Manufacturing Technology (2006) 27: 960–968, DOI 10.1007/s00170-004-2292-3.
- [21] E.S. Gadelmawla, Computer vision algorithms for measurement and inspection of spur gears, Measurement, Volume 44, Issue 9, November 2011, Pages 1669-1678, ISSN 0263-2241, <http://dx.doi.org/10.1016/j.measurement.2011.06.023>.
- [22] Harvey, E. S., and Shortis, M. R.. A system for stereo-video measurement of subtidal organisms. Journal of the Marine Technology Society, 1996.29(4): 10-22.
- [23] Harvey, E. S., and Shortis, M. R. Calibration stability of and underwater stereo-video system: Implications for measurement accuracy and precision. Journal of the Marine Technology Society, 1998.32(2): 3-17.
- [24] Zar, J. H. Biostatistical Analysis. (Second Edition eds.). 1984. Englewood Cliffs, New Jersey: Prentice Hall. 718 pp.
- [25] Thresher, R. E., and Gunn, J. S. Comparative analysis of visual census techniques for highly mobile, reef associated piscivores (Carangidae). Environmental Biology of Fishes, 1986.17: 93-116.

- [26] M. Weck, O. Guzman, P.W. Gold, Measuring the flank geometry of bevel gears on a multiple-coordinate measuring machine, *Precision Engineering*, Volume 2, Issue 2, April 1980, Pages 85-88
- [27] Anke Guenther, Karin Kniel, Frank Hartig, Ingo Lindner, Introduction of a new bevel gear measurement standard, *CIRP Annals - Manufacturing Technology*, Volume 62, Issue 1, 2013, Pages 515-518.
- [28] Ryohei Takeda, Masaharu Komori, Tatsuya Nishino, Yukihiko Kimura, Takayuki Nishino, Kenji Okuda, Shinji Yamamoto, Performance analysis of generated hypoid gear based on measured tooth flank form data, *Mechanism and Machine Theory*, Volume 72, February 2014, Pages 1-16.
- [29] Jun WANG, Xiao-chun WANG, Hong JIANG, Wen-jun FENG, Measurement and Compensation of Deviations of Real Tooth Surface of Spiral Bevel Gear, *Chinese Journal of Aeronautics*, Volume 16, Issue 3, August 2003, Pages 182-186.
- [30] Su-Ping Fang, Lei-Jie Wang, Masaharu Komori, Aizoh Kubo, Design of laser interferometric system for measurement of gear tooth flank, *Optik - International Journal for Light and Electron Optics*, Volume 122, Issue 14, July 2011, Pages 1301-1304
- [31] Jose A. Brandao, Ramiro Martins, Jorge H.O. Seabra, Manuel J.D. Castro, Calculation of gear tooth flank surface wear during an FZG micropitting test, *Wear*, Available online 9 January 2014.
- [32] Weidong Zhu, Biao Mei, Guorui Yan, Yinglin Ke, Measurement error analysis and accuracy enhancement of 2D vision system for robotic drilling, *Robotics and Computer-Integrated Manufacturing*, Volume 30, Issue 2, April 2014, Pages 160-171.
- [33] T. Jeyapoovan, M. Murugan, Surface roughness classification using image processing, *Measurement*, Volume 46, Issue 7, August 2013, Pages 2065-2072.
- [34] R.W. Furrow, H.H. Mabie, The measurement of static deflection in spur gear teeth, *Journal of Mechanisms*, Volume 5, Issue 2, Summer 1970, Pages 147-150.
- [35] Huseyin Imrek, Hayrettin Duzcukoglu, Relation between wear and tooth width modification in spur gears, *Wear*, Volume 262, Issues 3-4, 4 February 2007, Pages 390-394.
- [36] N.A Wright, S.N Kukureka, Wear testing and measurement techniques for polymer composite gears, *Wear*, Volume 251, Issues 1-12, October 2001, Pages 1567-1578.
- [37] Jozef Wojnarowski, Valentin Onishchenko, Tooth wear effects on spur gear dynamics, *Mechanism and Machine Theory*, Volume 38, Issue 2, February 2003, Pages 161-178.

- [38] Eiki Okuyama, Satoshi Kiyono, Hitoshi Moritoki, Investigation of an optical noncontact gear geometry measurement system: measurement of pitch errors and tooth profiles, *Precision Engineering*, Volume 16, Issue 2, April 1994, Pages 117-123.
- [39] Frank Hrrtig, Hu Lin, Karin Kniel, Zhaoyao Shi, Laser tracker performance quantification for the measurement of involute profile and helix measurements, *Measurement*, Volume 46, Issue 8, October 2013, Pages 2837-2844.
- [40] A. Guenther, R. Hocken, Evaluation of Runout Deviation at Bevel Gears based on Pitch Measurements, *CIRP Annals - Manufacturing Technology*, Volume 55, Issue 1, 2006, Pages 539-542.
- [41] Li Mei Song, Ming Ping Wang, Lu Lu, Huang Jing Huan, High precision camera calibration in vision measurement, *Optics & Laser Technology*, Volume 39, Issue 7, October 2007, Pages 1413-1420, ISSN 0030-3992.
- [42] M.A. Hotait, A. Kahraman, Experiments on the relationship between the dynamic transmission error and the dynamic stress factor of spur gear pairs, *Mechanism and Machine Theory*, Volume 70, December 2013, Pages 116-128.
- [43] Mu-Chen Chen, Roundness measurements for discontinuous perimeters via machine visions, *Computers in Industry*, Volume 47, Issue 2, February 2002, Pages 185-197, ISSN 0166-3615.
- [44] Maria Pia Sammartinia, Leonardo De Chiffre, Development and validation of a new reference cylindrical gear for pitch measurement, *Precision Engineering*, Volume 24, Issue 4, October 2000, Pages 302-309.
- [45] J.J. Aguilar, F. Torres, M.A. Lope, Stereo vision for 3D measurement: accuracy analysis, calibration and industrial applications, *Measurement*, Volume 18, Issue 4, August 1996, Pages 193-200, ISSN 0263-2241.
- [46] S.H. Suh, E.S. Lee, H.C. Kim, J.H. Cho, Geometric error measurement of spiral bevel gears using a virtual gear model for STEP-NC, *International Journal of Machine Tools and Manufacture*, Volume 42, Issue 3, February 2002, Pages 335-342.
- [47] Wei Gao, Masaru Furukawa, Satoshi Kiyono, Hiroshi Yamazaki, Cutting error measurement of flexspline gears of harmonic speed reducers using laser probes, *Precision Engineering*, Volume 28, Issue 3, July 2004, Pages 358-363.
- [48] G. Lanza, B. Viering, A novel standard for the experimental estimation of the uncertainty of measurement for micro gear measurements, *CIRP Annals - Manufacturing Technology*, Volume 60, Issue 1, 2011, Pages 543-546.

- [49] Hao Shen, Shuxiao Li, Duoyu Gu, Hongxing Chang, Bearing defect inspection based on machine vision, Measurement, Volume 45, Issue 4, May 2012, Pages 719-733, ISSN 0263-2241.
- [50] Wang Wen-cheng and Ji Tao, “ Future Intelligent Information Systems”, Lecture Notes in Electrical Engineering Volume 86, 2011, pp 7-13.
- [51] <http://www.engineersgarage.com/articles/image-processing-tutorial-applications>. Accessed on 15th November, 2013.
- [52] Ogesh Pandya, Anand Parey, Experimental investigation of spur gear tooth mesh stiffness in the presence of crack using photoelasticity technique, Engineering Failure Analysis, Volume 34, December 2013, Pages 488-500.
- [53] <http://homepages.inf.ed.ac.uk/rbf/HIPR2/erode.htm>. Accessed on 15th November, 2013.
- [54] http://www.aforgenet.com/framework/features/motion_detection_2.0.html. Accessed on 15th November, 2013.
- [55] <http://en.wikipedia.org/wiki/Grayscale>. Accessed on 15th November, 2013.